Benign Processing of High Performance Polymeric Foams of Poly(arylene ether sulfone)

Desmond J. VanHouten

Dissertation submitted to the faculty of the Virginia Polytechnic Institute and State University in partial fulfillment of the requirements for the degree of

DOCTOR OF PHILOSOPHY

In

Macromolecular Science and Engineering

Donald G. Baird, Chair
James E. McGrath
Scott W. Case
Richey M. Davis

December 2, 2008
Blacksburg, Virginia

Keywords: supercritical carbon dioxide, foaming, plasticizer, high performance polymer, poly(arylene ether sulfone)

Benign Processing of High Performance Polymeric Foams of Poly(arylene ether sulfone)

Desmond J. VanHouten

ABSTRACT

This work is concerned with the production of high performance polymer foams via a benign foaming process. The first goal of this project was to develop a process and the conditions necessary to produce a low density (>80% density reduction) foam from poly(arylene ether sulfone) (PAES). Water and supercritical carbon dioxide ($scCO_2$) were used as the blowing agents in a one-step batch foaming process. Both water and $scCO_2$ plasticize the PAES, allowing for precise control on both the foam morphology and the foam density. To optimize the foaming conditions, both thermogravimetric analysis and differential scanning calorimetery (DSC) were used to determine the solubility and the reduced glass transition temperature (T_g) due to plasticization of the polymer. It was determined that 2 hours was sufficient time to saturate the PAES with water and $scCO_2$ when subjected to a temperature of 220 ^oC and 10.3 MPa of pressure. Under these conditions, a combination of 7.5% of water and $scCO_2$ were able to diffuse into the PAES specimen, correlating to ~60 ^oC reduction in the T_g of the PAES. The combination of water and $scCO_2$ produced foam with up to an 80% reduction in density. The compressive properties, tensile modulus, and impact strength of the foam were measured. The relative compressive properties were slightly lower than the commercially available structural foam made of poly(methacrylimide).

The second objective of the dissertation was to enhance the compressive properties of the PAES foam, without concern for the foam density. Foam was produced over a range of density, by controlling the cell size, in order to optimize the compressive properties. Carbon nanofibers (CNFs) were also added to the PAES matrix prior to foaming to both induce heterogeneous nucleation, which leads to smaller cell size, and to reinforce the cell walls. Dynamic mechanical thermal analysis (DMTA), on saturated CNF-PAES, was used to determine the reduced T_g due to plasticization and establish the temperature for pressure release during foaming. DMTA proved to be more effective than DSC in establishing quantitative results on the reduction in the T_g. The CNF-PAES foam produced had compressive properties up to 1.5 times the compressive properties of the PAES foam.

Acknowledgements

I would like to thank my advisor, Dr. Donald G. Baird, for his thoughts and guidance on my project. The insightful conversations helped to spark new ideas and directions on my research. In addition I would like to thank my committee members, present and past, for their time and suggestions: Dr. Davis, Dr. Case, Dr. McGrath, and Dr. Riffle.

In addition my committee, I would like to thank the following people:

- The staff in both Chemical Engineering and the Macromolecular Science and Engineering program: Diane, Laurie, Millie, Angie, Mike, and Riley.
- Steve McCartney and Rick Caudill for time from their schedule to help me test my material.
- My best friend, my loving and caring wife, and my editor, Rachael. Throughout the process she has shown me tremendous support and encouragement. She was always there to keep my spirits high during the stressful times of graduate school, which helped me to persevere. I enjoyed being able to spend every lunch time with her over the past 4 ½ years and I look forward to the future that this opportunity will provide for us.
- My family: A special thank you goes to my grandparents, James and Theresa VanHouten, for raising me and always pushing me to work hard. Thank you also goes to Destiny and Joel Narloch, Dawn VanHouten, Doug Schrupp, Betty Zellner, Alex Zellner, Katie and Michael Abramczyk, and Kent and Stacy VanEgtern for their support.

- The men and woman of the Polymer Processing Lab whom I have had the pleasure of working with: Aaron, Chris S., David, Gregorio, Myoungbae, Chris M., Kevin, Chen, Mike, and Neeraj.
- My church family at Main Street Baptist Church for their support.
- Ultimately, I would like to thank God. Without His love and guidance in my life, nothing would be possible. My personal relationship with Him has gotten me through stress and dead-ends of my research.

Original Contributions

The following are considered to be original contributions of this research:

1. Development of a benign process, which utilized a dual plasticizer blowing agent system, to produce low density (>80% density reduction) foams from poly(arylene ether sulfone). A combination of water and supercritical carbon dioxide were used as the blowing agents.

2. The incorporation of carbon nanofibers into the poly(arylene ether sulfone) foam to greatly enhance the compressive properties of the foam via heterogeneous nucleation and reinforcement of the cell walls.

3. The use of dynamic mechanical thermal analysis on plasticized poly(arylene ether sulfone) to quantitatively determine the reduced T_g and to use the data to control the cell size by decreasing the temperature at which the foam is produced.

4. Incorporating the Williams-Landel- Ferry based equation into cell growth modeling to account for the increase of viscosity during the foaming of a polymer with blowing agents that plasticize the polymer.

Format of Dissertation

This dissertation is written in manuscript format. Chapters 3.0 through 5.0 are manuscripts which stand alone and describe the experiments, results, and conclusions for the work. With the exception of the literature review, chapter 2.0, the tables and figures are located after the references of each manuscript.

Table of Contents

Table of Tables xiii

Table of Figures xiii

1 Introduction 1

1.1 References 4

2 Literature Review 6

2.1 Role of Carbon Dioxide in Polymer Processing 6

2.1.1 Supercritical Carbon Dioxide Properties 6

2.1.2 Solubility in Polymers 7

2.1.3 Diffusivity in Polymers 10

2.1.4 Plasticization of Polymers 11

2.2 Structural Polymers and Composites 12

2.2.1 Structural Sandwich 13

2.2.1.1 Polymer Core Materials 13

2.2.1.1.1 Polyetherimide foam 14

2.2.1.1.2 Poly(methacrylimide) Rigid Foam 16

2.2.1.1.3 Polyimide foam 17

2.2.1.2 Honeycomb Core 18

2.2.1.3 Syntactic Foam Core 20

2.3 Benefits of Microcellular Foams 22

2.4 Processing of Microcellular Foams 24

2.4.1 Batch Processing 25

2.4.1.1 Two-Step Batch Processing 25

2.4.1.2 One-step Batch Process 27
2.4.2 Continuous and Semi-Continuous Processes 28
2.4.2.1 Continuous Extrusion Process 28
2.4.2.2 Continuous Injection Molding Process 31
2.4.2.3 Semi-continuous Extrusion Process 34
2.5 Parameters Affecting Microcellular Foaming 35
2.5.1 Control of Processing Parameters for Desired Foam Properties 36
2.5.1.1 Batch Processing 36
2.5.1.1.1 Cell Density 36
2.5.1.1.2 Cell Size 39
2.5.1.2 Continuous and Semi-continuous Processing 40
2.5.1.2.1 Cell Density 40
2.5.1.2.2 Cell Size 41
2.5.1.2.3 Expansion Ratio 42
2.5.1.2.4 Die Design 43
2.5.2 Polymer Properties Affecting Foam Production 45
2.5.2.1 Cell Density 45
2.5.2.2 Cell Size 45
2.6 Microcellular Foam Composites 46
2.6.1 Nanocomposite foam 46
2.6.1.1 Foaming of Polymer-Nanoclay Composites 47
2.6.1.2 Foaming of Polymer-Carbon Nanofiber Composites 49
2.6.2 Fiber Reinforcement 50

2.7 Modeling of Microcellular Foaming 51
2.7.1 Microcellular Nucleation Modeling 52
2.7.1.1 Classical Nucleation Theory 52
2.7.1.2 Microvoid Nucleation Model 55
2.7.2 Cell Growth Modeling 58
2.8 References 61
3 Generation of Low-Density High Performance Poly(arylene ether sulfone) Foams Using a Benign Processing Technique…… 73
3.1 Introduction 74
3.2 Experimental 78
3.2.1 Materials 78
3.2.2 Foaming Procedure 79
3.2.3 Thermal Analysis 79
3.2.4 Characterization 80
3.2.4.1 Foam Density 80
3.2.4.2 SEM Imaging 80
3.2.4.2.1 Determination of Cell Size and Cell Nucleation Density 80
3.2.5 Mechanical Properties 81
3.2.5.1 Tensile Testing 81
3.2.5.2 Compression Testing 82
3.2.5.3 Impact Testing 82
3.3 Results and Discussion 82
3.3.1 Determination of Plasticization of PAES resin 82

3.3.2 Characterization of the Foam Density and Morphology 85
3.3.3 Mechanical Properties of the PAES Foam 86
3.4 Conclusions 89
3.5 Acknowledgements 90
3.6 References 91
4 Generation and Characterization of Carbon Nano-fiber-Poly(arylene ether sulfone) Nanocomposite Foams 104
4.1 Introduction 105
4.2 Experimental 109
4.2.1 Materials 109
4.2.1.1 Preparation of the PAES-CNF Nanocomposite Material 110
4.2.2 Foaming Procedure 110
4.2.3 Thermal Analysis 111
4.2.4 Foam Density 113
4.2.5 Determination of Cell Size and Cell Nucleation Density from SEM Imaging… 113
4.2.6 Tensile Testing 114
4.2.7 Compression Testing 114
4.2.8 Impact Testing 115
4.3 Results and Discussion 115
4.3.1 Determination of CNF-PAES Plasticization from Presence of Water and CO_2 116
4.3.2 Characterization of Foam Morphology and Density 118

4.3.3 Determination of the Tensile, Compressive, and Impact Properties 121
4.4 Conclusions 123
4.5 Acknowledgements 124
4.6 References 125
5 Modeling of Cell Growth in Polymer Foaming with Dissolved Gas Blowing Agent by Incorporation of a Variable Viscosity Function 142
5.1 Introduction 143
5.2 Cell Growth Modeling 144
5.3 Determination of Viscosity, η 147
5.4 Solving the System of Equations 149
5.5 Determination of the Physical Parameters 150
5.6 Effect of Variable Viscosity on Cell Growth Modeling 151
5.7 Conclusions 152
5.8 Nomenclature 154
5.9 References 155
6 Recommendations 162
6.1 Determination of the Physical Parameters in the Cell Growth Model for PAES with Water and CO_2 163
6.2 References 165
Appendix A MATLAB Program for Cell Growth Modeling 166
Appendix B DMTA Data 170

Table of Tables

Chapter 3.0
Table 3.1 Foam Density and Morphology of PAES Foam 95

Table 3.2. Summary of the Mechanical Properties of the PAES Foam and Commercially Available PEI and PVC Foam 96

Chapter 4.0
Table 4.1. Summary of the Relative Tensile, Compressive, and Impact Properties for CNF-PAES foamed at Varying Release Temperatures 128

Chapter 5.0
Table 5.1. Estimated Physical Parameters Used in the Cell Growth Modeling. 157

Table of Figures

Chapter 2.0
Figure 2.1 Phase diagram of carbon dioxide[1]. Reprinted from *Progress in Polymer Science*, 31, 19-43, Copyright (2006), with permission from Elsevier..... 7

Figure 2.2 Schematic drawing of continuous extrusion process [81]. 29

Figure 2.3 Schematic drawing of the nozzle used in the IKV injection molding process[89]. Reprinted from *Cellular Polymers*, 23, 25-37, Copyright (2004), with permission from Rapra..... 32

Figure 2.4 Schematic drawing of the nozzle used in the University of Warwick injection molding process[89]. Reprinted from *Cellular Polymers*, 23, 25-37, Copyright (2004), with permission from Rapra..... 33

Figure 2.5 Comparison of modified classical nucleation theory to experimental data[111]. Discrete points represent experimental data and the line represents the model. 55

Chapter 3.0
Figure 3.1. Effect of saturation pressure on the diffusion of the blowing agents into the PAES resin. 97

Figure 3.2. TGA results quantifying the amount of blowing agents that were able to diffuse into the PAES resin. 98

Figure 3.3. DSC results quantifying the plasticized T_g of the PAES resin. 99

Figure 3.4. SEM image of PAES foam produce in a one-step batch process utilizing a combination of CO_2 and water as the blowing agents… 100

Figure 3.5. SEM image of PAES foam produce in a one-step batch process utilizing a combination of N_2 and water as the blowing agents…. 101

Figure 3.6. Stress-strain curve for PAES foam produced by using combination of CO_2 and water, and N_2 and water under a tensile load. 102

Figure 3.7. Relative compressive strength and foam density of the PAES foam produced by using CO_2 and water, and N_2 and water as the blowing agents. The compressive strength of commercially available PEI, PMI, and PVC foams are shown for comparison.[2,36] 103

Chapter 4.0
Figure 4.1. TGA results of 1 wt.% CNF-PAES saturated with CO_2 and water..... 129

Figure 4.2. DSC results of 1 wt.% CNF/PAES saturated with 7.6 % CO_2 and water. .. 130

Figure 4.3. DMTA results of 1 wt% CNF-PAES saturated with water and CO_2 (▲) and neat CNF-PAES (●).. 131

Figure 4.4. DMTA results of 1 wt% CNF-PAES saturated for release at 165 ^oC (●) and 220 ^oC (▲).. 132

Figure 4.5. SEM micrograph of the CNF-PAES foam produced from a one-step batch process utilizing water and CO_2 as the blowing agents at a release temperature of a) 165 ^oC, b) 180 ^oC, c) 200 ^oC, d) 220 ^oC, e) 227 ^oC..... 135

Figure 4.6. Cell size distribution of the CNF-PAES foam saturated with water and CO_2 at 165 ^oC, 180 ^oC, 200 ^oC, 220 ^oC, 227 ^oC..... 138

Figure 4.7. Effect of the release temperature on the cell nucleation density for CNF-PAES foamed with water and CO_2. 139

Figure 4.8. SEM micrograph of CNF-PAES foamed with water and CO_2 at a release temperature of 220 ^oC. The presence of heterogeneous nucleation can be seen in the micrograph. 140

Figure 4.9. Effect of foaming temperature on the bulk density of the CNF-PAES foams. 141

Chapter 5.0
Figure 5.1. Schematic for the modeling of the cell growth. An individual cell is assumed to be surrounded by a finite shell of gas-saturated polymer melt. 158

Figure 5.2. Schematic for the numerical simulation of the cell growth..... 159

Figure 5.3. Comparison of the cell diameter in the cell growth model when a constant viscosity term (●) versus a variable viscosity function (■) is used. 160

Figure 5.4. Comparison of the pressure inside the cell in the cell growth model when a constant viscosity term (●) versus a variable viscosity function (■) is used. 161

1 Introduction

Lightweight structural composites are comprised of a lightweight rigid core that is sandwiched between layers of facing material. The lightweight rigid core can be manufactured from polymeric foams, honeycomb material, or a syntactic foam core[1]. The choice of core material depends upon the application[2]. Polymeric foams are often cost effective and can be made from several different polymers. Honeycomb cores can be made from polymers, aramid or kraft paper, or metal. Most honeycomb materials are expensive and the mechanical properties are non-homogeneous throughout the core due to slight errors that arise in the manufacturing process. Syntactic foam cores are expensive to produce[3]. The benefit of a syntactic foam core is they provide materials that are high strength and have low water absorption[4]. Because of the cost effectiveness of production, polymeric foams will be the scope of the research.

Polymeric foam cores are often produced via processes that are harmful to the environment[5]. The structural polymeric foam is produced with either physical or chemical blowing agents. Chemical blowing agents produce cells in the polymer by decomposing into gases upon being heated. The gas can be either carbon dioxide, ammonia, or other toxic gases. Physical blowing agents are either liquids or gases. Some of the physical blowing agents are not environmentally safe. They are attributed to the production of smog, as well as the depletion of the ozone.

The use of carbon dioxide in processing polymers is an environmentally benign process which has been growing in interest. Supercritical carbon dioxide ($scCO_2$) has several properties that make it attractive for use in industrial applications. Upon using the $scCO_2$ in processes, the CO_2 is easily removed and can be recovered so it does not

contribute to green house gases.[6] This makes it environmentally attractive for several processes. It is also attractive for several industrial processes because it is non-toxic, non-flammable, chemically inert, and inexpensive.[6]

Carbon dioxide is also known to plasticize polymers, thus, significantly lowering the glass transition temperature[7]. The ability to lower the glass transition temperature of polymers aids in being able to melt process polymers at decreased temperatures, as well as being able to foam polymers with control over the cell size. The scope of this research relies on the ability to use supercritical carbon dioxide as a foaming agent for high performance polymers.

Supercritical carbon dioxide was first used in the early 1980's to produce microcellular foams of polystyrene[8]. The technique was developed to produce foam that had a uniform cell diameter smaller than the critical flaw size of the material, therefore, reducing the weight of the material while maintaining or improving upon the mechanical properties. Continued research extended the microcellular foaming technique to other polymers and exhibited improvements on the impact toughness of some polymers[9]. The ability to have control over the cell size, as well as the process being environmentally benign are attractive features for future research in this area.

Little research has been conducted in producing structural polymer foams using the microcellular foaming technique. In the research that has been done on using supercritical carbon dioxide to foam high performance polymers, the technique required long saturation times and minimal density reduction was achieved[10]. The objective of this research project was to use an environmentally process to produce high performance

polymer foam. The production method should be able to control both the size of the cells in the foam, as well as the density reduction.

Nanoparticles, both nanoclays and carbon nanofibers, have been added to polymers to improve mechanical properties[11-13]. In studies that nanoparticles were added to polymer foams, the nanoparticles acted as heterogeneous nucleating agents. This greatly reduced the cell size and increased the cell density in the polymer foam. An increase in the tensile and compression modulus was also observed in nanocomposite foams[12, 14, 15]. Nanoparticles have exhibited the ability to improve mechanical properties, as well as act as nucleating agents when utilized in polymeric foams.

Based on the literature, there is still a lot of information to be understood regarding the production of high performance foams by use of an environmentally friendly process.

The objectives of this research project are:

1. Develop an environmentally benign process to produce a low density foam (>80% density reduction) from poly(arylene ether sulfone).
2. Determine if carbon nanofibers will act as a nucleating agent in the benign foaming process, thus minimizing the cell size while maintaining a large density reduction.
3. Assess the tensile, compression, and impact properties of the resulting high performance polymeric and polymer composite foam.
4. Incorporate a variable viscosity function into the cell growth model equations to better describe the foaming of a polymer with blowing agents which plasticize the polymer

1.1 References

1. Karlsson, K.F. and B.T. Aström, *Manufacturing and Applications of Structural Sandwich Components.* Compos. Part A - Appl. S., 1997. **28**(2): p. 97-111.

2. Marshall, A.C., *Core Composite and Sandwich Structures*, in *International Encyclopedia of Composites*, S.M. Lee, Editor. 1990, VCH Publishers Inc. p. 488-507.

3. Kim, H.S., *Method of Forming Syntactic Foams*. 2006, The University of Newcastle Research Associates Ltd.: International Publication.

4. Gupta, N., *Characterization of Flexural Properties of Syntactic Foam Core Sandwich Composites and Effect of Density Variation.* J. Compos. Mater., 2005. **39**(24): p. 2197-2212.

5. *Polymeric Foams and Foam Technology*. 2nd ed, ed. D. Klempner and V. Sendijarevic. 2004, Cincinnatti: Hanser Gardener Publications. 584.

6. Nalawade, S.P., F. Picchioni, and L.P.B.M. Janssen, *Supercritical Carbon Dioxide as a Green Solvent for Processing Polymer Melts: Processing Aspects and Applications.* Prog. Polym. Sci., 2006. **31**: p. 19-43.

7. Shieh, Y.-T., et al., *Interaction of Supercritical Carbon Dioxide with Polymers. II. Amorphous Polymers.* J. Appl. Polym. Sci., 1996. **59**: p. 707-717.

8. Martini-Vvedensky, J.E., N.P. Suh, and F.A. Waldman, *Microcellular Closed Cell Foams and Their Method of Manufacture*. 1984, Massachusetts Institute of Technology: United States.

9. Collias, D.I. and D.G. Baird, *Impact toughening of polycarbonate by microcellular foaming.* Polym. J., 1994. **35**(18): p. 3978-3983.

10. Sun, H. and J.E. Mark, *Preparation, Characterization, and Mechanical Properties of Some Microcellular Polysulfone Foams.* J. Appl. Polym. Sci., 2002. **86**: p. 1692-1701.

11. Ray, S.S. and M. Okamoto, *Polymer/layered Silicate Nanocomposites: A Review From Preparation to Processing.* Prog. Polym. Sci., 2003. **28**: p. 1539-1641.

12. Shen, J., X. Han, and L.J. Lee, *Nanoscaled Reinforcement of Polystyrene Foams Using Carbon Nanofibers.* J. Cell. Plast., 2006. **42**: p. 105-126.

13. Shen, J., C. Zeng, and L.J. Lee, *Synthesis of Polystyrene-Carbon Nanofibers Nanocomposite Foams.* Polym. J., 2005. **46**: p. 5218-5224.

14. Okamoto, M., et al., *Biaxial Flow-Induced Alignment of Silitcate Layers in Polypropylene/Clay Nanocomposite Foam.* Nano. Lett., 2001. **1**(9): p. 503-505.

15. Han, X., et al., *Extrusion of Polystyrene Nanocomposite Foams with Supercritical CO_2.* Polym. Eng. Sci., 2003. **43**(6): p. 1261-1275.

2 Literature Review

2.1 Role of Carbon Dioxide in Polymer Processing

This section discusses how supercritical carbon dioxide interacts with polymers. It begins by addressing the solubility of supercritical and near supercritical carbon dioxide in polymers. The diffusivity of carbon dioxide in polymers is then addressed. Finally, the role of carbon dioxide as a plasticizer for many polymers is discussed.

2.1.1 Supercritical Carbon Dioxide Properties

Supercritical carbon dioxide ($scCO_2$) has several properties that make it attractive for use in industrial applications. Upon using the $scCO_2$ in processes, the CO_2 is easily removed and can be recovered so it does not contribute to greenhouse gases[1]. This makes it environmentally attractive for several processes. It is also attractive for several industrial processes because it is non-toxic, non-flammable, chemically inert, and inexpensive[1].

Supercritical fluids are obtained when the substance is subjected to pressures and temperatures above the critical pressure and temperature for that substance. Figure 2.1 illustrates the supercritical region of carbon dioxide using a pressure/temperature diagram. Super critical carbon dioxide can easily be obtained because the critical temperature and pressure are 304 ^{o}C and 7.1 MPa, respectively[2].

The properties of carbon dioxide can be tuned by controlling the proximity of the operating conditions to the critical pressure and temperature. Because supercritical fluids are compressible, the density can be varied with slight changes in pressure[3]. Varying the density affects the solvent properties of $scCO_2$. Though the low solubility parameter

suggests CO_2 behaves as a nonpolar hydrocarbon solvent such as hexane, Berens et al.[4] observed behavior similar to a slightly polar organic solvent for polymers. The solubility is also affected by the proximity to the critical point[5]. The solubility of $scCO_2$ in polymers is discussed further in the following section.

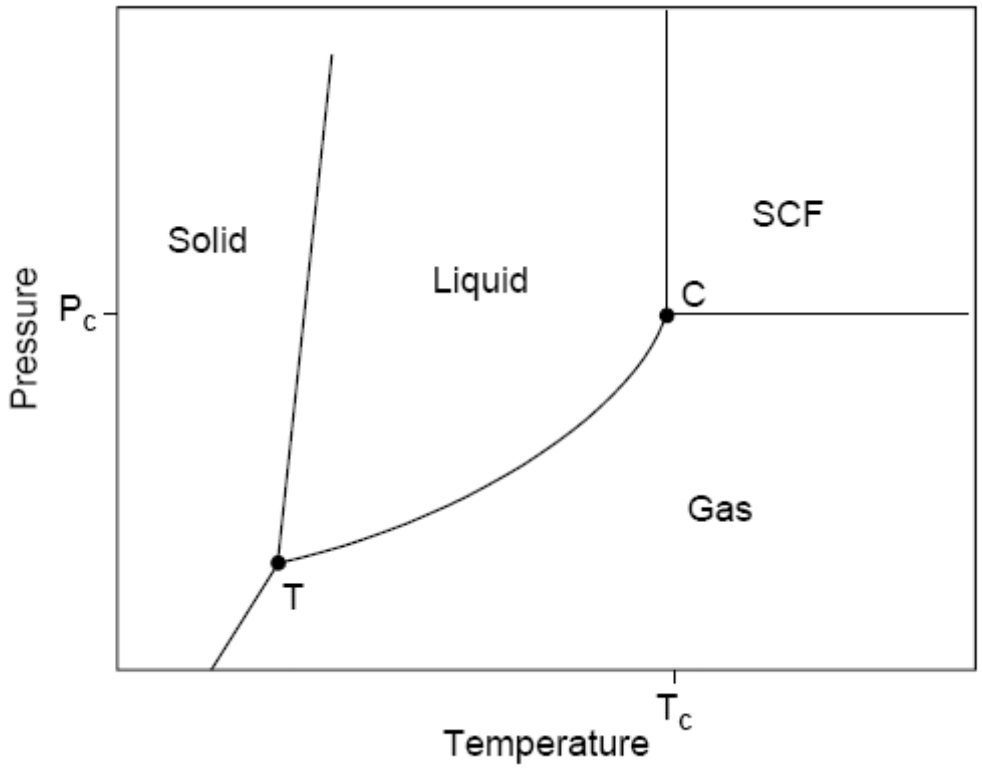

Figure 2.1 Phase diagram of carbon dioxide[1]. Reprinted from *Progress in Polymer Science*, 31, 19-43, Copyright (2006), with permission from Elsevier.

2.1.2 Solubility in Polymers

The solubility of $scCO_2$ varies between polymers. The solubility differences between the polymers is determined by the chain group substituents[1]. The chain flexibility as well as the presence of accessible carbonyl, ether, or nitrile groups in the polymer increases the solubility of $scCO_2$ in the polymer[4-6]. The solubility of $scCO_2$ in

polymers has also been shown to increase with the number of polar groups in a polymer[7]. Research has shown that near critical CO_2 resembles a highly volatile, polar solvent when interacting with polymers[4]. The solubility of $scCO_2$ in polymers is also affected by the morphology of the polymer[7, 8]. Because $scCO_2$ is absorbed into the amorphous regions of the polymers, a greater amount of crystallinity decreases the solubility of $scCO_2$ in a polymer[9]. Density of the polymer has been observed to have an effect on the solubility in polymers. In a study of chemically similar polymers, as the density of the polymer increased the solubility of $scCO_2$ decreased[6].

Several different techniques have been employed to determine the solubility of $scCO_2$ in polymers. Phase separation, pressure decay, gravimetric analysis, frequency modulation, and chromatographic methods have all been used to determine solubility. These methods all have distinct advantages and disadvantages.

The phase separation technique has been used to study the solubility of CO_2 in low viscosity polymers[1, 10]. In this technique, CO_2 is allowed to saturate and diffuse into molten polymer. Once the system has reached equilibrium, the polymer rich phase and CO_2 rich phase are separated. The solubility of CO_2 in the polymer is determined by the amount of CO_2 in the polymer rich phase.

Though pressure decay methods use relatively inexpensive equipment, they require large samples of polymer in order to determine the solubility[1, 5, 11]. A large sample of polymer is placed in an apparatus with a well known volume. The apparatus is then pressurized with CO_2, and the pressure is recorded. The polymer sample is then allowed to equilibrate with the CO_2. Because the polymer sample is large, the time required to reach equilibrium is long. Upon reaching equilibrium, the reduction in

pressure, along with the temperature and volume of the apparatus, is used to calculate the solubility of CO_2 in the polymer. This technique is also limited because the swelling of the polymer must also be taken into account (either measured or estimated from theoretical calculations) when determining the solubility.

The gravimetric method uses the kinetics of desorption to calculate the solubility of CO_2 in the polymer[1, 5]. A small sample of polymer is saturated with CO_2. The fully saturated sample is then placed on a microbalance and the amount of CO_2 that diffuses out of the polymer is calculated which is used to determine the solubility of CO_2 in the polymer. The advantages of this technique are that only a small sample is required, small changes in CO_2 are easily detected with the microbalance, and the measurement only requires a short time period. However, this technique requires the swelling of the polymer to be determined so the buoyancy can be accounted for in the calculations. This technique is also limited to polymers that are not rubbery or highly plasticized by CO_2. In situ gravimetric methods have also been used[5].

The chromatographic method is limited in that it can only determine relative solubilities[5]. In the chromatographic method, a thin film is used as a stationary phase and the CO_2 is used as a mobile phase[1]. As the CO_2 is phased through the polymer, the retention time is determined. The retention time is then used to determine the solubility of CO_2 in the polymer. The advantage of the chromatographic method is that equilibrium is quickly achieved due to the use of a thin film.

An accurate and quick method that has been used to determine the solubility of CO_2 in polymers is the frequency modulation method using a quartz crystal microbalance[5, 6]. A thin film is adhered to a thin quartz crystal and is then sandwiched

between two metal electrodes that create an alternating electric field across the crystal. The crystal vibrates due to the piezoelectric effect. The system is then subjected to CO_2. As the CO_2 absorbs into the polymer, the vibrating frequency of the crystal decreases. The decrease is linearly proportional to the mass of the CO_2 that absorbed into the polymer. The change in mass can then be calculated and used to determine the solubility. The difficulty in this method is getting the polymer to adhere to the quartz crystal.

By using the techniques described above, the solubility of CO_2 in several polymers has been determined. Tomasko et al.[5] published a summary of the methods used and the solubility of CO_2 in several polymers.

2.1.3 Diffusivity in Polymers

The diffusivity of CO_2 in polymers can be determined from some of the solubility experiments. Berens et al.[4] determined the diffusivity of several glassy polymers by using a gravimetric absorption and desorption experiment. In the experiments, it was found that the diffusivity approaches the range of 10^{-6} to 10^{-7} cm^2/sec, which is typical for rubbery materials. For molten polymers, it has been determined that the diffusivity is dependent upon the free volume. A summary of diffusion coefficients for molten polymers can be found in literature[5]. The diffusivity was also found to have a strong dependence on the concentration of CO_2[4, 12]. An increase in solubility, increased the diffusivity. Morphology effects the diffusivity in polymers. Crystalline materials provide a hindered path, thus decreasing the diffusivity[9].

2.1.4 Plasticization of Polymers

The absorption of CO_2 into a polymer matrix has been shown to reduce the glass transition temperature (T_g) of polymers. The gas absorption increases the free volume and chain mobility of the polymers leading to a decrease in the T_g[13]. The decrease in the plasticization of the polymer allows for controlled cell growth in microcellular foaming and the ability to process polymers at lower temperatures than unsaturated polymers[14-18]. The plasticization effect has shown promise in facilitating the processing of polymers that thermally degrade or high molecular weight polymers that are too viscous to be normally melt processed[17].

A few techniques have been used to determine the plasticized T_g of polymers that have been saturated with CO_2. Differential scanning calorimetry (DSC) has been widely used to determine the plasticized T_g[19-21]. Inaccuracies in the results arise due to desorption of CO_2 while the sample is tested. High pressure pans (up to 1000 psi) can be used to reduce desorption of gas during the testing. In situ creep compliance has also been used to determine the T_g of CO_2 saturated polymers[22-24]. The creep compliance as a function of pressure for several temperatures inside of a pressure vessel pressurized with CO_2 was determined. From this data, the reduced T_g was determined. Because the measurements are determined under pressure, desorption effects are eliminated with the in situ creep compliance technique. Inverse gas chromatography has been utilized to determine the plasticized T_g[13, 25]. Carbon dioxide is run through a column containing the polymer of interest. The retention time is then tracked as a function of temperature. As the temperature is increased through the T_g of the polymer, the retention mechanism changes. This data can then be used to determine the plasticized T_g. Regardless of the

technique used to determine the plasticized T_g, the reported values of T_g depression of the same polymer can differ depending on the experimental protocols in the testing procedures[5].

A summary of the T_g depression from the plasticization of CO_2 on various polymers can found in literature[5]. The amount of T_g depression depends upon the solubility of CO_2 in the polymer. The greater the solubility, the more the T_g is depressed. Thus, polymers which contain carbonyl or ether groups exhibit a greater T_g depression[7, 8, 26, 27]. Solubility can also be controlled by increasing the saturation pressure of CO_2. Though increasing the saturation pressure of CO_2 can increase the solubility of CO_2 in the polymer, the plasticization effect can be limited[22, 23, 27]. Initially, the T_g is greatly reduced by increasing the saturation pressure, but at moderate pressure (~2900 psi), it fails to be further reduced. It has been suggested that this is due to the hydrostatic pressure opposing the free volume increase provided by the absorption of CO_2.

Retrograde vitrification has also been observed with various polymers that were saturated with CO_2[22]. Retrograde vitrification occurs when the polymer transitions from a glass to a liquid with a decrease in temperature. This was observed when the solubility of the CO_2 in a polymer increases at lower temperatures. The greater amount of CO_2 absorbed into the polymer led to the polymer being plasticized, thus exhibiting rubbery behavior.

2.2 Structural Polymers and Composites

In this section the types of low density materials that are used as the core in structural sandwiches and the method of manufacturing the core materials are reviewed. There are three main groups of materials (polymeric foams, honeycomb, and syntactic

foams) that are used as the low density core in structural sandwich applications. High performance polymeric foams produced by conventional techniques of using physical and chemical blowing agents are discussed first. The manufacturing techniques and properties of honeycomb cores are then reviewed. The section concludes with a review of syntactic foam cores.

2.2.1 Structural Sandwich

Structural sandwiches, comprised of a facing material to carry the bending loads and a core to carry the shear loads, are currently used in structural applications where a low density material (less than 300 kg/m^3) is desired[28]. The core material can be either polymeric foam, honeycomb structured material, or syntactic foam[29]. The material chosen for the core depends upon the application, as the price and strength vary amongst the different types of cores. The manufacturing schemes, as well as the advantages and disadvantages of the core materials are discussed in the following subsections.

In a structural sandwich composite, the thickness of the core greatly affects the relative bending stiffness and strength[30]. As the core thickness is doubled, the relative stiffness increases by seven times and the relative strength is increased by 3.5 times. When the core is quadrupled, the relative stiffness increases by 37 times and the relative strength is increased to 9.2 times. Regardless of the material used for the core, the relative strength and stiffness increase greatly with an increase in core thickness.

2.2.1.1 Polymer Core Materials

Polymeric foams provide advantages in high performance applications[31]. Many types of polymeric foam are relatively inexpensive compared to other materials used in high performance applications. This is due to the wide variety of techniques and ease of

which polymeric foam materials can be produce and formed into usable parts. Closed cell polymeric foams also have little water absorption so material degradation due to water is of little concern. These desirable properties make polymeric foams good candidates as core materials in structural sandwich composites. The most common foams used as the core material for structural sandwiches are reviewed in further detail.

2.2.1.1.1 Polyetherimide foam

Physical blowing agents (PBA) have been utilized to produce low density (~95% density reduction) foams of various polymers. PBAs are either a liquid or gas, at standard temperature and pressure, which can undergo a reversible change of state[32]. The change of state in the PBA causes cell nucleation and growth in the polymer matrix.

In a patent issued to Krutchen et al.[33], low density foams of polyetherimide (PEI), polycarbonate (PC), and a blend of poly(phenylene oxide) (PPO) and polystyrene (PS) have been created by utilizing a PBA. The PPO and PS blends were created by combining 20 to 80 weight percent of either polymer. In this process methylene chloride, chloroform, 1,1,2-trichloroethane, and various combinations of the three were used as the PBA. The resulting foams typically had a density less than 20 lbs/ft^3, with the lowest density obtained being 2.5 lbs/ft^3 (40 kg/m^3).

The manufacturing process of the polymer foam was done in a two-step semi-continuous process[33]. The first step in the process was to saturate anhydrous polymer pellets with the methylene chloride, chloroform, 1,1,2-trichloroethane, and various combinations of the three. The pellets need to be anhydrous to prevent the formation of acid from water and the PBAs. The polymer pellets were subjected to the PBA vapor at high concentrations for up to 48 hours, which allowed for the PBA vapor to diffuse into

the polymer matrix. After 48 hours, the concentration of the PBA in the polymer matrix reached levels as high as 30%. The saturation of the polymer pellets with the PBA allowed for the pellets to be processed at a lower temperature in the second stage of manufacturing. For the second stage, the saturated pellets were extruded using a single screw extruder. During the pressure drop of the extrusion process, the PBA caused cells to nucleate and grow within the polymer matrix. The cell growth continued until the polymer was cooled to a temperature below the glass transition temperature, T_g, of the polymer. In order to produce a large pressure drop in the extrusion process, a small capillary die with a diameter of 0.080" (2.0 mm) or a circular slit die which will yield a foamed sheet of 0.090" (2.2 mm) thickness had to be used. By using this two-step process to create the polymer foams, densities of less than 20 lbs/ft^3 (312 kg/m^3) were regularly obtained.

Supercritical carbon dioxide ($scCO_2$) has also been used as a blowing agent to foam PEI. This was accomplished by Sun et al.[34] using the two-step batch processing technique. In this study, a sheet of PEI with a thickness of 1.6 mm had to be saturated with $scCO_2$ for 120 hours to reach equilibrium. Further details in the two-step batch processing technique can be found in section 2.4.1.1. Because $scCO_2$ took a long time to diffuse into the PEI, it was stated that the development of a new technique was needed to make microcellular foaming of PEI more feasible. Few foam properties were reported on the PEI foam. Good cell size and density were reported for the foam, with values of approximately 1 μm and 10^{10} to 10^{14} cells/cm^3, respectively. However, no data was reported on the bulk density of the PEI foam. Poly(ether imide) foam was successfully

produced using a two-step batch process technique with $scCO_2$ as the blowing agent, though the time scale was so long that it may not be feasible in an industrial setting.

A polymeric foam from a blend of PEI and poly(aryl ether ketone) (PAEK) was prepared by Brandom et al.[35] The foam was formed by using water as a blowing agent that was produced in situ via the reaction between diamine end groups that were present in the PEI with the ketone functional group from the PAEK. This foam production method exhibited the potential for producing foams with approximately a 60% density reduction.

The PEI/PAEK foam was produced in situ by mixing PEI and PAEK at high temperatures. Pellets of PEI and PAEK were melt blended in a single screw extruder. As the PEI and PAEK melt was mixed together, the diamine end groups on the PEI reacted with the ketone groups in the PAEK. This reaction produced water as a byproduct. At the high temperatures required for extruding the blend ($350^{o}C$) the water that was produced was a gas. The gaseous water acted as a blowing agent and produced a foam structure. At normal resonance times in the extruder, a foam with a density reduction of approximately 8% was obtained. When the PEI/PAEK blend was allowed to sit in the extruder for 5 minutes, foam with a density reduction of up to 60% was obtained. This foaming procedure has potential as a green process to produce moderate density reduction foams of high performance polymers, but more work would need to be conducted to optimize processing conditions.

2.2.1.1.2 Poly(methacrylimide) Rigid Foam

Closed-cell poly(methacrylimide) (PMI) rigid foam is a widely used foam core in the aerospace industry due to its high performance[30, 36]. PMI rigid foam has higher

strength and modulus of elasticity than any other polymer foam when compared based on density[36]. The density of PMI can be as low as 71 kg/m^3. Additional advantages of PMI rigid foam core is the material has a good resistance to many solvents, as well as the ability to be used at elevated temperatures (up to 177^{o}C)[30].

The production of PMI foam occurs during the cyclization of the imide structure. The process begins by mixing methacrylic acid and methacrylonitrile monomers for the polymerization[37]. Initiators and chemical blowing agents are added to the monomer mixture before the polymerization occurs. After combining everything, the mixture is placed in a glass vessel so the polymer is shaped into a block after the polymerization. The polymerization occurs by placing the glass vessel into a water bath, which maintains the optimum temperature for the polymerization process. Once the polymerization has occurred, the block is placed in an oven for postpolymerization. The foam is then generated by an additional heating between 180-250^{o}C for 3 to 5 hours.

2.2.1.1.3 Polyimide foam

Polyimide foam is generally used as a composite core in high temperature applications. Polyimide foam is unique because it can withstand temperatures over 800 °C for an extended period of time without burning and or exhibiting a loss of structural integrity[30, 38]. Polyimide foam has other applications in the aerospace industry. The aerospace industry uses polyimide foam in applications where good temperature stability over broad ranges is necessary because polyimide foam maintains good properties between -250 °C to 250 °C[38]. Polyimide foams have been produced with densities ranging between 1 and 800 kg/m^3. Foams with a wide variety of densities can be manufactured from polyimide materials with good temperature stability.

The production of polyimide foams is carried out during the polymerization and curing of the polymer. Several techniques have been employed to produce polyimide foams. In some techniques, foaming agents such as water, alcohols, acetone, ethyl glycol butyl ether, halogen substituted organic compounds, and ethers are used[38-40]. Other techniques rely on the production of water and alcohol during the polymerization process to act as the foaming agent[41]. However, the properties of polyimide foams made by producing the foaming agents *in situ* suffer at low densities[39].

2.2.1.2 Honeycomb Core

Honeycomb materials have unique properties and are widely used in high performance applications, such as the aerospace industry. The high strength combined with the low density of the honeycomb core is structurally efficient. There are two density ranges for honeycomb cores[28]. Low density cores are defined as having a density less than 16 kg/m^3. The high density cores are defined as having a density greater than 16 kg/m^3. Honeycomb cores have other advantageous properties besides structural performance. Because the honeycomb core consists of a lot of air due to the open voids (3-10 mm), the materials also exhibit good insulation properties. The structural efficiency and insulation properties of honeycomb materials have given rise to many high performance applications, especially in the aerospace industry.

Different materials and variations in the shapes of the holes lead to many different types of honeycomb materials which can be used for the core in a structural sandwich. The hole shape can be varied intentionally or the variations can arise from defects in the manufacturing process[30]. Slight variations in the shape lead to large changes in the properties of the material. Several different raw materials exist from which honeycomb

cores can be manufactured. These materials are diverse and result in different core properties. Common materials used to manufacture honeycomb cores are glass fiber/plastic, Kraft paper, aramid paper, carbon fiber/Kevlar, and stainless steel/titanium.

There are many different ways in which honeycomb cores can be manufactured. One of the first techniques patented involved stacking up corrugated materials and adhering the materials together to form the honeycomb structure[42-44]. In this process the materials must first be formed into a corrugated structure. The corrugated sheets are then covered with an adhesive and stacked such that the peak of one sheet touches the bottom of the valley of the adhering sheet. The stacked materials are then heated to cure the adhesive. Another technique used to manufacture honeycomb materials is to adhere a plurality of stacked sheets of material together[45, 46]. Equally spaced beads of adhesive are applied to sheets of material. These materials are stacked on top of each other, offsetting the beads of adhesive from the previous layer. A normal force can then be applied to the stacked sheets of material and a honeycomb structure will result. A third technique used to manufacture honeycomb cores is via an extrusion process[47, 48]. In the extrusion process, a die is designed such that the resulting extruded material will be a honeycomb structure. This requires the material to be soft enough to extrude but have the ability to harden once the material exits the die. All of these techniques can be used to produce honeycomb cores from various materials.

The techniques used to produce honeycomb cores have limitations which reduce the number of usable applications. Production cost is one limitation in the manufacturing process of honeycomb cores. The process of stacking and bonding corrugated sheets of material to produce honeycomb structures or the process of bonding a plurality of sheets

together is not time efficient. In some cases, the stacking is done by hand. Both the large amount of time and the manpower required to produce these materials lead to large production costs. Because the cost associated with producing the parts is large, most of the honeycomb materials produced are only used in the aerospace industry. The limit in part size is also a problem with the production methods. In the stacking processes, an oven is often required to cure the adhesive. The part size is then limited by the size of the oven. In the extrusion process the part can only be as big as the die that is used. Production costs, time, and part size all limit the applications where honeycomb materials are used.

Honeycomb materials are also sensitive to changes in production as well as use conditions. In a honeycomb core material, changing the geometry of the hole will affect the mechanical properties. Variation in the production can lead to slight changes in the cell structure of the honeycomb materials. A hexagonal structure will result in the best strength and stiffness for a honeycomb core[49]. In-service durability is also a major concern when using honeycomb materials. Several problems arise with in-service durability due to the presence of water, especially in liquid form[28]. Water can cause corrosion, debonding of the facing and the honeycomb due to cyclic freezing and thawing, and debonding or rupturing of cells due to steam pressure if heated over 100 ^{o}C. Though honeycomb materials are structurally efficient, the materials have been under scrutiny due to the sensitivity during production as well as the in-service durability.

2.2.1.3 Syntactic Foam Core

Syntactic foams are another material used as a core in structural sandwich composites. A unique property of syntactic foams is that unlike most foams, the density

before the cure is the same as the density after the material is cured[50]. Syntactic foams are becoming more widely recognized as a viable core material because they combine high strength, light weight, and low water absorption[51]. Because of the high manufacturing cost, syntactic foams are mainly used in high performance applications where cost is not a major factor[52]. Many of these high performance applications are in marine equipment, anti-submarine warfare, and packing materials for the aerospace and automotive industry.

Syntactic foams are manufactured by the combination of a low density material with a binding resin. The low density material can be microballoons, ceramic spheres, or other lightweight aggregate materials[50, 53, 54]. The microballoons can be manufactured from polymers, metals, glass, or ceramic materials[51]. The binding resin is used to provide the structural integrity of the foam core. Epoxies are often used as a binding material for syntactic foams because they provide good adhesion to the low density material and yield foam with good mechanical properties.

A few steps are needed to manufacture syntactic foams[52]. The first step involves combining the low density material with the binding resin. In the case where an epoxy is used for the binding resin, the curing agent and the epoxy are mixed together before the low density material is introduced into the system. The low density material and binding resin are then mixed to achieve a good dispersion. Care must be taken in the mixing process so that the low density material is not damaged. Once the low density material and the binding resin are combined the mixture is poured into a mold. The material is then cured to harden the binding resin. In some cases, a solvent can be added to the mixture. This reduces the viscosity, helping to facilitate in the mixing process.

The properties of syntactic foams can be controlled with great precision. Densities ranging between 90 and 1500 kg/m^3 have been reported[50, 55]. The density can be precisely varied in two different ways. One method to control the density is to vary the amount of low density material that is added to the binding material. A second method to control the density is to use the same type and volume of the low density material, which has a slightly different density. When using microballoons, this could be accomplished by varying the wall thickness. Retaining the original volume ratio of low density material to binding material makes the second method preferred because the physical properties of the foam will remain consistent[51]. The cell size can also be controlled with great precision. The cell size and distribution of sizes depends upon the material chosen for the low density material. Typical cell sizes are between 60 and 80 μm. One benefit of syntactic foam cores is the foam properties are precisely controlled because they depend upon the materials used, not the process for producing the foam.

2.3 Benefits of Microcellular Foams

This section begins with a highlight of the history of microcellular foams. A comparative study is then presented on the effect of microcellular foaming on the tensile strength of the material. The section concludes with a review on the effect the microcellular structure has on the impact properties of the material.

Microcellular foams were first developed to reduce the amount of material used in various commercial processes[56]. Microcellular foams are defined as having a cell size in the range of 1-10 μm. It was thought that by creating foamed samples with uniform cell sizes smaller than the critical flaw size of the polymer, the weight of the material would be reduced without decreasing the mechanical properties. Few mechanical

properties are reported, though in the few papers where mechanical properties are reported some improvements have been observed.

Studies have been conducted to characterize the effect of microcellular foaming on the tensile properties of the polymer. Kumar et al.[57] report an approximate decrease of 30% in the tensile modulus. Though the tensile modulus decreases, the tensile toughness has a tendency to increase compared to neat polymer[58]. An increase in tensile toughness is attributed to a greater elongation in the foamed samples. The tensile toughness decreases over time because trapped gas contributes to the toughness. As the gas diffuses out of the cells, the tensile toughness of the polymer decreases. Once all of the gas has diffused out of the cells, the tensile toughness is still 30% higher than the neat polymer. This increase in tensile toughness could be attributed to a decrease in necking during tensile testing[57]. Despite a decrease in the tensile modulus of microcellular foams, the tensile toughness still increases compared to neat polymer.

The effect of microcellular foaming on the impact strength varies depending upon the polymer being tested. Microcellular foaming did not improve the impact strength of polystyrene, styrene-acrylonitrile copolymer, or pure high density polyethylene[59, 60]. Though an increase was not seen in these polymers, microcellular foaming has been shown to greatly increase the impact strength in polycarbonate and high density polyethylene/polypropylene blends[60, 61]. In a study by Collias et al.[61], microcellular foaming increased the impact strength by 17 times compared to neat polycarbonate. For the study, microcellular foam with a cell size of 40 μm was subjected to a notched izod impact test. The impact failure changed from brittle fracture in neat polycarbonate to

ductile fracture in microcellular polycarbonate foam. The change from brittle to ductile fracture accounts for the large increase in impact strength.

2.4 Processing of Microcellular Foams

This section highlights studies that have been conducted involving the manufacturing processes of microcellular foams. Batch processes are discussed first, including both a one step process and a two step process. The section continues with discussions concerning continuous processes. These include single and twin screw extrusion, as well as injection molding. The section concludes with a semi-continuous process used to produce microcellular foams.

The generation of microcellular thermoplastic foams has been a topic of recent interest. In many of the microcellular foaming experiments, a batch process was employed to determine what parameters affected the foam properties. This batch process was either done in a one- or two-step technique. The knowledge obtained from these experiments was then utilized to investigate continuous and semi-continuous processes for use in industrial applications.

Microcellular foams have been produced via the introduction of a thermodynamic instability of a supersaturated gas into a polymer matrix[62]. The thermodynamic instability was introduced into the polymer matrix by diffusing a gas into the polymer under high pressure. Air, carbon dioxide (CO_2), nitrogen, and noble gases such as argon have all been used to produce microcellular foams[56], though carbon dioxide is the most widely used due to its ability to plasticize many polymers[63]. The plasticization effect allows for microcellular foams to be produced at processing temperatures at or below the glass transition, T_g, of the unplasticized polymer. The use of gases that do not plasticize

the polymer requires a processing temperature higher than the T_g of the polymer[16]. Because CO_2 is the most widely used gas in microcellular foaming, it will be the gas referred to in the microcellular sections. Once the gas saturation has reached equilibrium, the polymer is supersaturated with gas because the system is under high pressure. The polymer is then heated to around the glass transition temperature, T_g, and the CO_2 is rapidly released from the system causing a thermodynamic instability. The thermodynamic instability causes cells to nucleate and grow until the system becomes stable, leading to the production of foam.

2.4.1 Batch Processing

2.4.1.1 Two-Step Batch Processing

The two-step batch processing technique was the first technique developed in the early 1980's[16]. Since this time, several other people have used this technique to study the production of microcellular foams[9, 16, 34, 64-69]. Even though the two-step batch process requires a lot of time to produce microcellular foams and may not be feasible for industrial use, it has been used to determine what parameters affect the microcellular foaming of various polymers.

The first step in the two-step batch processing method involves the diffusion of CO_2 into the polymer matrix under high pressure. The polymer and CO_2 are combined in a pressure vessel and allowed to saturate over time. The amount of time required to saturate the sample depends upon the diffusion rate and the solubility of the foaming agent in the polymer as well as the sample thickness and can be between 2 hours[65] and 14 days[34]. After the solubility of CO_2 has reached equilibrium, the system is

depressurized at room temperature and the super-saturated polymer samples are removed from the pressure vessel.

The second step in the two-step batch process causes the nucleation and growth of the foam cells. After the polymer has been removed from the saturation vessel, it is placed in a hot bath. The temperature of the bath is dependent on the the T_g or melting temperature (T_m) of the polymer. For amorphous polymers, the temperature is normally slightly higher than the T_g of the polymer[9, 16, 34, 64-69]. When the polymer is heated, the dissolved CO_2 is released from the polymer matrix. The release of the CO_2 from the supersaturated polymer causes cells to nucleate and grow. The cell nucleation is controlled by the thermodynamics of the system. The cell growth is controlled by quenching the system. This is achieved by placing the sample in an ice bath or an ethanol/water mixture at room temperature, causing the temperature of the polymer to be lower than the T_g, which induces vitrification. The two-step process allows for more precise control of the cell size.

The two-step batch process can be used to obtain foamed samples with high cell densities, low cell sizes, and moderate bulk densities with great control. In studies conducted using the two-step batch process the bulk density reductions have been as high as 74%[34]. Polymeric foams exhibiting small cell sizes with a narrow range of cell size distributions are characteristic of the two-step process. Supercritical carbon dioxide has been used in a number of studies as the foaming agent to obtain foamed samples with cell sizes between 1 μm to 7 μm[34, 65]. Slightly larger cell sizes (~25 μm) have been achieved with the two-step process using nitrogen as the foaming agent[16]. Large cell densities have been obtained with the two-step batch process. In reported studies cell

densities in the range of 10^{10} to 10^{12} cells/cm^3 have been achieved using the two-step batch process[34, 65]. The two-step batch process can be used to obtain moderate bulk-density microcellular foams, with small cell size and large cell density with highly controlled structure (i.e. cell size and distribution).

2.4.1.2 One-step Batch Process

In the one-step batch process, the saturation as well as the cell nucleation is all conducted in the saturation vessel. Because the heat transfer occurs over the saturation time and the pressure drop is regulated by the release of the CO_2 from the pressure vessel, foam samples with a wide range of thickness can be produced. This process also eliminates the need for an additional hot bath in order to foam the polymer, and has been utilized throughout literature[14, 15, 63, 70-74]. Because a hot bath is not needed this process can be used at higher temperatures.

The one-step batch process is modeled after the two-step batch process. In the one-step batch process, the polymer and CO_2 are combined in a saturation vessel and allowed to saturate at high pressures and/or temperatures. Once the CO_2 diffusion reaches equilibrium, the temperature of the system is equilibrated near the T_g of the polymer. The CO_2 is rapidly released, which causes cell nucleation. The cell growth is inhibited by vitrification of the polymer[18, 63].

The one-step batch process can be used to produce low density microcellular foams, though the control of the foam properties is not as good as with the two-step process. Several experiments have been conducted on the foaming of polystyrene. Poly(methyl methacrylate) and styrene-co-acrylonitrile have also been foamed using the one-step batch processing technique. In these experiments the bulk density, cell

diameter, and cell density exhibit broad ranges depending upon the processing parameters. The bulk density of microcellular polystyrene ranged from 0.05 to 0.85 g/cm^3, which correlates to a density reduction up to 98%[15]. A range of cell sizes between 0.5 μm[18] to 75 μm[14] was achieved, with most of the foaming experiments yielding foams with cell sizes between 5 μm to 30 μm. This range is broader than in the two-step process because the foam samples cannot be controlled by quenching, as is done in the one-step process. The cell densities obtained in the one-step batch processing experiments had a broad range between 10^7 cells/cm^3 to 10^{12} cells/cm^3[18]. The average cell density for all of the experiments was 10^9 cells/cm^3. Lower density foams can be achieved using the one-step batch processing method, though the two-step process allows for a more precise control of the foam properties.

2.4.2 Continuous and Semi-Continuous Processes

2.4.2.1 Continuous Extrusion Process

The continuous extrusion process has been done using a single screw extruder[75-84], twin screw extruder[85], and a tandem of single screw extruders[86, 87]. The continuous extrusion process is similar for all three types of extruder configurations.

In all three processes a microcellular foam structure is achieved by a rapid depressurization when the polymer melt exits the die[81]. In order to achieve a large depressurization rate, a pressurized extruder is required. If a pressurized extruder were not used, premature nucleation would occur, which would result in a large cell structure foam.

A diagram of the continuous extrusion process for a single screw extruder can be seen in Figure 2.2. In this process, the polymer pellets are melted as they are conveyed

into the mixing zone. When the molten polymer reaches the mixing zone of the single screw extruder, a pump is used to inject the CO_2 into the system. Homogeneous mixing of the CO_2 and polymer are necessary in order to produce a microcellular foam structure. While some of the CO_2 is diffused into the polymer matrix, a lot of the CO_2 is introduced into the polymer through shear mixing[75]. To improve the distribution of the CO_2 in the polymer mixture, static mixers have been employed. The nucleation and growth of the cells occurs once the material exits the die. The number of cells which nucleate depend upon the depressurization rate. The cell growth is inhibited or terminated when vitrification occurs.

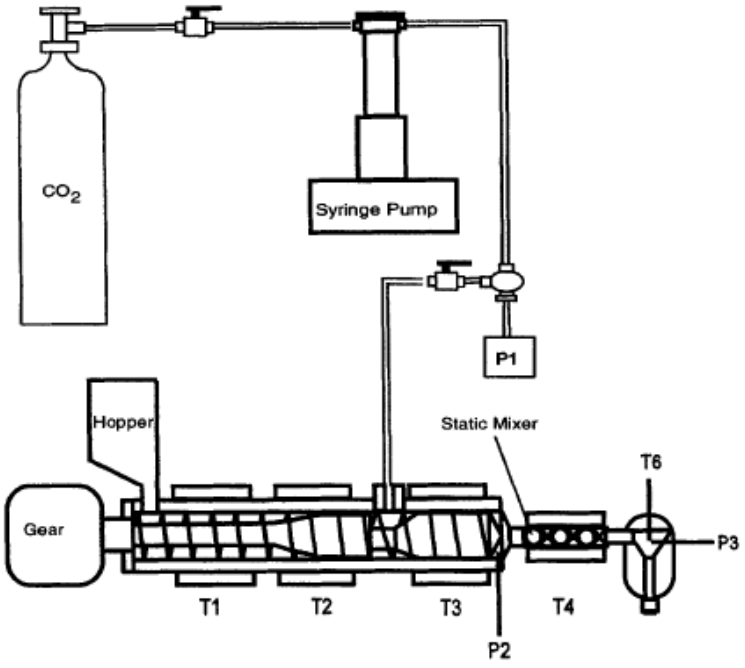

Figure 2.2 Schematic drawing of continuous extrusion process [81]. Reprinted with permission from John Wiley & Sons, Inc. Copyright (2002).

The continuous twin screw extrusion process is utilized to achieve higher mixing and diffusion of the CO_2/polymer system. Instead of using a static mixer at the end of the extruder, kneading elements are used downstream of the gas injection port[85]. The

kneading elements cause a greater shear force in the polymer, thus breaking up the large pockets of CO_2 and forcing the CO_2 to mix into the polymer. To minimize the pressure fluctuations in the CO_2 injection process, conveying elements should be used at the gas injection port instead of kneading elements.

The use of tandem single screw extruders in the continuous extrusion process was designed to improve the mixing of the CO_2/polymer system. In the tandem single screw extruder process, the first extruder is used to melt and initially mix the CO_2/polymer system. The second extruder is used to homogenize the CO_2/polymer system further. Static mixers are used at the end of the extrusion process to ensure a homogeneous mixture of the CO_2/polymer system.

The key step in the all three continuous extrusion processes is the diffusion and mixing the CO_2 into the polymer. In order to obtain a uniform microcellular foam structure, the CO_2/polymer system must be well homogenized. If there are any pockets of CO_2 before the rapid pressure drop, large voids are created. The single screw extrusion processes take advantage of static mixers, while the twin screw extrusion process uses kneading elements to mechanically mix the CO_2 into the polymer. The tandem single screw extrusion process also uses a longer residence time to allow for greater diffusion.

With the use of the continuous extrusion process, microcellular foams were successfully produced, though only foamed filaments have been reported. Orifice dies had to be used in order to get the proper pressure drop necessary to produce uniform microcellular foams. With the use of filament dies, the resulting foams had cell sizes and densities between 5-23 μm and 10^7-10^{10} cells/cm^3 respectively[75, 77-79, 81, 82]. The

use of a filament-die also allowed for a volume expansion ratio up to 23, which is much higher than has been achieved using batch processing[79]. Though microcellular foams with a large volume expansion ratio can be produced via a continuous extrusion process, the resulting parts may not be feasible for industrial use because the process only produces filaments with good foam properties. Also the size of the orifice must be quite small to produce a large pressure drop, so the final part thickness may be small.

2.4.2.2 Continuous Injection Molding Process

Several studies have been conducted to develop a continuous injection molding process to produce microcellular foams[88-91]. From these studies, three processes (Mucell™, IKV, University of Warwick) were able to successfully produce microcellular foams[89]. All of these processes are similar but vary in the gas delivery mechanism. The continuous injection molding process to produce microcellular foams involves the injection of the gas into the injection molding system, diffusion and mixing of the gas into the polymer, and injection of the polymer/gas mixture into the mold[90].

The only variance between the three methods is how the gas is injected into the system. The Mucell™ process uses a direct injection of the gas into the barrel of the injection molder. The gas is then mixed into the system from the shear of the rotating screw. In this process the gas also diffuses into the polymer as it is transmitted through the screw. This process requires equipment and licensing to be purchased. The IKV process has a different approach to introducing the gas into the system. In the IKV process an injection nozzle is incorporated into the system between the plasticizing unit and the shut-off nozzle of an injection molder. A picture of the nozzle can be seen in Figure 2.3. A static mixer is employed to help mix the gas into the polymer system. The

University of Warwick process was designed to minimize the amount of equipment necessary to produce microcellular foams via injection molding. This process incorporates the gas into the system by using a bolt-on gas injection port at the back of the nozzle. A schematic of the nozzle and injection port can be seen in Figure 2.4. In the University of Warwick process, the gas is mixed into the polymer via static mixers. If the there is a long residence time, the gas is also able to diffuse into the polymer. In the

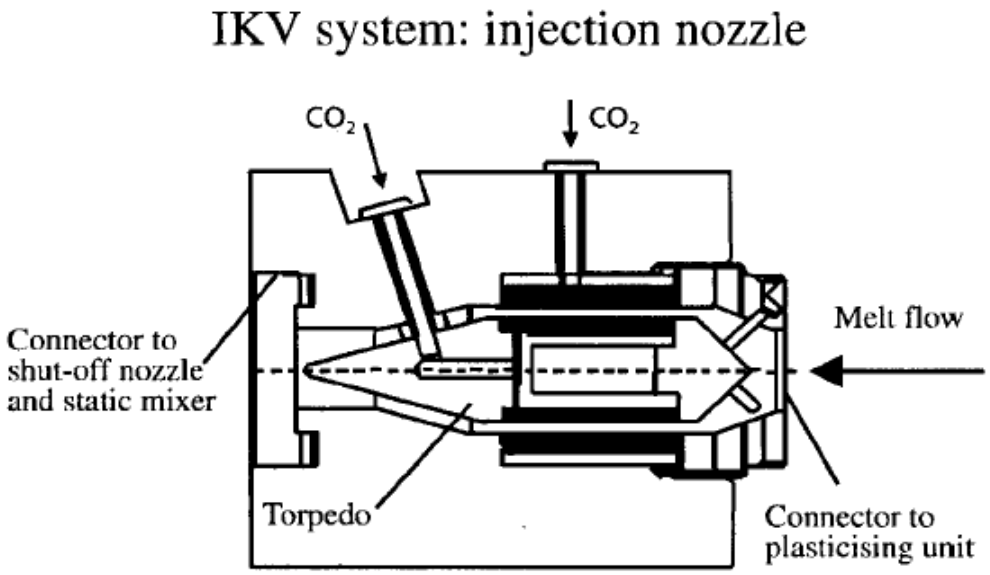

Figure 2.3 Schematic drawing of the nozzle used in the IKV injection molding process[89]. Reprinted from *Cellular Polymers*, 23, 25-37, Copyright (2004), with permission from Rapra.

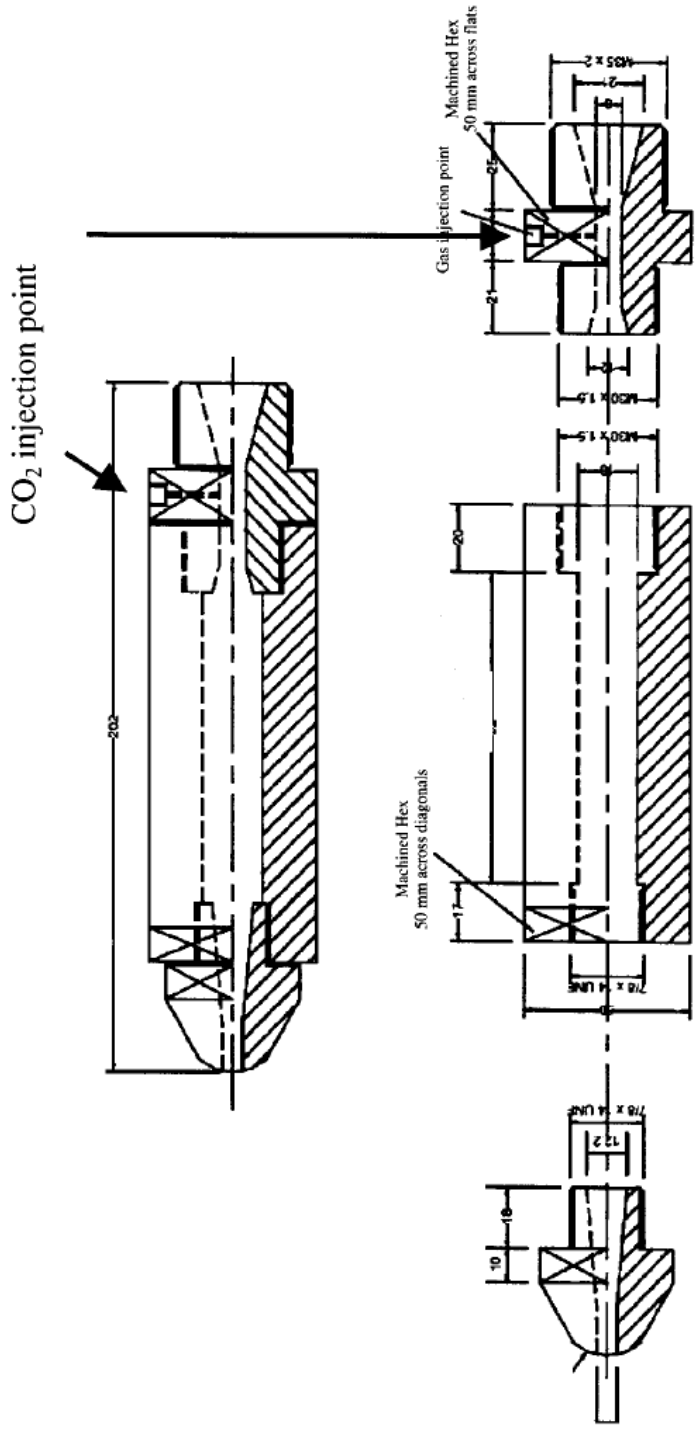

Figure 2.4 Schematic drawing of the nozzle used in the University of Warwick injection molding process[89]. Reprinted from *Cellular Polymers*, 23, 25-37, Copyright (2004), with permission from Rapra.

production of microcellular foams using a continuous injection molding process, it is important to introduce the gas into the system and form a single phase polymer/gas mixture.

Once the single gas/polymer phase is formed the formation of a microcellular foam is similar in all three processes. The single gas/polymer phase is injected into the mold. During the injection process a pressure drop occurs. This pressure drop introduces a thermodynamic instability into the system, which leads to microcellular foam formation. A short-shot is used to ensure cell morphology is not influenced by packing[91].

Few foam properties have been reported on any of the three microcellular injection molding processes. In the Mucell™ process studies the cell sizes have ranged between 30-90 μm[88, 90]. The largest reported density reduction for this process was 24%[88]. The IKV process reportedly yielded a higher density reduction of 60%[89]. Both of these processes would be feasible to use if a large density reduction was not necessary. The University of Warwick process did not report as high of density reduction as the other two processes. Foam production from the University of Warwick process only yielded density reductions up to 6.7%. It was also necessary to combine chemical blowing agents with the carbon dioxide to promote enough cell nucleation to produce microcellular foam. From the few foam properties reported on microcellular injection molding, the Mucell™ and IKV processes exhibit the best results.

2.4.2.3 Semi-continuous Extrusion Process

A semi-continuous extrusion process was described by Kumar[92] to alleviate the need of a complicated extruder setup. In the continuous extrusion process, it is necessary

to have an extruder that is modified to include a gas injection port. It is also necessary for the extruder to withstand large pressures within the barrel without losing gas. Both of these requirements are not necessary in the semi-continuous process.

The semi-continuous extrusion process involves two-steps in the microcellular foam processing. The first step in the process involves the saturation of the polymer pellets with CO_2 in a large pressure vessel filled with polymer pellets and pressurized with CO_2. The CO_2 is then given enough time to reach equilibrium in the diffusion process. The saturated pellets are then placed in the hopper of a standard compression single screw extruder. As the polymer pellets are heated, cell nucleation is initiated in the pellets which occurs due to a decrease in the solubility of CO_2 in the polymer because the polymer is at an elevated temperature. The polymer is then extruded under pressure through a die. When the cell nucleated CO_2/polymer melt reaches the end of the die, the nucleated cells are allowed to grow, which produces the microcellular foam.

The reported foam properties for the semi-continuous extrusion process were not as good as the continuous extrusion process. In the semi-continuous process, the average cell size ranged between 20 and 500 μm depending upon the processing parameters. A density reduction between 27 and 63% was also reported. These values could be higher than in the continuous extrusion process due to variations in die dimensions. In the continuous extrusion process, a filament die was used. In the semi-continuous process, a larger sheet die was used. If a filament die had been used in the semi-continuous process, the foam properties may have been more comparable to the continuous process.

2.5 Parameters Affecting Microcellular Foaming

This section presents a discussion on the various processing parameters that can be varied to control the microcellular foam properties such as cell size and cell density. The discussion begins with processing parameters that can be varied in the batch processing. The section continues with continuous processing parameters. The section on the continuous processing parameters includes a discussion of the effect of the processing on the expansion ratio.

2.5.1 Control of Processing Parameters for Desired Foam Properties

Cell density and cell size are important properties of microcellular foams regardless of whether the foam is produced in a batch or continuous process. Though the effect of processing parameters on cell size and density is discussed separately, the cell size and density in microcellular foaming are related[93]. Thus, changing the processing parameters to optimize one material property can have a detrimental affect on the other property. These material properties of the foam determine the usability of the material made from the process, which correlates to the usability of the process. In order to control these foam properties, several processing parameters can be varied.

2.5.1.1 Batch Processing

2.5.1.1.1 Cell Density

Several batch processing parameters can be used to control the cell density of a microcellular foamed polymer. The cell density can be increased or decreased to a desired level by controlling the saturation time and pressure, foaming temperature, and depressurization rate.

The saturation pressure can be used to control the cell density by limiting the amount of gas diffusion into the polymer and the depth of pressure release. As the pressure is increased, the amount of gas that is dissolved in the polymer also increases[65]. When more gas is dissolved in the polymer, the cell density increases exponentially[64, 68]. When more CO_2 particles are available in the polymer to foam, the interfacial tension and viscosity of the polymer are decreased, which leads to a greater number of nucleated cells[14]. The saturation pressure also affects the cell density by changing the depth of pressure release[15]. As the depth of pressure release is greater, a larger thermodynamic instability is generated in the polymer/gas mixture. This leads to a greater number of nucleated cells upon the release of the pressure. Nucleation theory supports the observations of an increase in the saturation pressure resulting in a greater cell density[67].

The saturation time affects the cell density by controlling the amount of gas dissolved in the polymer that is available for foaming[63, 93]. When the saturation times are increased, the amount of gas that diffuses into the polymer increases until equilibrium is reached. As discussed in the saturation pressure, more gas present in the polymer will decrease the cell density. Once equilibrium is reached, the cell density will no longer change as saturation time is increased.

The foaming temperature can be varied to obtain a desired cell density. In general, as the temperature is increased, the cell density decreases. There are three different discussions on the reasons for this relationship. Krause et al.[65] observed in microcellular foaming an upper and lower temperature exist at which foams can be generated, T_{upper} and T_{lower}, respectively. They propose that at a temperature below T_{lower},

cells do not nucleate because the polymer/gas system is below the T_g and is in a glassy state. As the temperature is increased, the cell density increases until a maximum is reached (at a temperature T_{max}). Once the temperature is above T_{max}, the cell density deceases due to an increase in gas diffusivity. When the diffusivity increases, the system will stabilize by gas diffusion rather than nucleation. At temperatures above T_{upper}, the diffusivity is so great that cell nucleation no longer occurs to stabilize the gas/polymer system. A second proposed idea relates the increase in the foaming temperature to a decrease in the viscosity of the polymer/gas system. This leads to an increased tendency for the nucleated cells to coalesce, thus generating a foam structure with a lowered cell density[71]. A third proposed idea is that the cell density decreases with an increase in temperature (at a constant pressure) due to the decreased solubility of the gas into the polymer at increased temperatures[10, 12, 16]. This decreased solubility of gas in the polymer leads to a smaller thermodynamic instability which decreases the cell nucleation[14, 15, 70]. Regardless of the mechanism, as the foaming temperature is increased, the resulting cell density of the foam decreases.

The cell density is dependent upon the pressure release rate. As the pressure release rate is increased, a greater thermodynamic instability is generated in the gas/polymer system. This large thermodynamic instability leads to a greater amount of cell nucleation which causes the cell density to increase[71]. In a one step batch process, the pressure release rate is controlled by the release mechanism and can be measured by timing the release during experimentation. In the two-step batch process the pressure release rate is determined by the heat transfer from the hot bath to the sample. In both processes, as the release rate is increased the cell density also increases.

2.5.1.1.2 Cell Size

The growth of cells in microcellular foaming is dependent upon the amount of gas available in the polymer after nucleation and the duration of the time before vitrification occurs or the sample is quench cooled. Both of these can be controlled via various processing parameters. The foaming temperature exhibits the largest effect on the cell size, though the pressure release rate, saturation pressure, and saturation time also affect the growth of cells in the foaming process.

The release rate, saturation pressure, and saturation time will affect the cell size by controlling the cell density. The saturation pressure and time limit the amount of gas that diffuses into the polymer. Increasing the saturation pressure or time increases the amount of gas that is able to diffuse into the polymer. Because the increase in gas diffusion correlates to a larger cell density, the cell size of the microcellular foam decreases. Though a change in the release rate, saturation pressure, or saturation time does not directly control the cell size, the cell size is affected due to its relationship to cell density[15].

The foaming temperature has been determined to have a large affect on cell growth in the microcellular foaming process by controlling both gas solubility in the polymer as well as the processing window in which cell growth can occur. Because an increase in temperature at a constant pressure yields a decrease in the gas solubility in a polymer, the cell size increases indirectly due to decreasing cell density[10, 12, 16]. Though this relationship can be considered, the cell size is most directly affected by the foaming temperature due to the change in viscosity of the polymer and the amount of time in which cells can grow[18]. When the foaming temperature is increased, the

viscosity of the polymer is decreased, as long as the temperature is above the T_g for the gas/polymer system[15, 34, 64]. The amount of time for cell growth is also increased because the onset of vitrification is delayed. Both of these phenomena lead to a larger cell foam structure.

2.5.1.2 Continuous and Semi-continuous Processing

Continuous processing of microcellular foams requires several parameters to be accounted for in the design of the process. The cell density, cell size, and expansion ratio can be controlled through various processing parameters in continuous processes. In order to produce microcellular foam in a continuous process, a die must be designed to promote cell nucleation. The section concludes with a discussion on the design of continuous processing dies to promote nucleation.

2.5.1.2.1 Cell Density

Cell density of the foamed polymer is controlled by both the initial cell nucleation as well as cell coalescence. To maximize the cell density, high initial cell nucleation and low cell coalescence is desired. Experiments have determined that the initial cell nucleation is controlled by the amount of CO_2 present in the polymer when the nucleation occurs, as well as how quickly the dissolved gas is released from the polymer[80, 94]. Cell nucleation occurs due to thermodynamic instabilities which arise because the gas solubility changes in the polymer via a pressure release. With greater thermodynamic instabilities present in the processing, more cell nucleation occurs. To achieve higher thermodynamic instabilities, either a higher CO_2 concentration or a rapid release of the gas can be used. This will lead to a greater change in the solubility.

Gas solubility in polymers is also controlled by the temperature and pressure of the system[77]. As the temperature of the polymer is increased at a constant pressure, the gas density in the polymer decreases. Because of the decrease in gas density with an increasing temperature, the processing temperature should be minimized to promote higher gas density. The processing temperature varies depending upon the polymer of interest. The maximum processing temperature to produce closed cell microcellular foams is the T_g for amorphous polymers and T_m for semicrystalline polymers[75]. A rapid pressure drop would also induce a large amount of cell nucleation[80, 81]. Because the solubility of a gas in a polymer decreases as pressure decreases, a large pressure drop would promote a large thermodynamic instability which promotes numerous cell nucleation sites. In an injection molding process, the pressure drop rate is determined by the injection rate. A faster injection rate correlates to a larger pressure drop rate[88, 91]. A pressure drop of 22 MPa or higher is needed to ensure a cell density of 10^9 cells/cm^3[77].

Once the cells have been nucleated, cell coalescence needs to be minimized to preserve the cell density. Cell coalescence occurs because the polymer melt becomes too weak to sustain the nucleated cells. An increase in the polymer melt strength is needed in order to reduce the amount of cell coalescence[94, 95]. The polymer melt strength can be controlled by reducing the temperature of the melt. In an extrusion process, cell coalescence can be nearly eliminated by decreasing the processing temperature to a temperature that approaches the plasticized T_g of the polymer[80].

2.5.1.2.2 Cell Size

Cell size is another important material property of microcellular foams that can be controlled through various processing parameters. In continuous and semi-continuous processing of microcellular foams, cell size can be controlled by the screw speed and processing temperature. Cell growth in an extrusion process occurs right after the cells are nucleated in the die[81]. The cells continue to grow until the polymer foam exits the die and the temperature is reduced below the T_g. If a lower processing temperature is used, the window for cell growth is smaller. This results in a foam with a smaller cell size. A longer residence time in the die, will lead to longer cell growth times. The residence time in the die is controlled by the screw speed. As the screw speed is increased, the residence time in the die decreases. This will lead to a small cell size since the cell growth time is short.

2.5.1.2.3 Expansion Ratio

The expansion ratio of the polymer foam is another important property in microcellular foaming. Expansion ratio is a comparison of the size of the extruded part to the size of the die. The expansion ratio of the extruded foam is dependent upon the viscosity of the polymer and can be controlled by the die temperature, CO_2 content, and pressure drop rate[86, 87]. In order to get a large pressure drop rate, filament dies are used to create large back pressure in the extruder. Large expansion ratios have been obtained using filament dies, though the resulting material still has a small diameter. During processing, there is a optimum viscosity for the expansion ratio. In experiments conducted by Lee et al.[86] the expansion ratio exhibited a strong dependence on the CO_2 concentration but only at low concentrations. The dependence started to decrease as the CO_2 content was increased. In these studies, a maximum expansion ratio was observed

when high CO_2 concentrations were investigated. These studies confirmed that an optimum viscosity was necessary to obtain foam with a maximum expansion ratio. If the viscosity was too low, the melt was not strong enough to support the cell structure and gas would be lost. With a high viscosity, the melt was too stiff thus inhibiting cell growth. The viscosity of the polymer melt needs to be optimized to obtain a large expansion ratio.

2.5.1.2.4 Die Design

Optimizing the die design is important in order to control the foam properties (i.e. cell size and cell density) in continuous processing of microcellular foams. Variations in the die design can change the cell nucleation, cell growth, and the final shape of the foamed polymer. The key design element to optimizing a die for microcellular foaming in a continuous process is controlling the location and overall amount of pressure drop in the die, as well as, a consistent control on temperature[76].

In order to facilitate the large amount of cell nucleation required for microcellular foams, a large pressure drop must be induced in the continuous processing. In several studies of continuous processing of microcellular foams, a large pressure drop was induced by use of a capillary die[76, 77, 84-86, 96]. The pressure drop in the capillary die resulted in a foam that had a large nucleation density that is required for microcellular foam.

The pressure drop through the capillary can be modeled by assuming the flow is representative of a fully developed flow through a nozzle. The flow rate, Q, through a nozzle for a power-law fluid is[97]:

$$Q = \left(\frac{\pi R^3}{s+3}\right)\left(\frac{R\Delta P}{2mL}\right)^s \tag{2.1}$$

Where

$$s = \frac{1}{n} \tag{2.2}$$

In equation (2.1), the radius of the nozzles is given by R, the length of the nozzle is denoted by L, m and n are the power law parameters, and ΔP is the pressure drop across the nozzle. Equation (2.1) can be solved for the pressure drop across the nozzle to yield:

$$\Delta P = \left(\frac{2mL}{R}\right)\left(\frac{Q(s+3)}{\pi R^3}\right)^{\frac{1}{s}} \tag{2.3}$$

If the power law parameters of the polymer are know, equation (2.3) can be used to calculate the pressure drop across the capillary die. For more accurate modeling, the power law parameters should be determined from data that were acquired on CO_2 plasticized polymer.

The pressure drop rate has also been determined as an important die design characteristic that needs be accounted for. The pressure drop rate through the capillary can be estimated as[96]:

$$\frac{\Delta P}{\Delta t} = 2m(3+s)^{\frac{1}{s}}\left(\frac{Q}{\pi R^3}\right)^{\frac{1}{s}+1} \tag{2.4}$$

In a study by Lee et al.[86], three different capillary dies were designed with the same pressure drop but varied in pressure drop rates. In this study, the pressure drop rate

affected the cell nucleation density. It was found that the larger pressure drop rate through the capillary led to an increase in cell nucleation density.

2.5.2 Polymer Properties Affecting Foam Production

Beyond optimizing the processing parameters to obtain the desired material properties, the choice of polymer used can have a great affect on the cell density and size. Polymer properties such as the degree of crystallinity and the presence of low molecular weight substituents affect the resulting material properties of the foam.

2.5.2.1 Cell Density

The cell density can be affected by the degree of crystallinity as well as the presence of low molecular weight substituents. The degree of crystallinity controls the diffusivity and solubility of gas into the polymer matrix[9]. When the polymer is more crystalline, there is less space for gas to dissolve into the polymer because gas only diffuses into the amorphous regions of a polymer[98]. This yields foams with a reduced cell density. The presence of low molecular weight substituents also contributes to a decrease in cell density[74].

2.5.2.2 Cell Size

Polymer properties can also be controlled to obtain a desired cell size in microcellular foaming. An increase in the degree of crystallinity in a polymer will lead to a larger, non-uniform cell structure[9]. This is attributed to the decreased solubility of gas in the polymer. Low molecular weight substituents have been observed to greatly affect the cell size. In a study by Stafford et al.[74] both commercial polystyrene and lab polymerized polystyrene were foamed using CO_2. The commercial polystyrene had a

remarkably larger cell structure, which prompted additional experiments. Upon further investigation, it was determined that cell size increased due to the presence of low molecular weight components. Incorporation of crystallinity or low molecular weight components into the polymer affects the resulting size of the foamed cells.

2.6 Microcellular Foam Composites

This section covers research that has been conducted on reinforced microcellular foams. The section begins with a discussion on reinforcing microcellular foams with nanoparticles. The discussion covers nanocomposites produced from nanoclays and highlights the advantages of these materials. The section then concludes with a discussion on the research conducted involving microcellular foams that are reinforced with wood fibers.

2.6.1 Nanocomposite foam

Nanoparticles have been combined with various polymers to improve several mechanical properties, thermal properties, and barrier properties[99]. Because nanoparticles could potentially improve material properties, studies have been conducted on the addition of nanoparticles to various microcellular foaming processes. During foaming, the added nanoparticles act as a nucleating agent, which leads to a greater number of nucleated cells with smaller cell diameter[100, 101].

The first step in the production of microcellular nanocomposite foams is the combination of the nanoparticles with the polymer of interest. Blending of the nanoparticles with the polymer matrix can be done by melt blending, *in-situ* polymerization, and solution blending[99]. Different types of nanocomposites can result

depending upon the blending method as well as the polymer/nanoparticle interaction. The nanocomposites can be intercalated or exfoliated. Intercalated nanocomposites occur when there is still order amongst the nanoparticles due to the inability to completely separate the nanoparticles. Exfoliated nanocomposites are achieved by completely separating the nanoparticles and are characterized by the polymer matrix completely surrounding the nanoparticles. Exfoliated nanocomposites lead to the largest improvement in material properties.

The second step in the production of microcellular nanocomposite foams is the foaming of the polymer matrix. The microcellular foaming can be carried out using either a continuous or batch process. The methods used are similar to those used in general to generate microcellular structures which were discussed in section 2.4.

2.6.1.1 Foaming of Polymer-Nanoclay Composites

The inclusion of nanoclays has shown a significant improvement on the reduction of cell size and the increase in cell density. In studies conducted, the cell size has decreased by 4 to 10 times that of neat foamed polymer with all other processing parameters the same[101, 102]. During the same studies, the cell density also increased by an order of magnitude. These improvements are attributed to several different phenomena that have been observed by including nanoclays in the foaming process. More gas is able to diffuse into the nanocomposites and the diffusion out of the sample is slower, which may contribute to the decrease in cell size and increase in cell density[78, 100]. One theory states that the additional gas in the system would lead to a more thermodynamically unstable system which would cause greater cell nucleation. The greater cell nucleation would then cause less gas to be available for cell growth, leading

to a smaller cell size. This is not likely the main reason for the smaller cell size and greater cell density since the amount of gas in the system only increased slightly. Other reports have stated that the inclusion of nanoclays leads to a decreased cell size and greater cell density because the nanoclays stabilize the melt[101]. It is expected that the stabilization would reduce the amount of cell coalescence. By decreasing the cell coalescence, the resulting foam would have a decreased cell size and a greater cell density. Several different experiments have shown a decrease in cell size and an increase in cell density with the inclusion of nanoclays in polymer foams.

The addition of nanoclays has also shown to increase mechanical properties in polymer foams. In a study by Okamoto et al.[103] the compression modulus of a foam made from polypropylene that was reinforced with nanoclay was shown to increase by a factor of seven. A paper by Han et al.[78] reported an increase in the reduced tensile modulus when compared to neat polymer foams. Both the neat and the nanocomposite foams exhibited a lower reduced tensile modulus than the unfoamed polymer. The increase in the compression and reduced tensile modulus are both attributed to the reinforcement by nanoclay in the cell wall. During the foaming process, the cell growth causes biaxial extension in the polymer. This causes the nanoclay to align around the cell wall, which increases mechanical properties in the foam.

While nanoclays have been shown to improve the mechanical properties of several microcellular foams, incorporation of the nanoclays into polymers with high glass transition temperatures (T_g) is difficult. Nanoclays are often organically modified to enhance the dispersion in polymer matrices[99]. Cation surfactacts, often alkylammonium or alkylphosphonium cations, are used to enhance the miscibility of the

nanoclays with the polymer. However, these cation surfactants tend to degrade at the high temperatures necessary to melt process these polymers.

2.6.1.2 Foaming of Polymer-Carbon Nanofiber Composites

Carbon nanofibers have also been incorporated into polymer matrices and then foamed using supercritical carbon dioxide as the foaming agent. Shen et al.[104, 105] have studied the effect of incorporating the carbon nanofibers (0.3 – 5 wt. %) into polystyrene. By incorporating well dispersed carbon nanofibers into the polystyrene matrix, it was found that the nanofibers were able to act as a heterogeneous nucleating agent. It was determined that the carbon nanofibers exhibited a greater nucleating efficiency than the nanoclays; thus the carbon nanofibers were able to nucleate more cells at a lower percent loading[105]. Like the nanoclays, the carbon nanofibers were shown to align around the nucleated cell walls, possibly increasing the mechanical properties of the nanocomposite foam[104].

Both tensile and compressive properties of microcellular polystyrene foams which were reinforced with carbon nanofibers (1 and 5 wt. % loading) were reported[104]. By incorporating carbon nanofibers, the reduced tensile modulus of the carbon nanofiber reinforced foam was greater than neat polystyrene (both foamed and unfoamed) for both 1 and 5 wt. % loading of fibers. However, the tensile strength was lower for the reinforced foam, making the reinforced foams less ductile. The ductility decreased with an increased weight percent of fibers. To study the effect of the carbon nanofibers on the compressive properties of the foam, two different density foams were produced (~80% reduction and ~50% reduction) with both 1 and 5 wt. % loading. The low density foam (~80% reduction) had a much lower compressive modulus than unfoamed polystyrene

regardless of the amount of carbon nanofibers. The medium density foam (~50% reduction) exhibited a compressive modulus that was higher than unfoamed polystyrene, with the 1 and 5 wt. % being statistically indifferent. Both the tensile and compressive modulus of microcellular polystyrene foams reinforced with carbon nanofibers were greater than neat polystyrene.

2.6.2 Fiber Reinforcement

Wood fibers have been used as reinforcement in microcellular foaming. However, in unfoamed polymer composites, the fibers decrease impact strength due to the increased stiffness of the material[106]. Microcellular foaming is carried out in order to increase the impact strength of the composite[107]. In studies conducted, the reinforcing fibers have increased the tensile modulus and impact strength compared to non-reinforced microcellular foams[106, 107]. Though an increase in mechanical properties was observed, there were more difficulties in the processing of the microcellular foams.

The addition of reinforcing fibers to the polymer matrix reduced the quality of the microcellular foam. An order of magnitude reduction of cell density was observed and the cell size increased by 3 to 8 times with the addition of the fibers[106, 107]. The decrease in the foam properties is attributed to the rapid gas loss during the foaming process. In the studies conducted, the polymer/fiber interface was weak causing channels to form. The channels formed an easy path for the CO_2 to escape instead of contributing to the foaming process. The studies also showed that the decreased foam properties are due to a decrease in the amount of CO_2 that is absorbed into the polymer. Since the fibers are not able to absorb CO_2, there is less CO_2 present to nucleate and grow the foam

cells. Though the addition of fibers led to a reduction in cell density and an increase in cell size, the fibers still increased the mechanical properties.

Fiber reinforced foamed composites have exhibited increased tensile modulus when compared to unreinforced foamed polymers. In a study of wood fiber reinforced poly(vinyl chloride), the tensile modulus slightly increased[107]. The increase was due to the addition of the reinforcing fibers. However, the foaming process had a negative effect on the tensile modulus. A decrease in tensile modulus was observed when comparing the foamed composite to the unfoamed composite.

Foaming the polymer/wood fiber composite led to an increase in impact strength. In a study by Matuana et al.[107] the impact strength of fiber reinforced microcellular poly(vinyl chloride) increased by 3 times compared to the unfoamed composite. An increase in the impact strength was also reported for fiber reinforced polypropylene[108]. The increase in impact toughness is attributed to the microcellular foam.

The use of reinforcing fibers to increase in the mechanical properties in microcellular foaming has been studied. The reinforcing fibers led to an increase in the tensile properties of the materials. Though the reinforcing fibers had a negative effect on the cell density and cell size, a slight increase in impact toughness was reported. A larger increase in mechanical properties may be observed if a process is developed that allows reinforced polymer to be foamed while still maintaining similar cell size and density to non-reinforced foamed polymers. The larger cell size and cell density negatively affect the mechanical properties, thus there is little benefit in reinforcing fibers.

2.7 Modeling of Microcellular Foaming

Several different models have been proposed to understand the nucleation in microcellular foaming. This section discusses the various models, the assumptions that each model makes, and the drawbacks of the various models. This section begins with classical nucleation theory, which was the first model that was used to estimate the nucleation in microcellular foaming. Next, a discussion on the microvoid model is presented. The section concludes with the modeling of the growth of the nucleated cells.

2.7.1 Microcellular Nucleation Modeling

The nucleation of cells can be broken down into either homogeneous or heterogeneous nucleation. Homogeneous nucleation occurs when cells form in a single phase system. Heterogeneous nucleation involves the formation of cells in a multiphase system. If there are two phases present, the bubbles will nucleate at the interface between the different phases.

2.7.1.1 Classical Nucleation Theory

The first model used in the nucleation of microcellular foams was based on classical nucleation theory that had been modified to include free volume and surface energy effects that arise due to the addition of additives and gases[109]. A more detailed derivation can be found in literature[110].

$$N_o = C_o f_o \exp\left(\frac{-\Delta G^*_{\text{hom}}}{kT}\right) \tag{2.5}$$

Where

$$\Delta G^*_{\text{hom}} = \frac{16\pi\gamma_{bp}^3}{3\Delta P^2} \tag{2.6}$$

Equation (2.5) has been derived to model the homogeneous nucleation rate, N_o. The concentration of the gas molecules is described by C_o. This is dependent on the gas saturation pressure and can be estimated by using Henry's Law. The frequency factor of gas molecules joining the nucleus is described by f_o. The temperature in Kelvin and Boltzman's constant are given by T and k, respectively. Gibbs free energy for homogeneous nucleation, ΔG^*_{hom}, is described in equation (2.6). In equation (2.6), γ_{bp} is the surface energy of the polymer/bubble interface and ΔP is the pressure of saturation.

The modified classical nucleation theory, which accounts for additives and dissolved gases, was also extended to heterogeneous nucleation[110]. Equation (2.7) describes the heterogeneous nucleation rate, N_1.

$$N_1 = C_1 f_1 \exp\left(\frac{-\Delta G^*_{het}}{kT}\right) \tag{2.7}$$

Where

$$\Delta G^*_{het} = \frac{16\pi\gamma^3_{bp}}{3\Delta P^2}\left(1/4\right)\left(2+\cos\theta\right)\left(1-\cos\theta\right)^2 \tag{2.8}$$

In equation (2.7), C_1 is the concentration of heterogeneous nucleation sites and f_1 represents the frequency factor of the gas molecules joining the nucleus. The temperature and Boltzman's constant are represented by T and k, respectively. Gibbs free energy of heterogeneous nucleation, ΔG^*_{het}, is calculated in equation (2.8). In this equation, γ_{bp} is the surface energy of the polymer/bubble interface and ΔP is the saturation pressure. The wetting angle of the polymer/additive/gas interface is described by θ.

Colton and Suh[110] propose that as the concentration additives approaches the solubility limit in the polymeric matrix, a mixed mode nucleation can occur. The model for the nucleation rate of mixed mode nucleation, which is described in equation (2.9), is

a combination of homogeneous and heterogeneous nucleation rates. In mixed mode nucleation, the heterogeneous nucleation will occur before homogeneous nucleation occurs. The gas will try to diffuse into the heterogeneously nucleated cells and, therefore, reduce the concentration of gas available for homogeneous nucleation, C_o. In the mixed mode model, the homogeneous nucleation rate, described in equation (2.10), is corrected for the reduction of C_o. In equation (2.10), t is the time since the beginning of heterogeneous nucleation and n_b is the number of gas molecules present in the nucleated bubbles.

$$N = N'_{\text{hom}} + N_{het} \tag{2.9}$$

$$N'_{\text{hom}} = \left(C_o - N_{het} t n_b\right) f_o \exp\left(\frac{-\Delta G^{**}_{\text{hom}}}{kT}\right) \tag{2.10}$$

$$\Delta G^{**}_{\text{hom}} \sim \Delta G^{*}_{\text{hom}} \tag{2.11}$$

The validity of the mixed mode model was tested by Colton and Suh.[111] To test both the mixed mode nucleation rates, a system of polystyrene and zinc stearate was foamed with different concentrations of zinc stearate and with varying saturation pressures. The results of the foaming study can be seen in Figure 2.5. From this graph, it can be seen that the mixed mode nucleation model accounts for the trends seen experimentally. As the pressure is increased, the nucleation rate also increases. The three regions of homogenous, heterogeneous, and mixed mode nucleation are also observed experimentally. The model, however, does not give a quantitatively accurate nucleation rate. At low concentrations of additives, the model over predicts the nucleation rate by two orders of magnitude. As the additive concentration is increased,

the model under predicts the nucleation rate by three orders of magnitude. The model also fails to predict homogeneous nucleation at low saturation pressures (35 atm) though nucleation occurs experimentally. The quantitative inaccuracies have also been observed with polycarbonate as well as unfilled polystyrene[112, 113].

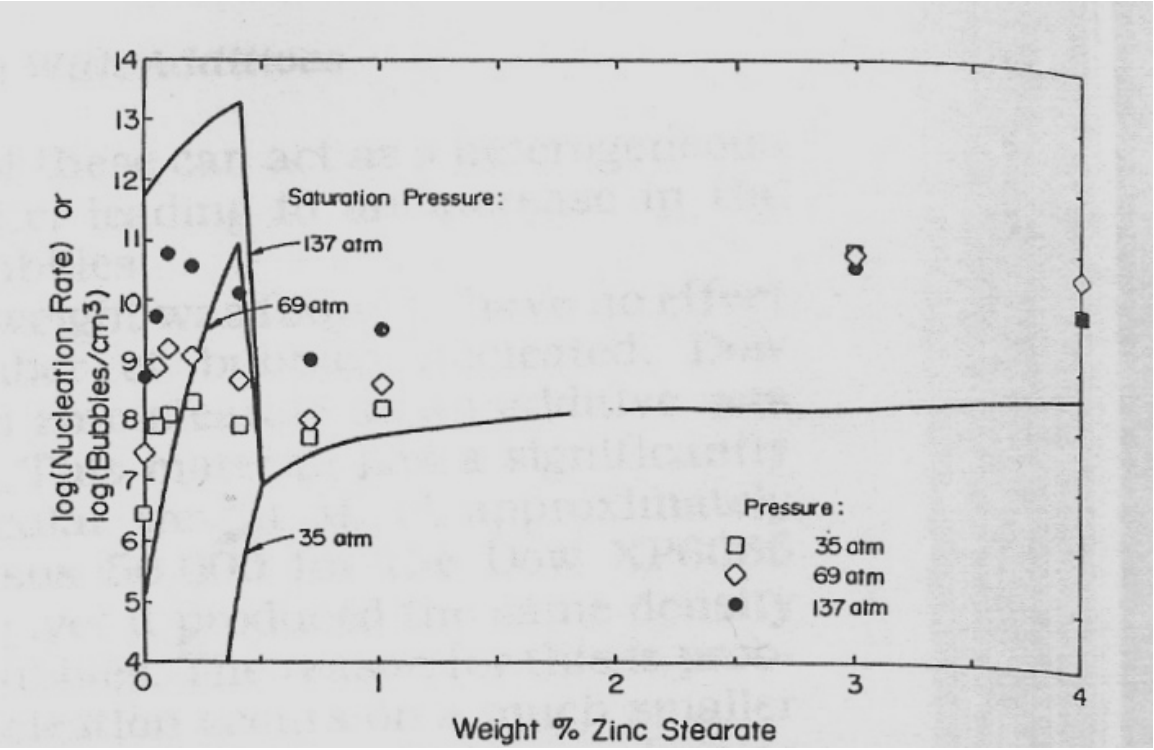

Figure 2.5 Comparison of modified classical nucleation theory to experimental data[111]. Discrete points represent experimental data and the line represents the model. Reprinted with permission from John Wiley & Sons, Inc. Copyright (1987).

2.7.1.2 Microvoid Nucleation Model

The microvoid nucleation model was developed by Kweeder et al.[114] and later modified by Ramesh et al.[115] The microvoid nucleation model is based on the assumption that as polymers are manufactured, small defects or microvoids are generated. It is hypothesized that during the microcellular foaming process, the

microvoids are responsible for the "nucleation" of the cells. In this model, it is assumed that there is a minimum radius of microvoid required to actually sustain cell growth.

$$N = \frac{N_o}{2} erfc\left(\frac{\ln\frac{r}{\xi}}{\psi}\right) \tag{2.12}$$

The microvoid model predicts the nucleation population by determining the minimum size microvoid that is required to sustain cell growth. In the microvoid nucleation model, the nucleation population is calculated by use of equation (2.12). Equation (2.12) assumes that there is a log-normal distribution of microvoids present in the polymer, and the number of voids with the minimum radius to sustain cell growth is described by the tail of the distribution. In this equation, N describes the population of voids that are large enough to sustain cell growth. The total number of voids present is described by N_o and r is the minimum radius required to sustain cell growth. The mean of the log-normal distribution and the standard deviation of the distribution are described by ξ and ψ, respectively. An initial value for r is assumed and the volume of polymer per void is calculated.

The assumption for the value of initial radius needed to sustain cell growth is validated using the Laplace Equation, described in equation (2.13), and the equation for the pressure of gas inside the nucleated microvoid, described in equation (2.14). The values of ΔP and P_{Gas} are calculated as the expansion of the bubble is simulated. During the simulation, if ΔP becomes larger than P_{Gas}, the value of r is increased slightly and the simulation is rerun. After a successful simulation, the value of the cell nucleation population is known.

$$\Delta P = \frac{2\sigma}{r} \tag{2.13}$$

The value of ΔP is calculated using the Laplace Equation. In equation (2.13), ΔP is the pressure difference across the bubble interface, r is the radius of the bubble, and σ is the surface tension. The equation assumes that the microvoid is spherical in shape.

$$P_{Gas} = \frac{-B + \sqrt{B^2 - 4m\left[\frac{4\pi}{3V_{PS}}\left(r^3 - r_o^3\right) - S(P)P_s\right]}}{2m} \tag{2.14}$$

The pressure of the gas inside the expanding bubble is calculated by using equation (2.14). This equation was determined by assuming the gas pressure was in equilibrium with the surrounding polymer and conducting a material balance on the void and polymer. A really short time scale for diffusion is also assumed in this material balance. In equation (2.14), P_{Gas} describes the gas pressure that is expanding the bubble. The expanding radius of the void is given by r and r_o describes the initial value of the radius. The volume of polymer that is supplying gas is described by V_{PS}, P_S is the saturation pressure, and $S(P)$ is the solubility as a function of the pressure. The values of m and B are determined from the slope and intercept of the solubility vs. pressure data respectively.

The validity of the microvoid nucleation model has been tested by using data for pure polystyrene as well as high impact polystyrene[114, 116]. For high impact polystyrene, the experimental data agreed with the predicted values for varying saturation pressures. Unlike the classical nucleation model, the micovoid model was able to predict cell nucleation at low saturation pressures[114].

The microvoid nucleation model exhibited a significant improvement in being able to model the nucleation population compared to classical nucleation theory. The experimental data for both polystyrene and high impact polystyrene correlated well with the model over a broad range of saturation pressures. In the microvoid nucleation model, it is important to fully understand the population of microvoids present in the polymer before foaming. Overall, this model provided a good understanding of the cell nucleation in microcellular foaming.

2.7.2 Cell Growth Modeling

Once the nucleation of cells is modeled, it is important to be able to model the cell growth in the microcellular foaming process. The cell growth in the system occurs by the gas pressure in the nucleated cell pushing out on the viscous polymer that is immediately surrounding the cell. In order to model the cell growth, it is necessary to understand the conservation of momentum, conservation of mass, and constitutive equations used to describe the polymer. Several papers have been published in which a detailed description of the derivation for bubble growth in polymeric materials was presented[117-120].

In order to model how the nucleated cell grows in the polymer, conservation of momentum is employed. Because the growth occurs in a viscous medium, the contribution from the inertial forces is negligible. It is also assumed that the bubble is spherical in shape. The gas inside the bubble is assumed to be an ideal gas. Using these assumptions, the conservation of momentum for bubble growth can be described by equation (2.15).

$$p_g - \frac{2\sigma}{R} = p_f - 2\int_R^S \frac{\tau_{rr} - \tau_{\theta\theta}}{r} dr \qquad (2.15)$$

In this equation p_g is the gas pressure inside the bubble, σ is the surface tension, p_f describes the pressure at the outer boundary of the polymer shell (S), and R describes the bubble radius. The terms τ_{rr} and $\tau_{\theta\theta}$ are components of the stress tensor that describe the deformation of the polymeric fluid. This can be accomplished by describing the fluid with a viscoelastic model or simplified by assuming a Newtonian fluid for a first approximation[117, 119].

In order to describe the diffusion of the gas that is dissolved in polymer surrounding the nucleated bubble into the bubble, the conservation of mass is required. As the bubble expands, the pressure inside decreases. The gas concentration at the bubble interface also decreases. It is assumed that the decrease in gas concentration at the bubble interface is described by Henry's Law[117]. A concentration gradient is created forcing diffusion of the dissolved gas from the polymer to the nucleated bubble. The diffusion of the dissolved gas is, therefore, described by equation (2.16).

$$\frac{\partial c}{\partial t} + v_r \frac{\partial c}{\partial r} = \frac{D}{r^2} \frac{\partial}{\partial r}\left(r^2 \frac{\partial c}{\partial r} \right) \tag{2.16}$$

In this equation, c is the concentration of the dissolved gas, v_r is the fluid velocity, and D is the diffusion coefficient.

Equations (2.15) and (2.16) are coupled by the continuity equation, described by equation (2.17).

$$v_r = \frac{R^2 \dot{R}}{r^2} \tag{2.17}$$

Equation (2.17) assumes that isothermal conditions are present. The conservation of mass, conservation of momentum, continuity equation, along with the constitutive equation to describe the deformation of the polymer, form a complete set of equations

used to describe the bubble growth. Because the set of equations involves a set of coupled partial differential equations, analytical solutions are not available. These equations must be solved numerically to model the growth of the bubble. Though the calculations are mathematically demanding, Advani and Arefmanesh[117] present several mathematical techiniques that can be employed to solve the set of equations.

2.8 References

1. Nalawade, S.P., F. Picchioni, and L.P.B.M. Janssen, *Supercritical Carbon Dioxide as a Green Solvent for Processing Polymer Melts: Processing Aspects and Applications.* Prog. Polym. Sci., 2006. **31**: p. 19-43.

2. Hyatt, J.A., *Liquid and Supercritical Carbon Dioxide as Organic Solvents.* J. Org. Chem., 1984. **49**(26): p. 5097-5101.

3. Cooper, A.I., *Polymer Synthesis and Processing Using Supercritical Carbon Dioxide.* J. Mater. Chem., 2000. **10**: p. 207-234.

4. Berens, A.R. and G.S. Huvard, *Interaction of Polymers with Near-Critical Carbon Dioxide*. Supercritical Fluid Science and Technology, ed. K.P. Johnston and J.M.L. Penninger. 1989, Washington, D.C.: American Chemical Society. 203-223.

5. Tomasko, D.L., et al., *A Review of CO_2 Applications in the Processing of Polymers.* Ind. Eng. Chem. Res., 2003. **42**: p. 6431-6456.

6. Aubert, J.H., *Solubility of Carbon Dioxide in Polymers by the Quartz Crystal Microbalance Technique.* J. Supercrit. Fluid., 1998. **11**: p. 163-172.

7. Shieh, Y.-T., et al., *Interaction of Supercritical Carbon Dioxide with Polymers. II. Amorphous Polymers.* J. Appl. Polym. Sci., 1996. **59**: p. 707-717.

8. Shieh, Y.-T., et al., *Interaction of Supercritical Carbon Dioxide with Polymers. I. Crystalline Polymers.* J. App. Polym. Sci., 1996. **59**: p. 695-705.

9. Doroudiani, S., C.B. Park, and M.T. Kortschot, *Effect of the Crystallinity and Morphology on the Microcellular Foam Structure of Semicrystalline Polymers.* Polym. Eng. Sci., 1996. **36**(21): p. 2645-2662.

10. Garg, A., E. Gulari, and C.W. Manke, *Thermodynamics of Polymer Melts Swollen with Supercritical Gases.* Macromolecules., 1994. **27**: p. 5643-5653.

11. Sato, Y., et al., *Solubilities of Carbon Dioxide and Nitrogen in Polystyrene Under High Temperature and Pressure.* Fluid Phase Equilibr., 1996. **125**: p. 129-138.

12. Sato, Y., et al., *Solubilities and Diffusion Coefficients of Carbon Dioxide in Poly(vinyl acetate) and Polystyrene.* J. Supercrit. Fluid., 2001. **19**: p. 187-198.

13. Kikic, I., et al., *Polymer Plasticization Using Supercritical Carbon Dioxide: Experiment and Modeling.* Ind. Eng. Chem. Res., 2003. **42**: p. 3022-3029.

14. Lee, K.-N., H.-J. Lee, and J.-H. Kim, *Preparation and morphology characterization of microcellular styrene-co-acrylonitrile (SAN) foam processed in supercritical CO2.* Polym. Int., 2000. **49**: p. 712-718.

15. Arora, K.A., A.J. Lesser, and T.J. McCarthy, *Preparation and Characterization of Microcellular Polystyrene Foams Processed in Supercritical Carbon Dioxide.* Macromolecules, 1998. **31**(4614-4620).

16. Martini-Vvedensky, J.E., N.P. Suh, and F.A. Waldman, *Microcellular Closed Cell Foams and Their Method of Manufacture*. 1984, Massachusetts Institute of Technology: United States.

17. Wilding, M., *Melt Processing of Thermally Unstable and High Molecular Weight Polymers with Supercritical Carbon Dioxide*, in *Chemical Engineering*. 2007, Virginia Polytechnic Institute and State University: Blacksburg. p. 215.

18. Goel, S.K. and E.J. Beckman, *Generation of Microcellular Polymeric Foams Using Supercritical Carbon Dioxide. II: Cell Growth and Skin Formation.* Polym. Eng. Sci., 1994. **34**(14): p. 1148-1156.

19. Chiou, J.S., J.W. Barlow, and D.R. Paul, *Plasticization of Glassy Polymers by CO_2.* J. App. Polym. Sci., 1985. **30**: p. 2633-2642.

20. Handa, Y.P., S. Lampron, and M.L. O'Neill, *On the Plasticization of Poly(2,6-dimethyl phenylene oxide) by CO_2.* J. Polym. Sci. Pol. Phys., 1994. **32**: p. 2549-2553.

21. Handa, Y.P., P. Kruus, and M. O'Neill, *High-Pressure Calorimetric Study of Plasticization of Poly(methyl methacrylate) by Methane, Ethylene, and Carbon Dioxide.* J. Polym. Sci. Pol. Phys., 1996. **34**: p. 2635-2639.

22. Condo, P.D. and K.P. Johnston, *In Situ Measurement of the Glass Transition Temperature of Polymers with Compressed Fluid Diluents.* J. Polym. Sci. Pol. Phys., 1994. **32**: p. 523-533.

23. Wang, W.-C.V., E.J. Kramer, and W.H. Sachse, *Effects of High-Pressure CO_2 on the Glass Transition Temperature and Mechanical Properties of Polystyrene.* J. Polym. Sci. Pol. Phys. Ed., 1982. **20**: p. 1371-1384.

24. Wissinger, R.G. and M.E. Paulaitis, *Glass Transition in Polymer/CO_2 Mixtures at Elevated Pressures.* J. Polym. Sci. Pol. Phys., 1991. **29**: p. 631-633.

25. Alessi, P., et al., *Plasticization of Polymer with Supercritical Carbon Dioxide: Experimental Determination of Glass-Transition Temperatures.* J. App. Polym. Sci., 2003. **88**: p. 2189-2193.

26. Canelas, D.A., A.L.C. Burke, and J.M. DeSimone, *Carbon Dioxide as a Continuous Phase for Polymer Synthesis.* Plast. Eng., 1997. **53**(12): p. 37-40.

27. Goel, S.K. and E.J. Beckman, *Plasticization of Poly(methyl methacrylate) (PMMA) networks by Supercritical Carbon Dioxide.* Polymer., 1993. **34**(7): p. 1410-1417.

28. Campbell, F. *The Case Against Honeycomb Core*. in *International SAMPE Symposium and Exhibition*. 2004. Long Beach, CA: Society for the Advancement of Material and Process Engineering.

29. Karlsson, K.F. and B.T. Aström, *Manufacturing and Applications of Structural Sandwich Components.* Compos. Part A - Appl. S., 1997. **28**(2): p. 97-111.

30. Marshall, A.C., *Core Composite and Sandwich Structures*, in *International Encyclopedia of Composites*, S.M. Lee, Editor. 1990, VCH Publishers Inc. p. 488-507.

31. Altstädt, V., et al., *Polymer Foams as Core Materials in Sandwich Laminates (Comparison with Honeycomb).* Polym. Polym. Compos., 1998. **6**(5): p. 295-304.

32. *Polymeric Foams and Foam Technology*. 2nd ed, ed. D. Klempner and V. Sendijarevic. 2004, Cincinnatti: Hanser Gardener Publications. 584.

33. Krutchen, C.M. and W.P. Wu, *Polymer Foam, Thermoformed Shapes and Methods of Forming It*. 1985, Mobil Oil Corporation: USA.

34. Sun, H. and J.E. Mark, *Preparation, Characterization, and Mechanical Properties of Some Microcellular Polysulfone Foams.* J. Appl. Polym. Sci., 2002. **86**: p. 1692-1701.

35. Brandom, D.K., et al., *New Method for Producing High-Performance Thermoplastic Polymeric Foams.* J. Appl. Polym. Sci., 1997. **66**: p. 1543-1550.

36. Pip, W. *Applications for PMI Foam-Cored Sandwich Material - Why PMI?* in *International SAMPE Technical Conference*. 1996. Seattle, Washington.

37. Servaty, S., et al., *Method for Producing Block-Shaped Polymethacrylimide Foamed Materials*. 2003, Roehm GmbH & Co KG: United States. p. 14.

38. Weiser, E.S., et al., *Polyimide Foams for Aerospace Vehicles.* High Perform. Polym., 2000. **12**: p. 1-12.

39. Vazquez, J.M., et al., *Polyimide Foams*. 2005, The United States of America as represented by the Administrator of the National Aeronautics and Space Administration: USA.

40. Barringer, J.R., et al., *Method for Producing Polyimide Foam of Desired Density*. 1991, Ethyl Corporation: USA.

41. Ishikura, M. and N. Watanabe, *Process for the Prepartation of Polyimide Foam*. 1994, Daicel Chemical Industries: USA.

42. Wentworth, C.H. and L.H. Wallner, *Method for Making Cellular Cores*. 1962, Hexcel Products, Inc: USA.

43. Duffy, J., et al., *Apparatus and Process for Stacking Sheets of Half-Cell Structure to Make a Honeycomb Core*. 1994, E. I. Du Pont de Nemours and Company: USA.

44. Jurisich, P.J., *Honeycomb Product and Process for Manufacture*. 1975: USA.

45. Hama, T., T. Tsuchihashi, and K. Ohya, *Honeycomb Core*. 1993, The Yokhama Rubber Co., Ltd., Japan: USA.

46. Gotoh, H., et al., *Honeycomb Core*. 1992, Mitsubishi Rayon Co., Ltd., Tokoyo, Japan: USA.

47. Blanding, W.S. and R.V.V. Dewoestine, *Extrusion Die*. 1978, Corning Glass Works: USA.

48. Ozaki, S., et al., *Die for Honeycomb Extruding Ceramic Honeycomb Structural Bodies*. 1987, NGK Insulators, Ltd.; Institute of Technology Precision Electrical Discharge Works: USA.

49. Jordan, W., *Using Embossing to Create a Fiber Reinforced Honeycomb Composite.* J. Eng. Mater-T ASME, 2005. **127**: p. 257-262.

50. Bunn, P. and J.T. Mottram, *Manufacture and Compression Properties of Syntactic Foams.* Composites., 1993. **24**(7): p. 565-571.

51. Gupta, N., *Characterization of Flexural Properties of Syntactic Foam Core Sandwich Composites and Effect of Density Variation.* J. Compos. Mater., 2005. **39**(24): p. 2197-2212.

52. Kim, H.S., *Method of Forming Syntactic Foams*. 2006, The University of Newcastle Research Associates Ltd.: International Publication.

53. Williams, M.K., et al., *Effects of Cell Structure and Density on the Properties of High Performance Polyimide Foams.* Polym. Advan. Technol., 2005. **16**: p. 167-174.

54. Sato, R., et al., *Foamed Polyimide Shaped Article and Process for Production of Same*. 2004, Ube Industried, Ltd. : USA.

55. Kim, H.S. and P. Plubrai, *Manufacturing and Failure Mechanisms of Syntactic Foam Under Compression.* Compos. Part A - Appl. S., 2004. **35**: p. 1009-1015.

56. Martini, J.E., N.P. Suh, and F.A. Waldman, *Microcellular Closed Cell Foams and Their Method of Manufacture*. 1984, Massachusetts Institute of Technology: USA. p. 7.

57. Kumar, V., et al., *Experimental Characterization of Tensile Behavior of Microcellular Polycarbonate Foams.* J. Eng. Mater-T ASME, 1994. **116**: p. 439-445.

58. Collias, D.I. and D.G. Baird, *Tensile Toughness of Microcellular Foams of Polystyrene, Styrene-Acrylonitrile Copolymer, and Polycarbonate, and the Effect of Dissolved Gas on the Tensile Toughness of the Same Polymer Matrices and Microcellular Foams.* Polym. Eng. Sci., 1995. **35**(14): p. 1167-1177.

59. Collias, D.I. and D.G. Baird, *Impact Behavior of Microcellular Foams of Polystyrene and Styrene-Acrylonitrile Copolymer, and Single-Edge-Notched Tensile Toughness of Microcellular Foams of Polystyrene, Styrene-Acrylonitrile Copolymer, and Polycarbonate.* Polym. Eng. Sci., 1995. **35**(14): p. 1178-1183.

60. Rachtanapun, P., S.E.M. Selke, and L.M. Matuana, *Relationship Between Cell Morphology and Impact Strength of Microcellular Foamed High-Density Polyethylene/Polypropylene Blends.* Polym. Eng. Sci., 2004. **44**(8): p. 1551-1560.

61. Collias, D.I. and D.G. Baird, *Impact toughening of polycarbonate by microcellular foaming.* Polym. J., 1994. **35**(18): p. 3978-3983.

62. Sun, X., et al., *Investigation on the Cell Nucleation and Cell Growth in Microcellular Foaming by Means of Temperature Quenching.* J. Appl. Polym. Sci., 2004. **93**: p. 163-171.

63. Goel, S.K. and E.J. Beckman, *Generation of Microcellular Polymeric Foams Using Supercritical Carbon Dioxide. I: Effect of Pressure and Temperature on Nucleation.* Polym. Eng. Sci., 1994. **34**(14): p. 1137-1147.

64. Kumar, V., *A Process for Making Microcellular Thermoplastic Parts.* Polym. Eng. Sci., 1990. **30**(20): p. 1323-1329.

65. Krause, B., et al., *Microcellular Foaming of Amorphous High-T_g Polymers Using Carbon Dioxide.* Macromolecules, 2001. **34**: p. 874-884.

66. Doroudiani, S., C.B. Park, and M.T. Kortschot, *Processing and Characterization of Microcellular Foamed High-Density Polyethylene/Isotactic Polypropylene Blends.* Polym. Eng. Sci., 1998. **38**(7): p. 1205--1215.

67. Baldwin, D.F., C.B. Park, and N.P. Suh, *A Microcellular Processing Study of Poly(Ethylene Terephthalate) in the Amorphous and Semicrystalline States. Part I: Microcell Nucleation.* Polym. Eng. Sci., 1996. **36**(11): p. 1437-1445.

68. Kumar, V. and J. Weller, *Production of Microcellular Polycarbonate Using Carbon Dioxide for Bubble Nucleation.* J. Eng. Ind., 1994. **116**: p. 413-420.

69. Krause, B., et al., *Open Nanoporous Morphologies from Polymeric Blends by Carbon Dioxide Foaming.* Macromolecules, 2002. **35**: p. 1738-1745.

70. Dai, X., et al., *High damping property of micrcellular polymer prepared by friendly environmental approach.* J. Supercrit. Fluids., 2005. **33**: p. 259-267.

71. Muratani, K., M. Shimbo, and Y. Miyano, *Correlation of Decompression Time and Foaming Temperature on the Cell Density of Foamed Polystyrene.* Cell. Polym., 2005. **24**(1): p. 15-27.

72. Jin, W., et al., *An investigation on the microcellular structure of polystyrene/LCP blends prepared by using supercritical carbon dioxide.* Polym. J., 2001. **42**: p. 8265-8275.

73. Wong, C.-M. and W.-C. Liang, *Porous Polystyrene Foam Produced at Supercritical Conditions.* J. Cell. Plast., 2004. **40**: p. 421-429.

74. Stafford, C.M., T.P. Russell, and T.J. McCarthy, *Expansion of Polystyrene Using Supercritical Carbon Dioxide: Effects of Molecular Weight, Polydispersity, and Low Molecular Weigth Components.* Macromolecules, 1999. **32**: p. 7610-7616.

75. Han, X., et al., *Effect of Die Temperature on the Morphology of Microcellular Foams.* Polym. Eng. Sci., 2003. **43**(6): p. 1206-1220.

76. Baldwin, D.F., *An Extrusion System for the Processing of Microcellular Polymer Sheets: Shaping and Cell Growth Control.* Polym. Eng. Sci., 1996. **36**(10): p. 1425-1435.

77. Park, C.B. and N.P. Suh, *Filamentary Extrusion of Microcellular Polymers Using a Rapid Decompressive Element.* Polym. Eng. Sci., 1996. **36**(1): p. 34-48.

78. Han, X., et al., *Extrusion of Polystyrene Nanocomposite Foams with Supercritical CO_2.* Polym. Eng. Sci., 2003. **43**(6): p. 1261-1275.

79. Behravesh, A.H., C.B. Park, and R.D. Venter. *Extrusion of Low-Density Microcellular HIPS Foams Using CO_2.* in *ASME International Mechanical Engineering Congress and Exposition*. 1996. Atlanta, Georgia: American Society of Mechanical Engineers

80. Park, C.B., A.H. Behravesh, and R.D. Venter, *Low Density Microcellular Foam Processing in Extrusion Using CO_2.* Polym. Eng. Sci, 1998. **38**(11): p. 1812-1823.

81. Han, X., et al., *Continuous Microcellular Polystyrene Foam Extrusion with Supercritical CO_2.* Polym. Eng. Sci, 2002. **42**(11): p. 2094-2106.

82. Lee, P.C., et al., *Increase of Open-Cell Content by Plasticizing Soft Regions With Secondary Blowing Agent.* Polym. Eng. Sci., 2005. **45**: p. 1445-1451.

83. Siripurapua, S., et al., *Generation of Microcellular Foams of PVDF and its Blends Using Supercritical Carbon Dioxide in a Continuous Process.* Polymer., 2002. **43**: p. 5511-5520.

84. Baldwin, D.F., C.B. Park, and N.P. Suh, *Microcellular Sheet Extrusion System Process Design Models for Shaping and Cell Growth Control.* Polym. Eng. Sci., 1998. **38**(4): p. 674-688.

85. Lee, M., C. Tzoganakis, and C.B. Park, *Extrusion of PE/PS Blends with Supercritical Carbon Dioxide.* Polym. Eng. Sci., 1998. **38**(7): p. 1112-1120.

86. Lee, J.W.S., K. Wang, and C.B. Park, *Challenge to Extrusion of Low-Density Microcellular Polycarbonate Foams Using Supercritical Carbon Dioxide.* Ind. Eng. Chem. Res., 2005. **44**: p. 92-99.

87. Lee, P.C., et al. *Extruded Open-cell Foams Using Brittle Polymers with CO_2.* in *ANTEC 2006 - Proceedings of the 64th Annual Technical Conference & Exhibition*. 2006. Charlottle, NC: Society of Plastics Engineers.

88. Xu, J. and D. Pierick, *Microcellular Foam Processing in Reciprocating-Screw Injection Molding Machines.* Journal of Injection Molding Technology, 2001. **5**(3): p. 152-159.

89. Goodship, V., et al., *Microcellular Foaming with Supercritical CO_2 in Injection Moulding.* Cell. Polym., 2004. **23**(1): p. 25-37.

90. Chandra, A., et al., *Microstructure and Crystallography in Microcellular Injection-Molded Polyamide-6 Nanocomposite and Neat Resin.* Polym. Eng. Sci, 2005. **45**(1): p. 52-61.

91. Xu, J. *Effect of Injection Molding Process Parameters on the Morphology and Quality of Microcellular Foams*. in *ANTEC 2006 - Proceedings of the 64th Annual Technical Conference & Exhibition*. 2006. Charlotte, NC: Society of Plastics Engineers.

92. Kumar, V., et al., *Extrusion of Microcellular Foams Using Pre-Saturated Pellets and Solid-State Nucleation.* Cell. Polym., 2004. **23**(6): p. 369-385.

93. Baldwin, D.F., C.B. Park, and N.P. Suh, *A Microcellular Processing Study of Poly(Ethylene Terephthalate) in the Amorphous and Semicrystalline States. Part II: Cell Growth and Process Design.* Polym. Eng. Sci., 1996. **36**(11): p. 1446-1453.

94. Suh, N.P., *Microcellular Plastics*, in *Innovation in Polymer Processing: Molding*, J.F. Stevenson, Editor. 1996, Hanser: New York. p. 93-133.

95. Behravesh, A.H., et al. *Effective Supression of Cell Coalescence During Shaping in the Extrusion of Microcellular HIPS Foams.* in *212th National ACS Meeting*. 1996. Orlando, Florida.

96. Xu, X., et al., *Effects of Die Geometry on Cell Nucleation of PS Foams Blown with CO_2.* Polym. Eng. Sci., 2003. **43**(7): p. 1378-1390.

97. Baird, D.G. and D.I. Collias, *Polymer Processing Principles and Design*. 1998, New York: John Wiley & Sons, INC.

98. Vieth, W.R., *Diffusion in and Through Polymers: Principles and Applications*. 1990, Munich: Hanser Gardner.

99. Ray, S.S. and M. Okamoto, *Polymer/layered Silicate Nanocomposites: A Review From Preparation to Processing.* Prog. Polym. Sci., 2003. **28**: p. 1539-1641.

100. Lee, Y.H., C.B. Park, and K.H. Wang, *HDPE-Clay Nanocomposite Foams Blown with Supercritical CO_2.* J. Cell. Plast., 2005. **41**: p. 486-502.

101. Nam, P.H., et al., *Foam Processing and Cellular Structure of Polypropylene/Clay Nanocomposites.* Polym. Eng. Sci., 2002. **42**(9): p. 1907-1918.

102. Strauss, W. and N.A. D'Souza, *Supercritical CO_2 Processed Polystyrene Nanocomposite Foams.* J. Cell. Plast., 2004. **40**: p. 229-241.

103. Okamoto, M., et al., *Biaxial Flow-Induced Alignment of Silitcate Layers in Polypropylene/Clay Nanocomposite Foam.* Nano. Lett., 2001. **1**(9): p. 503-505.

104. Shen, J., X. Han, and L.J. Lee, *Nanoscaled Reinforcement of Polystyrene Foams Using Carbon Nanofibers.* J. Cell. Plast., 2006. **42**: p. 105-126.

105. Shen, J., C. Zeng, and L.J. Lee, *Synthesis of Polystyrene-Carbon Nanofibers Nanocomposite Foams.* Polym. J., 2005. **46**: p. 5218-5224.

106. Matuana, L.M., C.B. Park, and J.J. Balatinecz, *Processing and Cell Morphology Relationships for Microcellular Foamed PVC/Wood-Fiber Composites.* Polym. Eng. Sci., 1997. **37**(7): p. 1137-1147.

107. Matuana, L.M., C.B. Park, and J.J. Balatinecz, *Cell Morphology and Property Relationships of Microcellular Foamed PVC/Wood-Fiber Composites.* Polym. Eng. Sci., 1998. **38**(11): p. 1862-1872.

108. Bledzki, A.K. and O. Faruk, *Microcellular Wood Fiber Reinforced PP Composites: Cell Morphology, Surface Roughness, Impact, and Odor Properties.* Cell. Polym., 2005. **41**: p. 539-550.

109. Colton, J.S. and N.P. Suh, *Nucleation of Microcellular Foam: Theory and Practice.* Polym. Eng. Sci., 1987. **27**(7): p. 500-503.

110. Colton, J.S. and N.P. Suh, *The Nucleation of Microcellular Thermoplastic Foam With Additives: Part 1: Theorectical Considerations.* Polym. Eng. Sci., 1987. **27**(7): p. 485-492.

111. Colton, J.S. and N.P. Suh, *The Nucleation of Microcellular Thermoplastic Foam with Additives: Part II: Experimental Results and Discussion.* Polym. Eng. Sci., 1987. **27**(7): p. 493-499.

112. Kumar, V. and J.E. Weller. *Bubble Nucleation in Microcellular Polycarbonate Foams*. in *Polymeric Materials: Science and Engineering (PMSE)*. 1992. Washington DC.

113. Kumar, V., *Phenomenology of bubble nucleation in the solid-state nitrogen-polystyrene microcellular foams.* Colloid Surface A., 2005. **263**: p. 336-340.

114. Kweeder, J.A., et al., *The Nucleation of Microcellular Polystyrene Foam.* SPE ANTEC Tech. Papers., 1991. **37**: p. 1398-1400.

115. Ramesh, N.S., D.H. Rasmussen, and G.A. Campbell, *The Heterogeneous Nulceation of Microcellular Foams Assisted by the Survival of Microvoids in Polymers Containing Low Glass Transition Particles. Part I: Mathematical Modeling and Numerical Simulation.* Polym. Eng. Sci., 1994. **34**(22): p. 1685-1697.

116. Ramesh, N.S., D.H. Rasmussen, and G.A. Campbell, *The Heterogeneous Nucleation of Microcellular Foams Assisted by the Survival of Microvoids in Polymers Containing Low Glass Transition Particles. Part II: Experimental Results and Discussion.* Polym. Eng. Sci., 1994. **34**(22): p. 1698-1706.

117. Advani, S.G. and A. Arefmanesh, *Chapter 10: Bubble Growth and Collapse in Viscoelastic Liquids*, in *Advances in Transport Processes IX*, A.S. Mujumdar and R.A. Mashelkar, Editors. 1993, Elsevier Science Publishers B.V.: New York. p. 445-499.

118. Otsuki, Y. and T. Kanai, *Numerical Simulation of Bubble Growth in Viscoelastic Fluid with Diffusion of Dissolved Foaming Agent.* Polym. Eng. Sci., 2005. **45**(9): p. 1277-1287.

119. Han, S., et al., *Numerical Analysis of Microcellular Injection Molding.* J. Cell. Plast., 2003. **39**: p. 465-485.

120. Amon, M. and C.D. Denson, *Study of Dynamics of Foam Growth: Analysis of Growth of Closely Spaced Spherical Bubbles.* Polym. Eng. Sci., 1984. **24**(13): p. 1026-1034.

3 Generation of Low-Density High Performance Poly(arylene ether sulfone) Foams Using a Benign Processing Technique

Desmond J. VanHouten[a], and Donald G. Baird[b*]

[a]Macromolecular Science and Engineering, Virginia Polytechnic Institute and State University, Blacksburg VA 24061
[b]Department of Chemical Engineering, Virginia Polytechnic Institute and State University, Blacksburg VA 24061

Polym. Eng. Sci, 2009. 49(1). 44-51.

Abstract

In this study, an environmentally benign process was used to successfully produce low density foam from poly(arylene ether sulfone) (PAES). Both carbon dioxide (CO_2) and water, as well as nitrogen and water were used as physical blowing agents in a one-step batch process. A large amount of blowing agents (up to 7.5%) was able to diffuse into the PAES resin in a 2 hour saturation time. Utilizing water and CO_2 as the blowing agents yielded foam with better properties than nitrogen and water because both the water and CO_2 are plasticizers for the PAES resin. PAES foam produced from CO_2 and water had a large reduction in foam density (~80 %) and a cell size of ~50 μm, while maintaining a primarily closed-cell structure. The small cell size and closed cell structure enhanced the mechanical properties of the foam when compared to the PAES foam produced from nitrogen and water. The tensile, compressive, and notched izod impact properties of the PAES foams were examined and the compressive properties were compared to commercially available structural foams. With reduced compression strength of 39 MPa and reduced compression modulus of 913 MPa, the PAES foam is comparable to polyetherimide and poly(vinylchloride) structural foams.

3.1 Introduction

Polymeric foams are one important class of lightweight materials under investigation because of their high strength to weight ratio. Polymeric foams can also posses other attractive features such as low moisture absorption, high thermal stability, and good sound and thermal insulation, which depend upon the polymer resin. They are cost effective compared to other lightweight, structural materials[1]. Because of these properties, these materials are used in the automotive, marine, wind-energy, rail, and aeronautical industries[2].

Currently, processes used to produce lightweight, structural, polymeric foams utilize physical blowing agents which are not environmentally friendly. Physical blowing agents, which have a relative high molecular weight and low diffusivity, are necessary to produce low density polymeric foams, especially when the foam is made from a thermoplastic resin[3]. High molecular weight physical blowing agents such as hydrochlorofluorocarbons are used, but they are being phased out because of the detrimental effects they have on the environment. Solvents, such as methylene chloride, are also currently used as physical blowing agents[4]. Because of the effects on the environment, new processes and foaming agents need to be utilized to produce lightweight, structural, polymeric foams.

Numerous studies have been conducted on producing polymeric foams by using supercritical carbon dioxide, $scCO_2$, which is environmentally benign, as the blowing agent[5-16]. These studies include both batch processing, in which the polymer can be molded, and continuous processing, in which polymer is foamed in the extruder or immediately on exiting a die. Regardless of the technique used, the underlying principles

for the production of polymeric foams from $scCO_2$ are the same[7,17]. A high pressure gas is allowed to diffuse into the polymer matrix. A supersaturated state of the gas is then obtained by either rapidly increasing the temperature of the saturated polymer or reducing the pressure. The supersaturated state causes cells to nucleate and grow until either the concentration of the gas becomes too low to cause cell growth or vitrification of the polymer occurs and inhibits the cell growth.

Supercritical carbon dioxide has several advantages in producing polymeric foams when compared to conventional physical blowing agents[17,18]. It is non-toxic, non-flammable, chemically inert, and inexpensive. Supercritical carbon dioxide is also known to plasticize a number of polymers, which reduces their viscosity at a given temperature and lowers their glass transition temperatures, T_g[19]. The plasticization of the polymers also allows for processing at lower temperatures and for the resulting cell size of the polymeric foam to be controlled[20].

Martini-Vvedensky et al.[21] first used $scCO_2$ as a blowing agent to produce foams that had microcellular foam morphology. Microcellular foams are defined as having a cell size less than 10 μm and a cell nucleation density between 10^9 and 10^{15} cells/cm^3. It was thought that if the cell size was kept smaller than the size of the critical flaw, lightweight material could be produced without compromising the mechanical integrity of the foam. Since the initial development of microcellular foams, very little research has been reporting concerned with extending the technique to high T_g thermoplastics.

Microcellular morphologies enhance some of the mechanical properties of the foam. Because of an increase in the elongation at break under a tensile load, the

toughness of the foams increases when compared to the neat polymer[22]. The presence of small cells also increases the notched impact toughness of some polymeric foams[23,24]. When the impact failure mode changes from brittle fracture to ductile fracture, due to the crack blunting capabilities of the small cells, the impact toughness greatly increases.

Sun et al.[25,26] have applied the technique to several high performance polymers. The polymers were foamed using $scCO_2$ as the blowing agent in a two-step process. Polymer sheets (1.5 mm thick) of poly(phenylsulfone) (Radel R-5000) were saturated at room temperature for 70 hours. After saturating the sheets for 70 hours, it was determined that 8.0% of carbon dioxide was able to diffuse into the sample. The saturated polymer sheet was then submerged into an oil bath in order to induce cell nucleation and growth. The samples were quenched in order to induce vitrification, thus stopping cell growth. By using carbon dioxide as the blowing agent in a two-step batch process, foam with a density of 500 kg/m^3 (approximately 60% density reduction) for the poly(phenylsulfone) was obtained. Because many applications require a foam with a density less than 300 kg/m^3, a greater reduction in density is desired.

In the work by Sun et al.[25,26], the density reductions of the foams were limited by the choice of blowing agent. Though the authors reported 8.0% $scCO_2$ was able to diffuse into the polymer, the cell growth was inhibited by the rapid loss of the $scCO_2$ out of the polymer during the foaming process. In order to obtain foam with a higher density reduction, either more cells would need to be nucleated initially and allowed to grow to the same size as the authors reported or the process would need to be altered to allow for a larger cell growth.

Water has also been used as a benign blowing agent to produce polymeric foams. In a study published by Brandom et al.[27], a blend of polyetherimide (PEI) and poly(aryl ether ketone) (PAEK) was foamed utilizing water as the blowing agent. Pellets of the PEI and PAEK were melt blended in a single screw extruder. Upon mixing in the extruder, the diamine end groups on the PEI reacted with the ketone groups in the PAEK and produced water as a byproduct. Because the extrusion was taking place at 350 ^{o}C, the water produced was in the gaseous form. The gaseous water acted as a blowing agent for the polymer. By varying the residence time of the polymer in the extruder, the foam density was controlled, with a maximum of 60% reduction in foam density obtained.

Water could be used as an ideal physical blowing agent for certain polymer resins. An ideal physical blowing agent must not react with the polymer, be readily incorporated in the polymer matrix, thermally stable in the gaseous state, nontoxic, economically feasible, and environmentally safe[28]. It must also possess low vapor pressure at room temperature, a low rate of diffusion in the polymer, and low flammability or combustibility. Water inherently possesses several of these characteristics. Also, the polymer could become supersaturated with water rapidly if the water was quickly transformed from liquid to a gas. Water can remain a liquid at temperatures well above 100 ^{o}C, as long as sufficient pressure is applied. The necessary pressure is readily obtained from a water phase diagram. If incorporated into polymer that is compatible with water, water could be used as an environmentally benign physical blowing agent.

Poly(arylene ether sulfone) (PAES) has several characteristics that are desired in lightweight, structural applications. PAES is thermally stable at high temperatures, exhibits outstanding toughness, and is combustion resistant[29]. In addition to these

properties, water is also readily absorbed into the polymer resin at high temperatures and pressures (220 ^{o}C and 1500 psi, respectively).

Our research incorporates the concepts of microcellular foaming, along with the use of water as a benign blowing agent to produce foam with a density of 250 kg/m^3 (~80% density reduction) from PAES. PAES was foamed utilizing a combination of blowing agents in a one-step batch processing scheme. Both $scCO_2$ and water, as well as nitrogen and water, were used as the blowing agents in the process. At a pressure greater than 2.2 MPa, the water remains liquid at the elevated processing temperature (220 ^{o}C)[30]. The polymer becomes saturated with the liquid water and upon rapid depressurization of the system, the liquid turns to gas causing cell nucleation and growth. The use of gas and water as the blowing agents produces foam with a large density reduction. The foam morphology, as well as tensile, compressive, and impact properties of the resulting foams are presented. Because the foams exhibit a potential for use in structural applications, the mechanical properties of the foams are compared to several commercially available polymeric structural foams with similar foam densities (110 to 320 kg/m^3).

3.2 Experimental

3.2.1 Materials

Poly(arylene ether sulfone) (PAES, Radel® R-5800) was generously supplied by Solvay Advanced Polymers (Alpharetta, GA). The glass transition temperature (T_g) and density of the polymer were 220 ^{o}C and 1.29 g/cm^3, respectively. Carbon dioxide and compressed nitrogen were obtained from Airgas, Inc.

3.2.2 Foaming Procedure

The PAES foams were produced using a one-step batch process method. A cylindrical stainless steel mold measuring 3 cm in diameter by 12.5 cm in length was filled with the PAES resin and liquid water (a 2:1 w/v ratio was used for polymer:water). The mold was placed inside a pressure vessel. The pressure vessel was sealed and charged with a predetermined amount of either carbon dioxide (5.5 MPa) or nitrogen (6.9 MPa). The pressure vessel was heated to 220 ^{o}C, the T_g of the unsaturated polymer, which caused the pressure to increase to between 10 - 11 MPa. Foaming has been performed at temperatures from 165 to 220 ^{o}C. However, a temperature of 220 ^{o}C yielded foam with the greatest density reduction. The gas was allowed to diffuse into the PAES for 2 h, which assured full saturation. The pressure was rapidly released (less than 2 s) and the mold was removed. The mold was allowed to cool to room temperature before removing the foamed specimen.

3.2.3 Thermal Analysis

A TA Q1000 differential scanning calorimeter (DSC) was used to determine the T_g of the samples. Scans were conducted under nitrogen from -20 to 260 ^{o}C at a heating rate of 10 ^{o}C/min. PAES was saturated with the gas and water at 220 ^{o}C and 10.3 MPa for 2 hours. The temperature was cooled to room temperature, to eliminate blowing agent loss due to foaming, and the PAES was removed from the vessel. The PAES sample was sealed in the DSC pan immediately after removal from the vessel. High volume DSC pans with rubber seals (TA instruments) were used to minimize the loss of blowing agents during testing.

A TA Q500 thermogravimetric analyzer (TGA) was used to determine the amount of blowing agents present in the PAES resin. PAES was saturated with the blowing agent(s) at 220 ^{o}C and 10.3 MPa or 17.2 MPa for 2 hours. The temperature was cooled to room temperature, to eliminate blowing agent loss due to foaming, and the PAES was removed from the vessel. The test was begun immediately after removal from the vessel. Samples were run from 25 ^{o}C to 600 ^{o}C at a heating rate of 10 ^{o}C/min under a nitrogen atmosphere.

3.2.4 Characterization

3.2.4.1 Foam Density

The foam density was determined using the water displacement method. A foam specimen was weighed and then submerged in water. The displaced water was then measured to determine the volume of the foam. Because the foam has a thin skin layer on the surface and a predominately closed cell structure, water uptake is negligible during the measurements.

3.2.4.2 SEM Imaging

The cell size and structure of the foamed polymer was determined using a Leo 1550 field emission scanning electron microscope (FE-SEM). The foam specimen was freeze fractured and sputter coated with 20 nm of gold. The FE-SEM was operated at 5 kV.

3.2.4.2.1 Determination of Cell Size and Cell Nucleation Density

The SEM images were analyzed using ImageJ image processing software. Typically micrographs containing 25 to 50 cells were used to determine the average cell diameter and 100 to 200 cells to determine the cell nucleation density.

The cell nucleation density, N_o, was calculated using the method reported by Kumar and Weller and given by Eq. (3.1)[31]. In Eq.(3.1), n is the number of cells in the micrograph, M is the magnification, A is the area micrograph in cm^2, and V_f is the void fraction of the foam. V_f can be estimated from Eq.(3.2), where D represents the average diameter of the cells.

$$N_o = \left(\frac{nM^2}{A} \right)^{3/2} \frac{1}{\left(1 - V_f\right)} \tag{3.1}$$

$$V_f = \frac{\pi}{6} D^3 \left(\frac{nM^2}{A} \right)^{3/2} \tag{3.2}$$

3.2.5 Mechanical Properties

3.2.5.1 Tensile Testing

The tensile properties of the foam were determined using an Instron 4204 and ASTM D638 was used as a guide for testing. Due to sample size limitation the ASTM test method was not followed exactly. Five rectangular samples measuring 45 mm in length, 10 mm in width, and 3 mm in thickness were cut from a large specimen of the PAES foam. The gauge length was set to 20 mm and the samples were tested at a constant speed of 1.27 mm/min. The strain was calculated from the displacement of the crosshead. The modulus was determined by applying a least-squares fit through the initial linear region of the stress-strain curve. The modulus represents an average of the five foam specimens.

3.2.5.2 Compression Testing

The compressive properties of the foam were measured using a MTS (model 826.75) 50,000 lbs servo hydraulic test system. ASTM D1621 was used as a guide for testing, however, due to sample size limitations the test method was not followed exactly. Five cylindrical samples measuring 30 mm in diameter and 40 mm length were cut from a large specimen of the PAES foam and the foam properties were determined from the average of the five samples. A lathe was used to cut the samples to ensure the cuts were perpendicular to the cylinder wall. The samples were compressed at a rate of 2.5 mm/min. The strain was calculated from the displacement of the crosshead and the modulus was determined by applying a least-squares fit through the initial linear region of the stress-strain curve.

3.2.5.3 Impact Testing

The impact strengths of the foams were determined using ASTM D256-06a. Five samples measuring 63 mm in length, 12.7 mm in width, and 3.2 mm thick were cut from a large specimen of the PAES foam. A sharp notch was cut into the sample using a Tinius Olsen Model 899 specimen notcher (Horsham, PA) turning at a high rotational speed. The notched specimens were tested using a Tinius Olsen 897 machine (Horsham, PA). Because the specimens were thinner than the ideal ASTM thickness, care was taken to ensure the samples did not buckle during impact.

3.3 Results and Discussion

3.3.1 Determination of Plasticization of PAES resin

All of the foams were produced using the one-step batch processing method. In the one-step batch process, the polymer was first saturated with the blowing agents of

interest. As the polymer was saturated with the blowing agents, plasticization occurred which caused a reduction in the T_g[17]. The saturated resin was then subjected to a rapid pressure drop. The rapid pressure release causes a thermodynamic instability which nucleates the cells and the cells grow. During the nucleation and growth process, the blowing agents diffuse out of the polymer resin, which causes the suppressed T_g to increase. Cell growth is inhibited by vitrification once the suppressed T_g reaches the foaming temperature which is just below the Tg of the neat polymer. Because the cell growth is inhibited by vitrification, the cell size can be controlled by the amount of plasticization or by the rate of diffusion of the blowing agent out of the polymer[7].

The effect of the saturation pressure on the diffusion of the blowing agents into the PAES resin was determined with TGA and the results are shown in Figure 3.1. For both saturation pressures of 10.3 and 15.2 MPa, the same amount of CO_2 and water were able to diffuse into the polymer during the saturation time. Because there was not a significant effect on the diffusion of the blowing agents into the PAES at the different pressures, the lower pressure of 10.3 MPa was chosen for the rest of the experiments.

The amount of blowing agents in the resin affects the suppression of the T_g of the polymer. TGA was used to quantify the amount of blowing agents that diffused into the polymer, and the results are shown in Figure 3.2**.** From TGA, it was determined that ~2.8% of CO_2 was able to diffuse into the PAES during the 2 hour saturation time at 220 ^oC and 10.3 MPa. However, when both $scCO_2$ and water were used as the blowing agents, 7.5% of CO_2 and water combined diffused into the polymer. Because only 2.8% of CO_2 diffused into the PAES under the saturation conditions, the additional 4.7% is attributed to the water. When nitrogen and water were used, a combined level of 4.3% of

the blowing agents diffused into the polymer, of which 3.9% is attributed to water. As can be seen in Figure 3.2, the solubility of nitrogen in the PAES is 0.4%.

The amount of water increases significantly when CO_2 and water are the blowing agents, as compared to saturating the polymer with nitrogen and water. The increased solubility of water in the PAES is believed to be due to the carbon dioxide. Water is known to be soluble in scCO_2[32]. Thus, more water is present in the PAES which contributes to the formation of a lower density PAES foam.

The DSC thermograms of the plasticized PAES resin are shown in Figure 3.3. The DSC results exhibited a plasticized T_g for the saturated polymer, followed by an endothermic peak. The endothermic peak is attributed to the adiabatic expansion of the gas as it diffuses out of the polymer once the plasticized T_g is surpassed.

The combination of CO_2 and water yielded the greatest reduction in T_g, which correlates to the greater amount of blowing agents determined from TGA. When CO_2 and water were utilized as the blowing agents, the T_g was reduced from 220 to 160 ^oC. When the combination of N_2 and water was used the T_g was only suppressed to 175 ^oC. The additional suppression of the T_g is attributed to the CO_2 which acts also as a plasticizer.

Quantifying the amount of blowing agents in the polymer and the suppression of the T_g is important for understanding the fundamentals of the foam production and for controlling the foam density. Because cell growth is inhibited by vitrification in the one-step batch processing method, the suppression of the T_g controls the cell size and, ultimately, the foam density. In the one-step batch foaming process both a foaming temperature, T_f, and the plasticized T_g exist. Research by Krause et al.[7] showed that if

T_f was less than the plasticized T_g, no foaming could occur. This is because the viscosity of the polymer is infinitely large. Therefore, T_f must be higher than the plasticized T_g. The magnitude of the difference between the plasticized T_g and T_f can be used to control the cell size. The further that T_f is from the plasticized T_g, the longer the cells can grow before vitrification occurs and, thus, larger cells are obtained. The research by Krause et al.[7] also showed that the T_f is bound by an upper limit. The upper limit is near the T_g of the unsaturated (neat) polymer. Because the upper limit on T_f is controlled by a material property and cannot be changed, a larger suppression of the T_g is necessary to produce foam with a large density reduction using the one-step batch processing method.

3.3.2 Characterization of the Foam Density and Morphology

The foam densities of the PAES foams are shown in Table 3.1. As expected, based on the DSC and TGA results, the combination of CO_2 and water as the blowing agents for the PAES resin yielded foam with a greater density reduction than when N_2 and water were used. As determined from the DSC, the combination of CO_2 and water reduced the T_g of the PAES by 60 ^oC, where as the nitrogen and water reduced the T_g by 45 ^oC. This additional plasticization yielded foam with a greater reduction in the foam density. A foam density of 244 kg/m^3, obtained from CO_2 and water, represents a 50% decrease in foam density relative to previous efforts which also utilized a benign foaming process[25,26].

The cell size and nucleation density were determined from SEM images, which can be seen in Figures 3.4 and 3.5, respectively. Although the CO_2 and water yield PAES foam with a larger reduction in foam density than N_2 and water, the cell size is smaller and cell nucleation density is larger when the CO_2 and water are used. Both combinations

of blowing agents yielded foam which had a predominantly closed cell structure, which is important for enhanced mechanical properties[33].

3.3.3 Mechanical Properties of the PAES Foam

The mechanical properties of the PAES foams were measured to determine their potential for use in structural applications. The tensile, compressive and impact properties of the PAES foams were tested. Compressive properties of various commercial structural foams are used as a comparison for the PAES foams.

Tensile results are shown in Figure 3.6 and Table 3.2 for the PAES foams. From Figure 3.6, the PAES foam produced from CO_2 and water yields a material that is both stronger and more ductile when compared to the foam produced from N_2 and water. The increases in strength and ductility are attributed to the smaller cell size of the foam. The tensile modulus is also greater when CO_2 and water are used, shown in Table 3.2. The foam produced from CO_2 and water has a modulus of 177.1 MPa, whereas the foam produced from nitrogen and water has a modulus of 122.4, despite having a greater foam density. The increase observed in the tensile modulus of the foam produced from CO_2 and water is attributed to the smaller cell size and the greater abundance of a closed cell structure.

The tensile moduli for both of the foams are lower than unfoamed PAES, which is expected from conventional foam theory[33]. The theory states that the modulus of the foam decreases as a function of the foam density, as can be seen in Eq.(3.3). In Eq. (3.3), E represents the modulus and ρ represents the foam density, and the subscripts f and s denote the foam and the solid polymer, respectively. The moduli of the foams, as predicted by conventional foam theory, can be seen in Table 3.2. The modulus of the

foam produced with CO_2 and water is higher than the theoretical modulus, and this is attributed to the foam having a predominantly closed cell structure[33]. However, the foam produced with N_2 and water has a modulus which is slightly less than predicted.

$$\frac{E_f}{E_s} = \left(\frac{\rho_f}{\rho_s}\right)^2 \tag{3.3}$$

The properties of the PAES foam when subjected to a compressive load were also determined. The relative compressive strengths and moduli of the PAES foams are shown in Figure 3.7 and Table 3.2, respectively. As was observed in the tensile properties, the PAES foam produced with CO_2 and water exhibits significantly greater compressive properties than the foam produced with N_2 and water. This is also attributed to the smaller cell size of the foam produced with CO_2 and water.

Three commercially available structural foams, Airex® R82 (polyetherimide foam, PEI), Rohacell® WF (polymethacrylimide foam, PMI), and Divinycell® H (poly(vinyl chloride) foam, PVC), were used as a comparison for the compressive properties of the PAES foams. The commercial foams are referred to as their polymer abbreviation, followed by a number denoting the foam density in kg/m^3. The PVC and PMI foams were chosen for the comparison because they are both used in structural applications. Both PMI (T_g = 140 ^oC) and PVC (T_g = 81 ^oC) have low T_g's compared to PAES, and, thus the structural properties of the foams significantly decrease at temperature greater than 140 ^oC. The PEI110 (T_g = 225 ^oC) was chosen because it has a similar T_g to the PAES. All of the commercial foams have cell sizes between 300 and 600 μm, which are significantly greater than the PAES foams[34,35].

A comparison of the compressive properties to commercially available structural foams with similar densities is shown in Table 3.2 and Figure 3.7. Because of slight variations among the densities of the foams, the relative compressive strengths are used for the comparison. Both PAES foams exhibit relative compressive strengths that are comparable to or better than PEI110, PVC250 and PVC300[2,36]. However, the relative compressive strengths are much less than that of the PMI200 and PMI300, despite having a smaller cell size. The PMI foams have some of the highest strength to weight ratios of any polymeric foam, but these foams have limited high temperature applications[2]. The PAES foams have greater relative compression moduli than PEI110. However, the relative compression modulii of the PAES foams are significantly lower than PVC250 and PVC300. The cell size does not affect the compressive properties between the foams produced from different polymer resins, but when comparing the two different PAES foams the smaller cell size leads to greater compressive properties.

The impact strength of the PAES foams was determined by using a notched izod impact test. The results of the test are shown in Table 3.2. The notched izod impact results follow the same trend as the tensile and compressive properties. The PAES produced from CO_2 and water has greater relative compression strength than the PAES foam produced from nitrogen and water. Like the tensile and compressive properties, this is attributed to a smaller cell size and greater cell nucleation density. When compared to unfoamed PAES, the relative impact strength is lower for the PAES foams. Collias and Baird[24] report that a 15.7 times increase in the notched impact strength of polycarbonate foam compared to unfoamed polycarbonate, which was attributed to the fracture going from brittle in the unfoamed polycarbonate to ductile in the polycarbonate

foam. Because the unfoamed PAES already exhibited ductile fracture, it was not expected that the PAES foams would have greater impact strength than unfoamed PAES.

3.4 Conclusions

PAES foam was successfully produced by means of an environmentally benign process. Both CO_2 and water, as well as, N_2 and water were used as blowing agents to produce the PAES foam in a one-step batch foaming process. PAES foam produced using the combination of N_2 and water had a foam density ranging between 350 to 490 kg/m^3. This correlates to a density reduction of 62 to 72%. The cell size and cell nucleation density of the foam was 156 μm and $7.03x10^5$ $cells/cm^3$, respectively. The PAES foam produced using CO_2 and water as the blowing agents exhibited much better properties. The foam density was 250 kg/m^3, an 81% reduction in foam density, which is comparable to several commercially available structural foams. The cell size was 54 μm and the cell nucleation density was $1.85x10^7$ $cells/cm^3$, which are both improvements upon the PAES foam produced from N_2 and water.

The mechanical properties of the resulting PAES foams were also determined. Though both foams exhibited much lower reduced tensile and compressive properties than unfoamed PAES polymer, the PAES foamed produced using CO_2 and water as the blowing agents performed relatively well. The tensile modulus was much better than theoretically predicted from conventional foam theory. The relative impact strength of the PAES foams was less than unfoamed PAES, which was expected because unfoamed PAES already fractured in a ductile manner during impact. Also the compressive properties were similar to some polymeric structural foams which are used commercially. Because the mechanical properties compare well with the commercial foams, the PAES

foam produced using CO_2 and water as the blowing agents exhibit a potential for use in future structural foam applications.

3.5 Acknowledgements

Parts of this work were carried out using instruments in the Nanoscale Characterization and Fabrication Laboratory, a Virginia Tech facility operated by the Institute for Critical Technology and Applied Science. The authors would also like to acknowledge the Wood Engineering Lab at Virginia Tech for use of the MTS compression testing machine.

3.6 References

1. Altstädt, V., et al., *Polymer Foams as Core Materials in Sandwich Laminates (Comparison with Honeycomb).* Polym. Polym. Compos., 1998. **6**(5): p. 295-304.

2. Marshall, A.C., *Core Composite and Sandwich Structures*, in *International Encyclopedia of Composites*, S.M. Lee, Editor. 1990, VCH Publishers Inc. p. 488-507.

3. Lee, S.T., C.B. Park, and N.S. Ramesh, *Polymeric Foams: Science and Technology*. Polymeric Foams Series, ed. S.T. Lee. 2007, Boca Raton: CRC Press.

4. Krutchen, C.M. and W.P. Wu, *Polymer Foam, Thermoformed Shapes and Methods of Forming It*. 1985, Mobil Oil Corporation: USA.

5. Doroudiani, S., C.B. Park, and M.T. Kortschot, *Effect of the Crystallinity and Morphology on the Microcellular Foam Structure of Semicrystalline Polymers.* Polym. Eng. Sci., 1996. **36**(21): p. 2645-2662.

6. Kumar, V., *A Process for Making Microcellular Thermoplastic Parts.* Polym. Eng. Sci., 1990. **30**(20): p. 1323-1329.

7. Krause, B., et al., *Microcellular Foaming of Amorphous High-T_g Polymers Using Carbon Dioxide.* Macromolecules, 2001. **34**: p. 874-884.

8. Doroudiani, S., C.B. Park, and M.T. Kortschot, *Processing and Characterization of Microcellular Foamed High-Density Polyethylene/Isotactic Polypropylene Blends.* Polym. Eng. Sci., 1998. **38**(7): p. 1205--1215.

9. Baldwin, D.F., C.B. Park, and N.P. Suh, *A Microcellular Processing Study of Poly(Ethylene Terephthalate) in the Amorphous and Semicrystalline States. Part I: Microcell Nucleation.* Polym. Eng. Sci., 1996. **36**(11): p. 1437-1445.

10. Kumar, V. and J. Weller, *Production of Microcellular Polycarbonate Using Carbon Dioxide for Bubble Nucleation.* J. Eng. Ind., 1994. **116**: p. 413-420.

11. Lee, K.-N., H.-J. Lee, and J.-H. Kim, *Preparation and morphology characterization of microcellular styrene-co-acrylonitrile (SAN) foam processed in supercritical CO2.* Polym. Int., 2000. **49**: p. 712-718.

12. Goel, S.K. and E.J. Beckman, *Generation of Microcellular Polymeric Foams Using Supercritical Carbon Dioxide. I: Effect of Pressure and Temperature on Nucleation.* Polym. Eng. Sci., 1994. **34**(14): p. 1137-1147.

13. Stafford, C.M., T.P. Russell, and T.J. McCarthy, *Expansion of Polystyrene Using Supercritical Carbon Dioxide: Effects of Molecular Weight, Polydispersity, and Low Molecular Weigth Components.* Macromolecules, 1999. **32**: p. 7610-7616.

14. Baldwin, D.F., *An Extrusion System for the Processing of Microcellular Polymer Sheets: Shaping and Cell Growth Control.* Polym. Eng. Sci., 1996. **36**(10): p. 1425-1435.

15. Park, C.B. and N.P. Suh, *Filamentary Extrusion of Microcellular Polymers Using a Rapid Decompressive Element.* Polym. Eng. Sci., 1996. **36**(1): p. 34-48.

16. Lee, M., C. Tzoganakis, and C.B. Park, *Extrusion of PE/PS Blends with Supercritical Carbon Dioxide.* Polym. Eng. Sci., 1998. **38**(7): p. 1112-1120.

17. Cooper, A.I., *Polymer Synthesis and Processing Using Supercritical Carbon Dioxide.* J. Mater. Chem., 2000. **10**: p. 207-234.

18. Nalawade, S.P., F. Picchioni, and L.P.B.M. Janssen, *Supercritical Carbon Dioxide as a Green Solvent for Processing Polymer Melts: Processing Aspects and Applications.* Prog. Polym. Sci., 2006. **31**: p. 19-43.

19. Tomasko, D.L., et al., *A Review of CO_2 Applications in the Processing of Polymers.* Ind. Eng. Chem. Res., 2003. **42**: p. 6431-6456.

20. Wilding, M., *Ph.D. Thesis: Melt Processing of Thermally Unstable and High Molecular Weight Polymers with Supercritical Carbon Dioxide*, in *Chemical Engineering*. 2007, Virginia Polytechnic Institute and State University: Blacksburg. p. 215.

21. Martini-Vvedensky, J.E., N.P. Suh, and F.A. Waldman, *Microcellular Closed Cell Foams and Their Method of Manufacture*. 1984, Massachusetts Institute of Technology: United States.

22. Collias, D.I. and D.G. Baird, *Tensile Toughness of Microcellular Foams of Polystyrene, Styrene-Acrylonitrile Copolymer, and Polycarbonate, and the Effect of Dissolved Gas on the Tensile Toughness of the Same Polymer Matrices and Microcellular Foams.* Polym. Eng. Sci., 1995. **35**(14): p. 1167-1177.

23. Rachtanapun, P., S.E.M. Selke, and L.M. Matuana, *Relationship Between Cell Morphology and Impact Strength of Microcellular Foamed High-Density Polyethylene/Polypropylene Blends.* Polym. Eng. Sci., 2004. **44**(8): p. 1551-1560.

24. Collias, D.I. and D.G. Baird, *Impact toughening of polycarbonate by microcellular foaming.* Polym. J., 1994. **35**(18): p. 3978-3983.

25. Sun, H., G.S. Sur, and J.E. Mark, *Microcellular foams from polyethersulfone and polyphenylsulfone: Preparation and mechanical properties.* Eur. Polym. J., 2002. **38**: p. 2373-2381.

26. Sun, H. and J.E. Mark, *Preparation, Characterization, and Mechanical Properties of Some Microcellular Polysulfone Foams.* J. Appl. Polym. Sci., 2002. **86**: p. 1692-1701.

27. Brandom, D.K., et al., *New Method for Producing High-Performance Thermoplastic Polymeric Foams.* J. Appl. Polym. Sci., 1997. **66**: p. 1543-1550.

28. *Polymeric Foams and Foam Technology*. 2nd ed, ed. D. Klempner and V. Sendijarevic. 2004, Cincinnatti: Hanser Gardener Publications. 584.

29. Domine, J.D., *Radel poly(phenylsulfone) - a new, tough, engineering polymer.* Technical Papers, Regional Technical Conference - Society of Plastics Engineers, 1977(Injection Molding Eng. Thermoplast., June 8-9): p. 96-104.

30. in *Perry's Chemical Engineers' Handbook*, R.H. Perry and D.W. Green, Editors. 1997, McGraw-Hill.

31. Kumar, V. and J.E. Weller, *Microcellular polycarbonate - Part I: Experiments on bubble nucleation and growth.* SPE ANTEC Tech. Papers., 1991. **37**: p. 1401-5.

32. Sabirzyanov, A.N., et al., *Solubility of Water in Supercritical Carbon Dioxide.* High Temp., 2002. **40**(2): p. 231-234.

33. Gibson, L.J. and M.F. Ashby, *Cellular Solids: Structure and Properties*. 1988, New York: Pergamon.

34. Anderson, W.B. and R.S. Lakes, *Size effects due to Cosserat elasticity and surface damage in closed-cell polymethacrylimide foam.* J. Mater. Sci., 1994. **29**(24): p. 6413-19.

35. Thomsen, O.T., et al., *Sandwich Structures 7: Advancing with Sandwich Structures and Materials*. 2005. 1031 pp.

36. Kuwabara, A., et al., *Basic mechanical properties of balloon-type TEEK-L polyimide-foam and TEEK-L filled aramid-honeycomb core materials for sandwich structures.* Advanced Composite Materials, 2005. **14**(4): p. 343-363.

Table 3.1 Foam Density and Morphology of PAES Foam

Blowing Agent	Foam Bulk Density kg/m^3	Average Cell Size μm	Cell Nucleation Density $cells/cm^3$
CO_2/water	244	54	$1.85x10^7$
N_2/water	490	156	$7.03x10^5$

Table 3.2. Summary of the Mechanical Properties of the PAES Foam and Commercially Available PEI and PVC Foam

	Density kg/m^3	Tensile Modulus MPa	Stress at Break MPa	Theoretical Tensile Modulus MPa	Relative Compressive Modulus MPa	Relative Impact Strength J/m
Unfoamed PAES	1290	2300	70	-	-	537.4 ± 6.2
PAES CO_2/water	245	177.1 ± 27.4	9.7	82.3	912.5 ± 60.2	305.5 ± 55.6
PAES N_2/water	335	122.4 ± 16.1	6.2	154.2	518.6 ± 70.0	225.4 ± 80.7
PEI-110 [36]	110	-	-	-	504.3	-
PVC-250 [2]	250	-	-	-	1187	-
PVC-300 [2]	300	-	-	-	1376	-

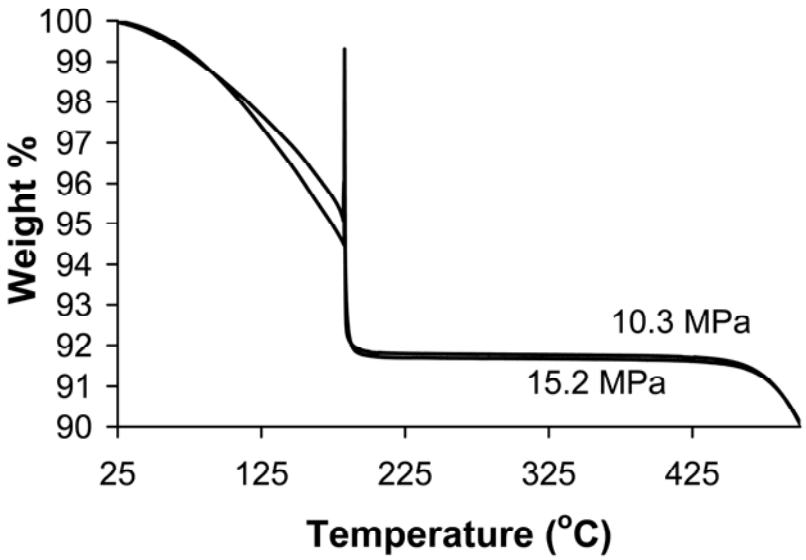

Figure 3.1. Effect of saturation pressure on the diffusion of the blowing agents into the PAES resin. The PAES resin was saturated with CO_2 and water at 220 °C for 2 hours at 10.3 MPa and 15.2 MPa. The TGA was run at a heating rate of 10 °C/min under a nitrogen atmosphere.

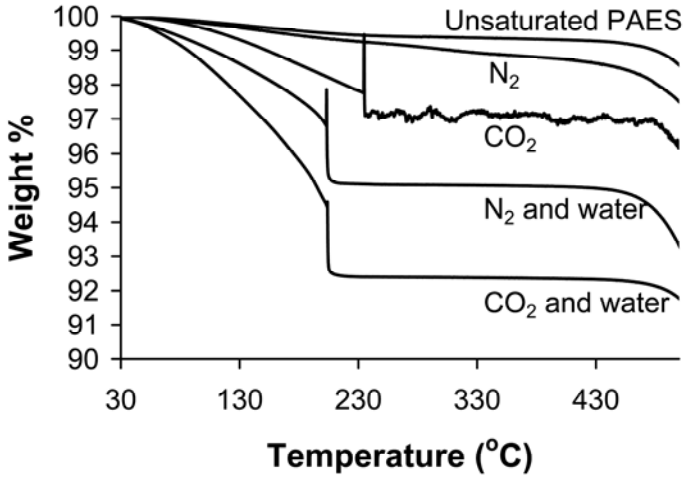

Figure 3.2. TGA results quantifying the amount of blowing agents that were able to diffuse into the PAES resin. The resin was saturated for 2h at 220 ^{o}C and a pressure of 10.3 MPa. Results are shown for unsaturated PAES, PAES saturated with N_2, PAES saturated with CO_2, PAES saturated with CO_2 and water, and PAES saturated with N_2 and water. The TGA was run at a heating rate of 10 ^{o}C/min under a nitrogen atmosphere.

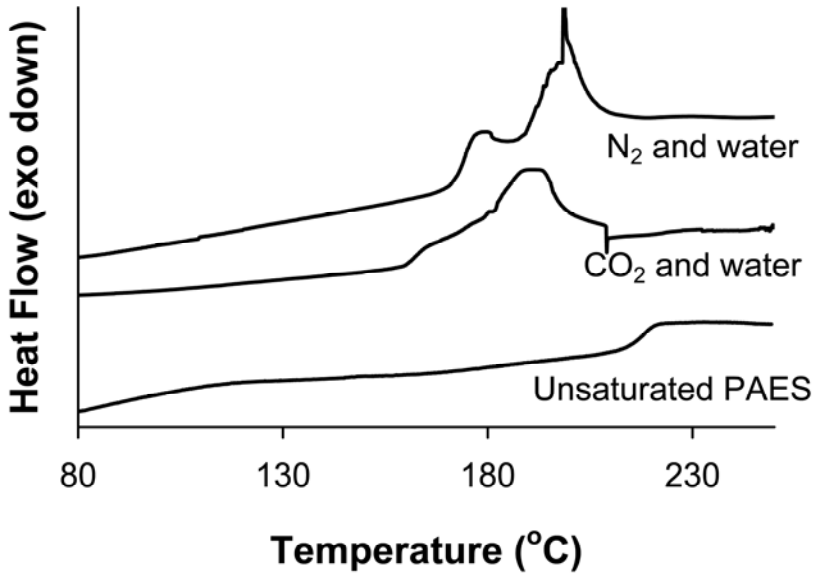

Figure 3.3. DSC results quantifying the plasticized T_g of the PAES resin. The resin was saturated for 2h at 220 ^oC and a pressue of 10.3 MPa. Results are shown for unsaturated PAES, PAES saturated with CO_2 and water, and PAES saturated with N_2 and water. The DSC was run at a rate of 10 ^oC/min in a nitrogen atmosphere. The data has been shifted so the results could be seen more clearly.

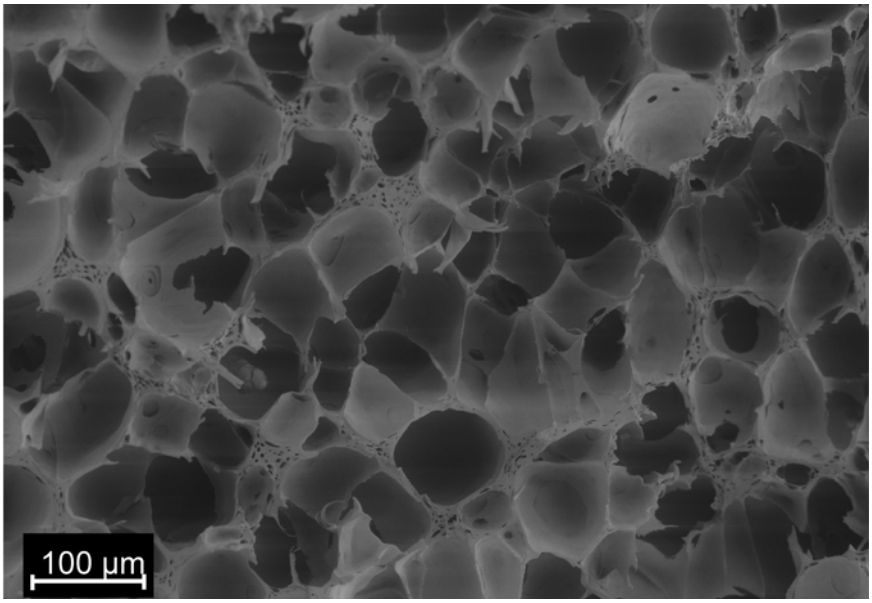

Figure 3.4. SEM image of PAES foam produce in a one-step batch process utilizing a combination of CO_2 and water as the blowing agents. The PAES subjected to the CO_2 and water for 2 hours at 220 ^{o}C under a pressure of 10.3 MPa and foamed at a temperature of 220 ^{o}C.

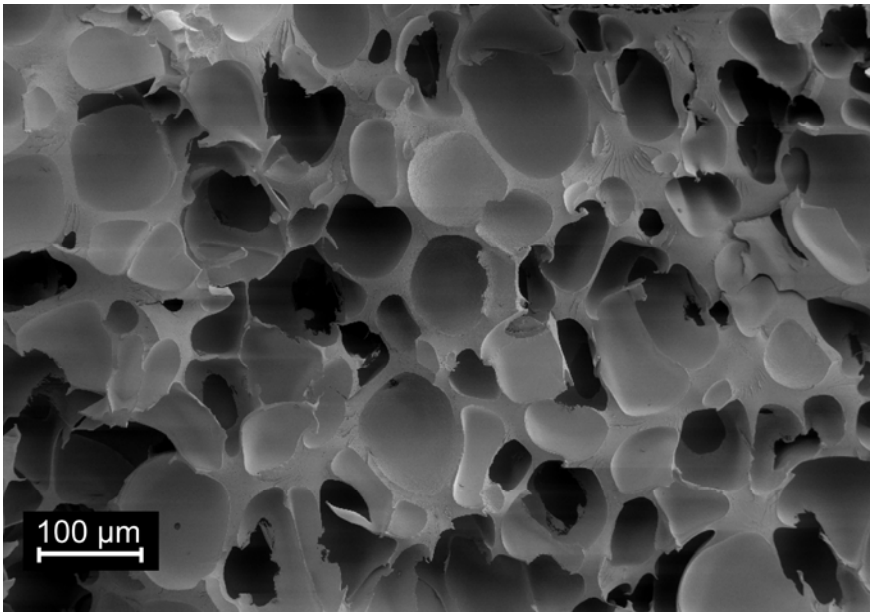

Figure 3.5. SEM image of PAES foam produce in a one-step batch process utilizing a combination of N_2 and water as the blowing agents. The PAES subjected to the N_2 and water for 2 hours at 220 ^{o}C under a pressure of 10.3 MPa and foamed at a temperature of 220 ^{o}C.

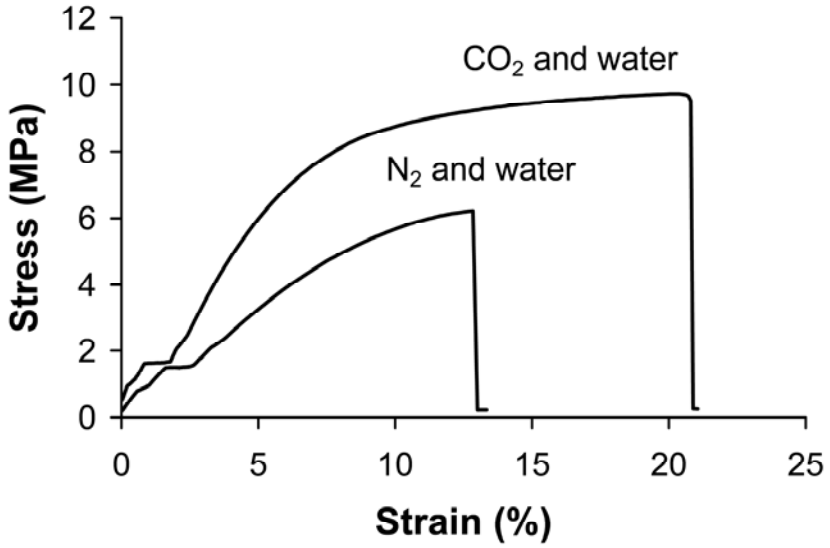

Figure 3.6. Stress-strain curve for PAES foam produced by using combination of CO_2 and water, and N_2 and water under a tensile load. The samples were tested at a rate of 1.27 mm/min.

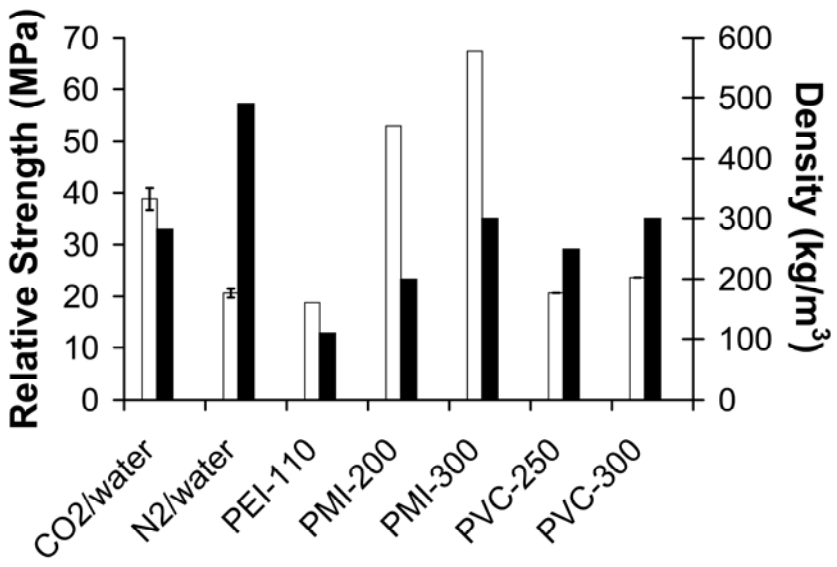

Figure 3.7. Relative compressive strength (□) and foam density (■) of the PAES foam produced by using CO_2 and water, and N_2 and water as the blowing agents. The compressive strength of commercially available PEI, PMI, and PVC foams are shown for comparison.[2,36] The samples were compressed at a rate of 2.5 mm/min.

4 Generation and Characterization of Carbon Nano-fiber-Poly(arylene ether sulfone) Nanocomposite Foams

Desmond J. VanHouten[a], and Donald G. Baird[b*]
[a]Macromolecular Science and Engineering, Virginia Polytechnic Institute and State University, Blacksburg VA 24061
[b]Department of Chemical Engineering, Virginia Polytechnic Institute and State University, Blacksburg VA 24061

Abstract

In this study, carbon nano-fibers (CNFs) were used to increase the compressive properties of poly(arylene ether sulfone) (PAES) foams. The polymer composite pellets were produced by melt blending the PAES resin with CNFs in a single screw extruder. The pellets were saturated and foamed with water and CO_2 in a one-step batch process method. Dynamic mechanical thermal analysis (DMTA) was used to determine the reduced glass transition temperature (T_g) of the CNF-PAES as a result of plasticization with water and CO_2. Sharp transitions were observed as peaks in the tan delta leading to accurate quantitative values for the T_g. By accurately determining the reduced T_g, the foaming temperature could be chosen to control the foam morphology. Foams were produced which ranged in density from 290 to 1100 kg/m^3. The foams had cell nucleation densities between 10^9 and 10^{10} cells/cm^3, two orders of magnitude higher than unreinforced PAES foam, suggesting that the CNFs acted as heterogeneous nucleating agents. The CNF-PAES foam exhibited improved compressive properties compared to unreinforced PAES foam produced from a similar method. Both the relative compressive modulus and strength increased by over 1.5 times that of unreinforced PAES foam. The relative compressive strength of 59 MPa for the CNF-PAES foam is similar to that of commonly used high performance structural foam, poly(methacrylimide foam).

4.1 Introduction

The development of lightweight, structural materials is important in aerospace, automotive, marine, rail, and wind energy applications[1]. Polymeric foams are gaining interest for use in these applications because they have a large strength to weight ratio, as well as being cost effective when compared to other lightweight, structural materials[2]. The compressive properties of foams are important because structural foams are often used in applications where compressive forces are applied. Poly(methacrylimide) (PMI) foams have high relative compressive strength properties, up to 67 MPa[1]. However, PMI is limited in it upper use temperature, with the compressive properties greatly decreasing at temperatures above 177 ^{o}C.

In order to increase the strength to weight ratio of polymers, microcellular foams were developed[3]. Microcellular foams are characterized by having a cell size less than 10 μm and a cell nucleation density greater than 10^9 cells/cm^3. It was hypothesized that if the cell size of the foam was smaller than the critical flaw size of the polymer, the microcellular foam would maintain the mechanical properties of the polymer matrix while increasing the impact toughness [3, 4].

In an effort to improve the mechanical properties of microcellular foams, microcellular nanocomposite foams have been produced by combining nano-clays and polymer matrices, including polystyrene[5-7], PMMA[5, 6], polypropylene[7, 8], polyethylene[9, 10], and polyethylene-octene[11]. The nanocomposites produced were either intercalated and featured agglomerates of clay particles or were exfoliated and the nano-particles were well dispersed throughout the polymer matrix. In all of the studies involving composites made using nano-clays, the addition of the particles improved the

cell morphology of the foam. When the particles were present, heterogeneous nucleation was dominant, which led to cell morphology with a smaller cell size and an increased cell nucleation density. The cell size distribution was also narrowed when compared to the neat polymer foam. As long as the particles were exfoliated and well dispersed, even at low levels of nano-clays (0.5%), they were able to act as a heterogeneous nucleating agent leading to numerous small cells[5, 6, 12]. The dispersion of the nano-clays was the most important factor in the resulting microcellular foam structure. If the nano-clays were exfoliated and well dispersed, there was more surface area on which cells could nucleate. The resulting foam had small cell sizes and a large cell density.

The dispersion and exfoliation were also important for increasing the tensile and compressive properties of the nanocomposite foam. Two studies were performed, one involving polystyrene and one involving PMMA. The tensile properties of the nanocomposite foams were lower than the unfoamed polymer, regardless of the clay dispersion, even if the tensile properties were normalized to account for the lower density. However, the tensile properties were improved when compared to the neat polymer foam as long as good dispersion of the clays was observed[5, 12]. The increase in the tensile properties of the nanocomposite foam was also attributed to the reinforcing nature of the clay. As the nanocomposites were foamed, the biaxial extension of bubble growth caused the nano-clays to orient. As a result, the nano-clays helped to reinforce the cell wall by aligning around the nucleated bubble. Transmission electron microscopy has been used to show this phenomenon in literature[7, 8].

While nano-clays have been shown to improve the mechanical properties of several microcellular foams, incorporation of the nano-clays into polymers with high

glass transition temperatures (T_g) is difficult. Nano-clays are often organically modified to enhance the dispersion in polymer matrices[13]. Cation surfactacts, often alkylammonium or alkylphosphonium cations, are used to enhance the miscibility of the nano-clays with the polymer. However, these cation surfactants tend to degrade at the high temperatures necessary to melt process these polymers.

Carbon nano-fibers have also been incorporated into polymer matrices and then foamed using supercritical carbon dioxide as the foaming agent. Shen et al.[14, 15] have studied the effect of incorporating carbon nano-fibers (0.3 – 5 wt. %) into polystyrene. By incorporating well dispersed carbon nano-fibers into the polystyrene matrix, it was found that the nano-fibers were able to act as a heterogeneous nucleating agent. It was determined that the carbon nano-fibers exhibited a greater nucleating efficiency than the nano-clays. Thus, the carbon nano-fibers were able to nucleate more cells at a lower percent loading[15]. Like the nano-clays, the carbon nano-fibers were shown to align around the nucleated cell walls, possibly increasing the mechanical properties of the nanocomposite foam[14].

Both tensile and compressive properties of microcellular polystyrene foams which were reinforced with carbon nano-fibers (1 and 5 wt. % loading) were reported[14]. By incorporating carbon nano-fibers, the reduced tensile modulus of the carbon nano-fiber reinforced foam was greater than that of the neat polystyrene (both foamed and unfoamed) for both 1 and 5 wt. % loading of fibers. However, the tensile strength was lower for the reinforced foam, making the reinforced foams less ductile. The ductility decreased with an increased weight percent of fibers. To study the effect of the carbon nano-fibers on the compressive properties of the foam, two different density foams were

produced (~80% reduction and ~50% reduction) with both 1 and 5 wt. % loading. The low density foam (~80% reduction) had a much lower compressive modulus than unfoamed polystyrene regardless of the amount of carbon nano-fibers. The medium density foam (~50% reduction) exhibited a compressive modulus that was higher than unfoamed polystyrene, with the values from the samples containing 1 and 5 wt. % nano-fibers being statistically indifferent. Both the tensile and compressive moduli of microcellular polystyrene foams reinforced with carbon nano-fibers were greater than those values of neat polystyrene.

Foams of poly(arylene ether sulfone) (PAES) have demonstrated relatively high compressive properties. Microcellular foams of PAES were first produced by Sun et al.[16, 17]. Supercritical carbon dioxide ($scCO_2$) was used as the blowing agent to produce the microcellular foams in a two-step process. The two-step process yielded foam with cell sizes of 1 to 7 μm, cell nucleation density of 10^{11} cells/cm^3, and up to 60% reduction in bulk density. The resulting foams exhibited relative compressive properties which were reported to be greater than theoretical predictions. The actual values of the compressive strength and modulus were not reported.

VanHouten and Baird[18, 19] introduced a new process for foaming PAES to further reduce the foam density. A one-step batch process was utilized with a dual plasticizer blowing agent system to produce the PAES foam. The process produced foam which had a cell size of 54 μm, cell nucleation density of 10^7 cells/cm^3, and up to 80% reduction in foam density. The compressive strength and modulus were compared to several commercially available polymeric foams. The relative compressive modulus and strength were 913 MPa and 38 MPa, respectively. While the compressive strength was

better than several of the commercially available structural foams, the compressive modulus was slightly lower.

The objective of this research was to determine whether foams produced from CNF reinforced PAES over a range of foam densities, would exhibit enhanced compressive properties, tensile modulus, and impact strength compared to the neat PAES foam [19]. Foams were produced which had cell sizes ranging from 1 to 100 μm and foam densities ranging from 290 to 1100 kg/m^3. The effect of the foam morphology on the compressive properties, tensile modulus, and impact strength of the CNF-PAES foams is discussed.

A second objective of this research was to more fully exploit the use of the blowing agents of water and CO_2, which both plasticize the polymer, to control the cell size and density. In particular, dynamic mechanical thermal analysis (DMTA) is utilized to more accurately determine the suppression of the Tg, when compared to differential scanning calorimetry, and thereby more carefully select temperatures at which foaming occurs.

4.2 Experimental

4.2.1 Materials

Poly(arylene ether sulfone) (PAES, Radel® R-5800) was generously supplied by Solvay Advanced Polymers (Alpharetta, GA). The glass transition temperature (T_g) and density of the polymer were 220 ^{o}C and 1.29 g/cm^3, respectively. Vapor grown carbon nano-fibers (PR-19-XT-LHT) were obtained from Pyrograf Products (Cedarville, OH). The fibers had an average diameter of 150 nm and a length of 50 to 200 μm. Carbon dioxide was obtained from Airgas, Inc.

4.2.1.1 Preparation of the PAES-CNF Nanocomposite Material

Prior to melt blending, the PAES pellets and carbon nano-fibers were weighed and dry mixed with an industrial blender. The mixture was dried at 100 ^{o}C for 18-24 h under vacuum to remove the moisture. The dried PAES and carbon nano-fibers were compounded with a Killion extruder (L/D = 18, barrel diameter = 25.2 mm, and variable screw diameter from 16.6 mm at the feed to 21.45 mm at the exit) with a temperature profile of 310 ^{o}C – 330 ^{o}C – 350 ^{o}C, a die temperature of 350 ^{o}C, and screw speed of 25 rpm. A 3 mm diameter capillary die was used to produce a strand. The strand was drawn down to a diameter of 1 mm, cooled in a 1 m water bath, and fed into a pelletizer.

4.2.2 Foaming Procedure

The PAES foams were produced using a one-step batch process method. A cylindrical stainless steel mold measuring 3.0 cm in diameter by 12.5 cm in length was filled with the PAES resin and liquid water (a 2:1 w/v ratio was used for polymer:water). The mold was placed inside a pressure vessel which was sealed and charged with a predetermined amount of carbon dioxide (4.5 MPa). The pressure vessel was heated to 265 ^{o}C causing the pressure to increase to between 10 and 11 MPa. A saturation temperature of 265 ^{o}C was used to facilitate the sintering of the pellets during the saturation process, yielding a foamed specimen without weld lines after the foaming process. The gas was allowed to diffuse into the PAES for 1 h. The temperature was decreased to the desired temperature (165 ^{o}C to 227 ^{o}C), and the pressure was increased to 10.3 MPa using a high pressure pump. The pressure vessel was held at the desired temperature for one hour to assure full saturation. The pressure was rapidly released (less

than 2 s) and the mold was removed from the pressure vessel. The mold was allowed to cool to room temperature before removing the foamed specimen.

Several obstacles must be overcome to produce a foamed sample which is of sufficient size and shape for mechanical testing, when using a one-step batch processing method. Although foaming a preformed polymer sheet or plug would result in the strongest foam, the sample would have to be several millimeters thick which would require long saturation times. Minimizing the diameter of the pellets is desirable to reduce saturation time by decreasing the distance which the gas has to diffuse. However, individually foamed pellets must be sintered together during processing to provide a usable part. Therefore, a higher initial saturation temperature (265 ^{o}C) was chosen to facilitate sintering of the CNF-PAES composite pellets during the saturation process. Because the water and CO_2 plasticize the PAES matrix, the viscosity of the composite material at 265 ^{o}C was reduced enough to induce flow of the pellets. The flowing of the pellets caused the composite material to form a flat cylindrical sheet in the mold. Once foamed, the sample exhibited no visible weldlines from the sintered pellets as was determined from visual analysis of a fractured surface.

4.2.3 Thermal Analysis

Differential scanning calorimetry (DSC), thermogravimetric analysis (TGA) and DMTA were conducted on CNF-PAES samples which had been saturated with water and carbon dioxide. CNF-PAES was saturated with scCO_2 and water at 265 ^{o}C and 10 to 11 MPa for 1 h. The temperature was cooled to 220 ^{o}C and pressure regulated to 10.3 MPa, and the sample was saturated for an additional hour. The temperature was cooled to room temperature to eliminate the loss of blowing agents due to foaming, and the CNF-

PAES was removed from the vessel. The saturated specimen was immediately tested upon removal from the pressure vessel. However, experiments proved that no appreciable loss of blowing agents occurred when the saturated specimen was subjected to ambient temperature and pressure for up to an hour after release.

CNF-PAES plaques were compression molded, prior to saturation, for DMTA testing. A Carver Laboratory Press was used to produce 2 mm thick sheets of CNF-PAES. The polymer pellets were placed in a rectuangular mold and placed inside of the press, which was heated to 300 ^{o}C. A pressure of 11.5 MPa was applied to the mold for 10 minutes. The mold was cooled to room temperature, and the plaque was removed.

A DSC (TA Instruments, model Q1000) was used to determine the T_g of the samples. Scans were conducted under nitrogen from -20 to 260 ^{o}C at a heating rate of 10 ^{o}C/min. High volume DSC pans with rubber seals (TA instruments) were used to minimize the loss of blowing agents during testing.

A TGA (TA Instruments, model Q500) was used to determine the amount of blowing agents present in the PAES resin. Samples were run from 25 ^{o}C to 600 ^{o}C at a heating rate of 10 ^{o}C/min in a nitrogen atmosphere.

DMTA was performed on a Rheometrics RMS-800. Strips measuring 45 mm long, 4 mm wide, and 2 mm thick were cut from the plaque of CNF-PAES that was saturated with water and CO_2. A dynamic torsional test was conducted at a frequency of 1 s^{-1} and 1% strain leading to the measurement of the storage (G') and loss (G") moduli from which the tan δ was determined as a function of temperature from 50 to 240 ^{o}C.

4.2.4 Foam Density

The foam density was determined using the water displacement method. A foam specimen was weighed and submerged in water. The displaced water was measured to determine the volume of the foam. Because the foam has a thin skin layer on the surface and a predominately closed cell structure, water uptake is negligible during the measurements.

4.2.5 Determination of Cell Size and Cell Nucleation Density from SEM Imaging

The cell size and structure of the foamed polymer was determined using a Leo 1550 field emission scanning electron microscope (FE-SEM) operated at 5 kV. The foam specimen was freeze fractured and sputter coated with 20 nm of gold. The SEM images were analyzed using ImageJ (National Institute of Health) image processing software. Typically, micrographs containing 25 to 50 cells were used to determine the average cell diameter and 100 to 200 cells were used to determine the cell nucleation density.

The cell nucleation density, N_o, was calculated using the method reported by Kumar and Weller and given by Eq. (4.1)[20]. In Eq. (4.1), n is the number of cells in the micrograph, M is the magnification, A is the area micrograph in cm^2, and V_f is the void fraction of the foam. V_f can be estimated from Eq. (4.2), where D represents the average diameter of the cells.

$$N_o = \left(\frac{nM^2}{A} \right)^{3/2} \frac{1}{\left(1 - V_f\right)} \tag{4.1}$$

$$V_f = \frac{\pi}{6} D^3 \left(\frac{nM^2}{A} \right)^{3/2} \tag{4.2}$$

4.2.6 Tensile Testing

The tensile modulus of the foam were determined using an Instron 4204 and ASTM D638 was used as a guide for testing. Due to sample size limitation the ASTM test method was not followed exactly. Five rectangular samples measuring 45 mm in length, 10 mm in width, and 3 mm in thickness were cut from a large specimen of the PAES foam. The gauge length was set to 20 mm and the samples were tested at a constant speed of 1.27 mm/min. The strain was calculated from the displacement of the crosshead. The modulus was determined by applying a least-squares fit through the initial linear region of the stress-strain curve. The modulus represents an average of five foamed specimens.

4.2.7 Compression Testing

The compressive properties of the foam were measured using a MTS (model 826.75) 50,000 lbs servo hydraulic test system. ASTM D1621 was used as a guide for testing. However, due to sample size limitations, the test method was not followed exactly. Five cylindrical samples measuring 30 mm in diameter and 40 mm in length were cut from a large specimen of the PAES foam and the foam properties were determined from the average of the five samples. A lathe was used to cut the samples to ensure the cuts were perpendicular to the cylinder wall. The samples were compressed at a rate of 2.5 mm/min. The strain was calculated from the displacement of the crosshead and the modulus was determined by applying a least-squares fit through the initial linear region of the stress-strain curve.

4.2.8 Impact Testing

The impact strengths of the foams were determined using ASTM D256-06a as a guide. Five samples measuring 63 mm long, 12.7 mm wide, and 3.2 mm thick were cut from a large specimen of the PAES foam. A sharp notch was cut into the sample using a Tinius Olsen Model 899 specimen notcher (Horsham, PA) turning at a high rotational speed. The notched specimens were tested using a Tinius Olsen 897 machine (Horsham, PA). Because the specimens were thinner than the ideal ASTM thickness, care was taken to ensure the samples did not buckle during impact.

4.3 Results and Discussion

The production of CNF-PAES foams using water and CO_2 as the blowing agents and the associated mechanical properties are addressed in three parts. First, the amount of blowing agents absorbed under various conditions and their plasticization of the CNF-PAES are considered. Secondly, based on the information obtained in the first part of the research, the conditions for foaming of the CNF-PAES to obtain various degrees of density reduction and cell size are discussed. In particular, results from DMTA helped to refine the foaming process by quantifying the plasticization of the CNF-PAES with the water and CO_2. By understanding the thermal transitions, foams were produced by releasing the pressure at varying temperatures to control the cell morphology and foam density. We then conclude this section with a presentation of the mechanical properties obtained for the CNF-PAES foams of various morphologies (cell size and densities).

4.3.1 Determination of CNF-PAES Plasticization from Presence of Water and CO_2

Thermogravimetric analysis was conducted to determine the amount of water and CO_2 that diffused into the CNF-PAES polymer composite during saturation. In order to induce a large thermodynamic instability during foaming, a large solubility is desired[21, 22]. The CNF-PAES was prepared in a similar manner to previously reported techniques which exhibited a large solubility of water and CO_2[19]. It is shown in Figure 4.1 that ~7.6% of water and CO_2 were able to diffuse into the CNF-PAES matrix during the 2 hour saturation time, at 10.3 MPa. Similar amounts of water and CO_2 were able to diffuse into the neat PAES [19]. Therefore, the addition of the CNFs does not affect the solubility or diffusivity of the water and CO_2 in the PAES matrix.

DSC was used to determine how much the T_g of the CNF-PAES polymer composite was reduced by the presence of the 7.6% water and CO_2. VanHouten and Baird[19] previously demonstrated that when PAES was saturated with water and CO_2, the lowered T_g due to plasticization was observed followed by an endothermic peak attributed to the loss of the blowing agents from the polymer matrix. Similar thermograms were observed with the CNF-PAES polymer composite. It is shown in Figure 4.2 that the water and CO_2 (7.6%, Figure 4.1) reduce the T_g of the CNF-PAES to approximately 160 ^oC. A large endothermic peak was observed directly after the T_g inflection. It was difficult to quantify the degree of suppression of the T_g of the polymer due to plasticization using DSC because the endothermic peak was much larger than the inflection due to the T_g.

To better quantify the plasticization of the CNF-PAES with water and CO_2, DMTA was conducted. Dynamic torsional testing was conducted on strips of CNF-

PAES. The storage modulus and tan delta are shown in Figure 4.3 for CNF-PAES saturated with 7.6% CO_2 and water and CNF-PAES which had not been saturated. The data from the storage modulus suggests that the loss of water and CO_2 did not occur before the CNF-PAES was heated to the lowered T_g due to plasticization. If the blowing agents were able to diffuse out of the CNF-PAES matrix, an increase in the storage modulus would be observed. Because no appreciable amount of blowing agents are lost during the DMTA testing of the PAES saturated with water and CO_2, DMTA was a viable option for quantitatively determining the plasticization of the polymer.

The T_g can be observed as either a rapid decrease in the storage modulus or a peak in the tan delta. The storage modulus and tan delta exhibited only one transition in the CNF-PAES samples containing no blowing agents. This transition was observed at 227 ^oC, which was close to the T_g of the PAES. When the CNF-PAES sample was saturated with CO_2 and water, three distinct transitions were observed as peaks in the tan delta. The first transition was observed at 160 ^oC, which is attributed to the plasticized T_g of the CNF-PAES due to the presence of both the CO_2 and water. Once 160 ^oC was reached, the CO_2 was able to rapidly diffuse out of the PAES matrix while a majority of the water remained in the polymer. The broadening of the decrease in the storage modulus at 160 ^oC is due to the loss of the CO_2. This loss of CO_2 from the PAES matrix led to an increase in the T_g, which yielded another transition at 189 ^oC. This transition is attributed to the plasticized T_g due to water. Once 189 ^oC was reached, the water was able to escape by both diffusion and nucleation of bubbles from the PAES matrix. Because the water completely escaped from the PAES matrix, a transition at 227 ^oC was observed, which is the T_g of the CNF-PAES matrix without blowing agents.

DMTA was used to determine the effect of the release temperature on the diffusion and solubility of the blowing agents. During the saturation process, the temperature was decreased from 265 ^{o}C to the desired temperature for pressure release and held for an hour. Because the temperatures varied greatly, the solubility of the blowing agents could be affected. To prepare the DMTA samples, the CNF-PAES sample was saturated at 265 ^{o}C and 10.3 MPa for 1 hour. The temperature was lowered to either 165 ^{o}C or 220 ^{o}C, the pressure regulated to 10.3 MPa, and CNF-PAES sample was saturated for an additional hour. The DMTA results for the samples saturated at 165 and 220 ^{o}C are shown in Figure 4.4. From this figure, it can be seen that the decrease in temperature does not affect the diffusion or solubility of the blowing agents as both curves exhibit the same transitions.

4.3.2 Characterization of Foam Morphology and Density

Using blowing agents, which also plasticized the CNF-PAES, allowed for better control of the foam morphology. Samples were foamed at four different release temperatures, which corresponded to significant transitions on the DMTA curve. The release temperature is defined as the temperature of the pressure vessel at which the pressure was released. The SEM micrographs of these samples, shown in Figure 4.5, show the effect foaming temperature had on cell morphology. It can be seen that as the foaming temperature is increased, cell size increases. When the release temperature is close to the plasticized T_g of the CNF-PAES, the cells do not have a lot of time to grow before vitrification is induced because the viscosity is becoming infinitely large. As the release temperature is increased, the cells have a longer time to grow and cell coalescence can occur, leading to larger diameter cells. Cell coalescence occurs when the growth of

two or more cells impinge on each other and the cell walls become so thin that surface tension can no longer keep the cells separate. Cell coalescence can be seen in the SEM micrographs when the pressure was released at a temperature of 180 ^{o}C or higher. At the higher temperatures, cell coalescence occurs more frequently. Cell coalescence which led to macrocellular size cells occurred when the pressure was released at a temperature of 227 ^{o}C. Despite the cell coalescence at the higher temperatures, cells less than 1 μm are present for all temperatures. The number of the cells less than 1 μm decreases as the foaming temperature is increased.

The presence of a broad distribution of cell sizes can be seen in Figures 4.5 and 4.6. In all of the micrographs, small cells (>1 μm) can be seen in the cell walls of the larger cells. The presence of distinctly different diameter cells suggests that there is more than one nucleation mechanism present during the foaming process. Upon rapid release of the pressure, the cells first nucleate due to the supersaturation of the CO_2 in the PAES matrix. Nucleation due to the supersaturation of the water occurs after the CO_2 nucleation. The bimodal distribution of cell sizes occurs because the two blowing agents nucleate the cells at different rates.

The DMTA confirms that two nucleation processes could occur during foaming when water and CO_2 are used as the blowing agents. The nucleation processes can be seen by the distinct transitions in the DMTA. At 160 ^{o}C, the CO_2 is able to be released from the PAES matrix. At this temperature, the CO_2 can begin to nucleate cells, while the water is still stable in the PAES matrix. When the temperature reaches 189 ^{o}C in the DMTA, the transition due to the water is observed. At this temperature, the water is unstable in the PAES matrix and can begin to nucleate cells. The difference in the

stabilities of the blowing agents in the PAES matrix confirms that nucleation due to water and CO_2 occurs at different rates.

The cell nucleation density was calculated from the SEM micrographs, and it was determined that cell nucleation density was affected by the temperature at which the pressure was released. A plot of cell nucleation density is shown in Figure 4.7. As the temperature of pressure release increased, the cell nucleation density decreased. The cell nucleation density decreased because of cell coalescence during the cell growth. As the cells grow together, the population of the cells decreases and this was observed as a decrease in the cell nucleation density.

For the CNF-PAES foam, the cell nucleation density ranged between 10^9 and 10^{10} cells/cm^3. The cell nucleation density was two orders of magnitude higher than neat PAES foam produced with water and CO_2 under the same saturation and foaming conditions[19]. The significant increase was attributed to the CNFs promoting heterogeneous nucleation. When heterogeneous nucleating agents are present, the activation energy of nucleation is significantly decreased so nucleation occurs much more easily, thus leading to a larger nucleation density[15, 23]. Heterogeneous nucleation was observed in the SEM images and is shown in Figure 4.8. In the micrograph, it can be seen that a CNF protrudes from the initially nucleated cell. The presence of heterogeneous nucleation produces a larger population of smaller cells, which can lead to better mechanical properties[14].

While the temperature of pressure release could be used to control the cell size, there was a tradeoff between cell size and the foam density. The effect of release temperature on the foam density is shown in Figure 4.9. As the release temperature was

increased, the foam density decreased. CNF-PAES foams were produced with a reduction in foam density ranging from 290 to 1100 kg/m^3, a 78 to 15 % density reduction, by only controlling the temperature at which the pressure was released.

4.3.3 Determination of the Tensile, Compressive, and Impact Properties

The tensile, impact and compressive properties of the CNF-PAES foams were tested and are shown in Table 4.1. The temperature in the sample name refers to the release temperature at which the corresponding foam was produced. Previously reported values[19] for the tensile, impact, and compressive properties of unreinforced PAES foam produced using water and CO_2 are also reported in Table 4.1 to determine the effect the CNFs had on the mechanical properties of the foams. All of the values are relative values, normalized by the foam density, to eliminate differences in the mechanical properties due to foam density.

The effect of both the cell morphology and the addition of the CNFs on the tensile modulus can be seen in Table 4.1. By comparing the PAES foam to the CNF-PAES foam (both foamed at 220 ^{o}C) it was determined that the addition of the CNFs yielded no effect on the foams because both foams exhibited tensile moduli which were statistically similar. Through comparison of the CNF-PAES foams produced at different release temperatures, the effect of the cell morphology on the tensile modulus of the foams was determined. The tensile modulus improved slightly as the cell size increased. As the foaming temperature was increased, up to 220 ^{o}C, the thickness of the cell walls also increased. The higher release temperature caused the cells with thin walls to coalesce. At a release temperature of 220 ^{o}C, a majority of the cell walls appeared to be greater than 1 μm, thus yielding a higher relative tensile modulus than the foams produced at the

lower release temperatures. The increase in the cell growth, at a release temperature of 227 ^{o}C, led to a decrease in the cell wall thickness. The decrease in cell wall thickness led to a slight decrease in the relative tensile modulus. It should be noted that the improvement in the relative tensile modulus due to the foam morphology was minimal.

The addition of the CNFs to the PAES yielded foam which had a significantly lower relative notched izod impact strength. When compared to unreinforced PAES foam, the relative impact strength of the CNF-PAES foam decreased by approximately 40%. The decrease in the impact strength from the addition of the CNFs was due to the strengthening characteristics of the CNFs. The CNF-PAES was more rigid than the unreinforced PAES foam. The rigidity of the foam allowed energy transfer to occur more easily in the foam. Therefore, the sample did not recoverably deform, and little energy from the impact was lost due to deformation[24]. The cell morphology did not cause a statistically significant difference in the impact strength of the CNF-PAES foams.

The compressive properties, modulus and strength, were most affected by the addition of the CNFs to the PAES. Both the relative compressive modulus and relative compressive strength increased over 1.5 times that of the unreinforced PAES foam to values of 1.5 GPa and 59 MPa, respectively. The CNF-PAES foam compared well with commercially available structural foams. The commercial structural foams that have high compressive properties have relative compressive moduli and strength values around 1.4 GPa and 70 MPa[1]. Shen et al.[14] observed an increase in the compressive properties, compared to the unreinforced polystyrene foam, when they foamed CNF reinforced polystyrene with CO_2 as the blowing agent. It was determined that during foaming, the CNFs aligned around the cell walls and helped to reinforce the walls during compression.

The relative compressive properties of the CNF-PAES foam were also affected by the foaming temperature. Similarly to the relative tensile modulus results, a higher release temperature, up to 220 ^{o}C, produced foam with greater relative compression modulus and strength than the lower release temperatures. As was argued for the tensile modulus, this increase was attributed to the greater cell wall thicknesses observed in the foam produced at 220 ^{o}C. However, at 227 ^{o}C the compressive properties were greatly decreased. The large reduction in the relative compressive properties is attributed to the inclusion of many macrocellular cells.

4.4 Conclusions

DMTA was demonstrated to be a more useful method than DSC to quantitatively determine the reduced $T_{g,}$ due to plasticization, of the CNF-PAES saturated with water and CO_2. In the DMTA, two distinct T_g's were observed for the plasticized samples. The sharp peaks in the tan delta provided more quantitative results than in the DSC. The loss of the blowing agents yielded a large endothermic peak in the DSC thermograms, which overlapped with the reduced T_g, and hindered quantitatively determining the T_g.

The DMTA results were used to refine the foaming process. Different foaming temperatures, corresponding to the thermal transitions observed in the DMTA, were chosen to control the cell morphology and foam density. Both the cell diameter and cell nucleation density were greatly affected by the temperature at which the pressure was released. As the temperature was increased, the cell size increased and the cell nucleation density decreased. The increase in the cell size was attributed to the longer cell growth times and cell coalescence. Cell coalescence accounts for the decrease in the cell nucleation density. The foam density was also significantly affected by the temperature

at which the pressure was released. At 165 ^{o}C, the foam density was the greatest because the cells did not have time to grow. At 227 ^{o}C, the cells had a longer time to grow and the foam density was reduced by 78%.

The addition of the CNFs where shown to greatly increase the compressive properties while slightly decreasing the impact strength of the foams. By adding in only 1% of the CNFs, both the relative compressive modulus and relative compressive strength were increased by over 1.5 times the modulus and strength of the unreinforced PAES foam. The relative compressive modulus and strength are greater than several commercial polymeric structural foams. However, the CNFs decreased the relative impact strength of the foams. By adding the CNFs to the PAES, the foam was much more rigid and less energy was absorbed by the sample bending during impact testing.

4.5 Acknowledgements

The authors would like to acknowledge the National Science Foundation IGERT (DMR-0114346) for partial funding. Parts of this work were carried out using instruments in the Nanoscale Characterization and Fabrication Laboratory, a Virginia Tech facility operated by the Institute for Critical Technology and Applied Science. The authors would also like to acknowledge the Wood Engineering Lab at Virginia Tech for use of the MTS compression testing machine and Christopher McGrady for his assistance with running the RMS-800.

4.6 References

1. Marshall, A.C., *Core Composite and Sandwich Structures*, in *International Encyclopedia of Composites*, S.M. Lee, Editor. 1990, VCH Publishers Inc. p. 488-507.

2. Altstädt, V., et al., *Polymer Foams as Core Materials in Sandwich Laminates (Comparison with Honeycomb).* Polym. Polym. Compos., 1998. **6**(5): p. 295-304.

3. Martini-Vvedensky, J.E., N.P. Suh, and F.A. Waldman, *Microcellular Closed Cell Foams and Their Method of Manufacture*. 1984, Massachusetts Institute of Technology: United States.

4. Collias, D.I. and D.G. Baird, *Impact toughening of polycarbonate by microcellular foaming.* Polym. J., 1994. **35**(18): p. 3978-3983.

5. Fu, J. and H.E. Naguib, *Effect of Nanoclay on the Mechanical Properties of the PMMA/Clay Nanocomposite Foams.* J. Cell. Plast., 2006. **42**: p. 325-342.

6. Manninen, A.R., et al., *The Effect of Clay Content on PMMA-Clay Nanocomposite Foams.* Cell. Polym., 2005. **24**(2): p. 49-70.

7. Nam, P.H., et al., *Foam Processing and Cellular Structure of Polypropylene/Clay Nanocomposites.* Polym. Eng. Sci., 2002. **42**(9): p. 1907-1918.

8. Okamoto, M., et al., *Biaxial Flow-Induced Alignment of Silitcate Layers in Polypropylene/Clay Nanocomposite Foam.* Nano. Lett., 2001. **1**(9): p. 503-505.

9. Lee, Y.H., et al., *Effects of Clay Dispersion on the Foam Morphology of LDPE/Clay Nanocomposites.* J. App. Polym. Sci., 2007. **103**: p. 2129-2134.

10. Lee, Y.H., C.B. Park, and K.H. Wang, *HDPE-Clay Nanocomposite Foams Blown with Supercritical CO_2.* J. Cell. Plast., 2005. **41**: p. 486-502.

11. Chang, Y.-W., D. Lee, and S.-Y. Bae, *Preparation of Polyethylene-Octene Elastomer/Clay Nanocomposite and Microcellular Foam Processed in Supercritical Carbon Dioxide.* Polym. Int., 2006. **55**: p. 184-189.

12. Han, X., et al., *Extrusion of Polystyrene Nanocomposite Foams with Supercritical CO_2.* Polym. Eng. Sci., 2003. **43**(6): p. 1261-1275.

13. Ray, S.S. and M. Okamoto, *Polymer/layered Silicate Nanocomposites: A Review From Preparation to Processing.* Prog. Polym. Sci., 2003. **28**: p. 1539-1641.

14. Shen, J., X. Han, and L.J. Lee, *Nanoscaled Reinforcement of Polystyrene Foams Using Carbon Nanofibers.* J. Cell. Plast., 2006. **42**: p. 105-126.

15. Shen, J., C. Zeng, and L.J. Lee, *Synthesis of Polystyrene-Carbon Nanofibers Nanocomposite Foams.* Polym. J., 2005. **46**: p. 5218-5224.

16. Sun, H., G.S. Sur, and J.E. Mark, *Microcellular foams from polyethersulfone and polyphenylsulfone: Preparation and mechanical properties.* Eur. Polym. J., 2002. **38**: p. 2373-2381.

17. Sun, H. and J.E. Mark, *Preparation, Characterization, and Mechanical Properties of Some Microcellular Polysulfone Foams.* J. Appl. Polym. Sci., 2002. **86**: p. 1692-1701.

18. VanHouten, D.J. and D.G. Baird. *Benign Processing of High Performance Polymeric Foams of Poly(arylene ether sulfone)*. in *ANTEC 2008 - Proceedings of the 66th Annual Technical Conference & Exhibition*. May 4-8, 2008. Milwaukee, WI: Society of Plastic Engineers.

19. VanHouten, D.J. and D.G. Baird, *Generation of Low-Density High Performance Poly(arylene ether sulfone) Foams Using a Benign Processing Technique.* Polym. Eng. Sci., 2008. ***In press***.

20. Kumar, V. and J.E. Weller, *Microcellular polycarbonate - Part I: Experiments on bubble nucleation and growth.* SPE ANTEC Tech. Papers., 1991. **37**: p. 1401-5.

21. Kumar, V., *A Process for Making Microcellular Thermoplastic Parts.* Polym. Eng. Sci., 1990. **30**(20): p. 1323-1329.

22. Kumar, V. and J. Weller, *Production of Microcellular Polycarbonate Using Carbon Dioxide for Bubble Nucleation.* J. Eng. Ind., 1994. **116**: p. 413-420.

23. Colton, J.S. and N.P. Suh, *Nucleation of Microcellular Foam: Theory and Practice.* Polym. Eng. Sci., 1987. **27**(7): p. 500-503.

24. Fanegas, N., et al., *Optimizing the Balance Between Impact Strength and Stiffness in Polypropylene/Elastomer Blends by Incorporation of a Nucleating Agent.* Polym. Eng. Sci., 2008. **48**: p. 80-87.

Table 4.1. Summary of the Relative Tensile, Compressive, and Impact Properties for CNF-PAES foamed at Varying Release Temperatures

	Density	Relative Tensile Modulus	Relative Compressive Modulus	Relative Compressive Strength	Relative Impact Strength
	kg/m^3	MPa	MPa	MPa	J/m
Unfoamed CNF-PAES	1290	1105.7 ± 90.9	-	-	496.6 ± 66.4
CNF-PAES 165 ^oC	1087	622.0 ± 82.8	1222.9 ± 17.6	62.3 ± 3.7	137.8 ± 19.6
CNF-PAES 180 ^oC	730	600.6 ± 71.1	962.5 ± 95.1	43.1 ± 6.6	101.1 ± 36.6
CNF-PAES 200 ^oC	532	758.8 ± 92.6	1134.7 ± 188.3	58.7 ± 10.1	171.6 ± 50.0
CNF-PAES 220 ^oC	362	813.8 ± 98.1	1507.1 ± 188.0	58.7 ± 10.1	175.1 ± 50.9
CNF-PAES 227 ^oC	287	759.0 ± 171.9	948.2 ± 91.5	62.8 ± 5.2	188.2 ± 33.1
PAES 220 ^oC	245	936.1 ± 144.7	912.6 ± 60.2	38.8 ± 2.2	305.5 ± 55.6

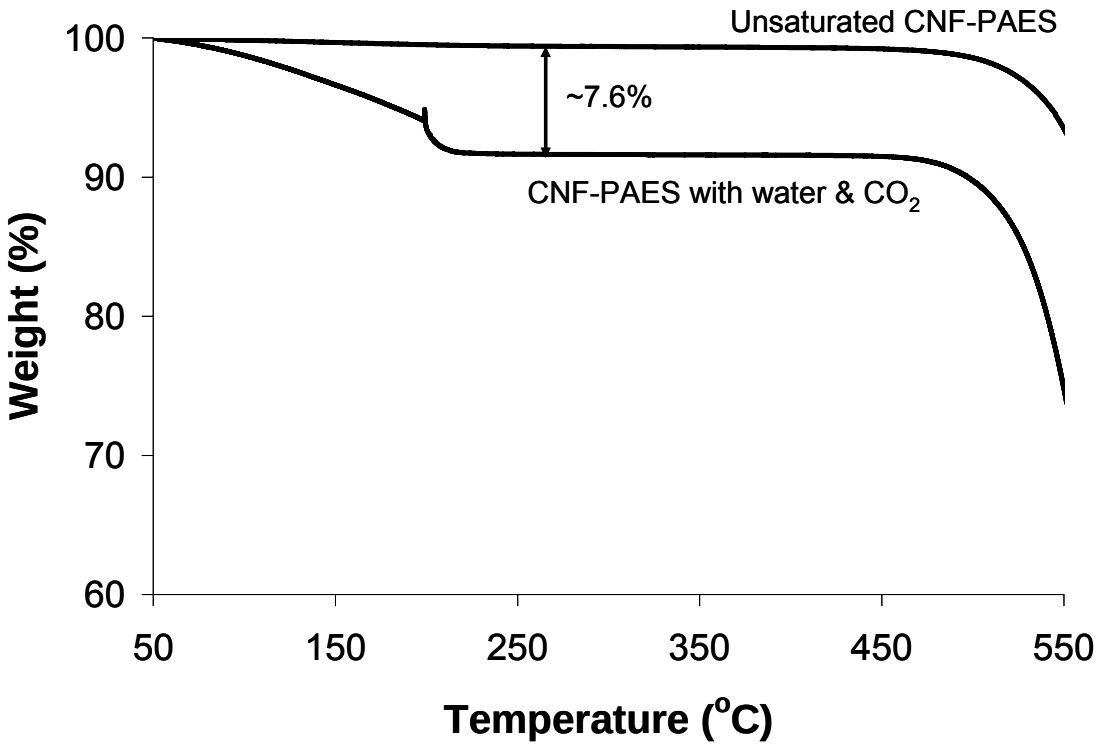

Figure 4.1. TGA results of 1 wt.% CNF-PAES saturated with CO_2 and water. The TGA was run in a nitrogen atmosphere at a heating rate of 10 ^oC/min.

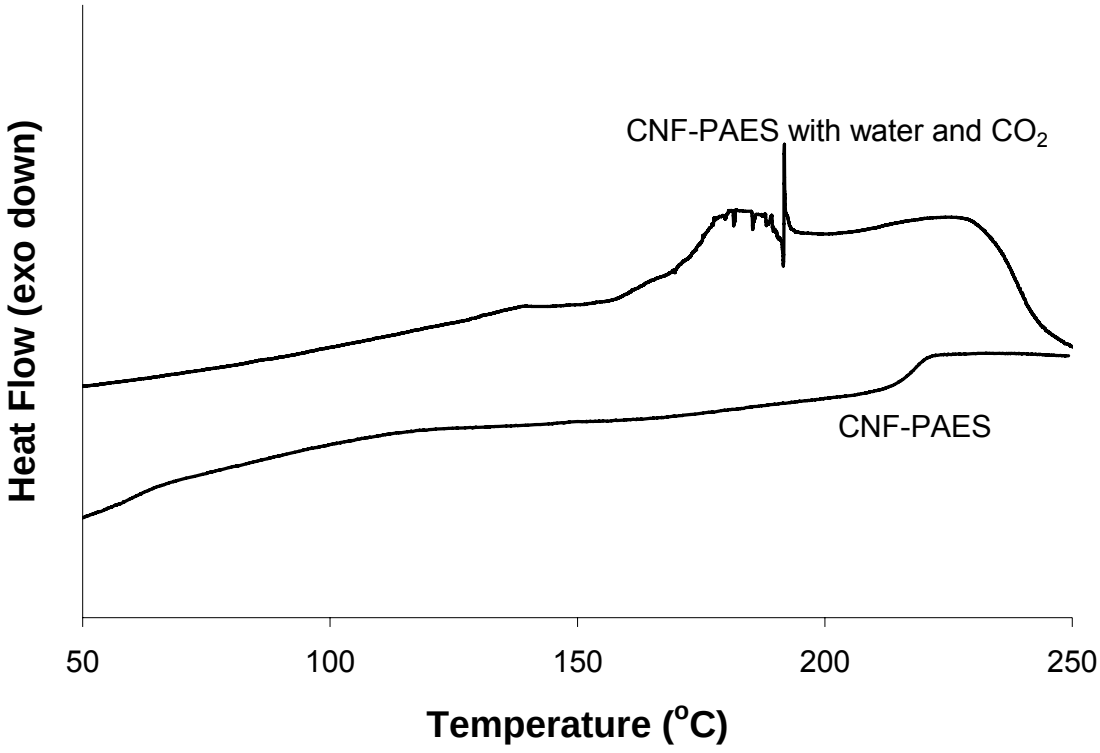

Figure 4.2. DSC results of 1 wt.% CNF/PAES saturated with 7.6 % CO_2 and water. The DSC was run at a rate of 10 ^oC/min in a nitrogen atmosphere. The data has been shifted so the results could be seen more clearly.

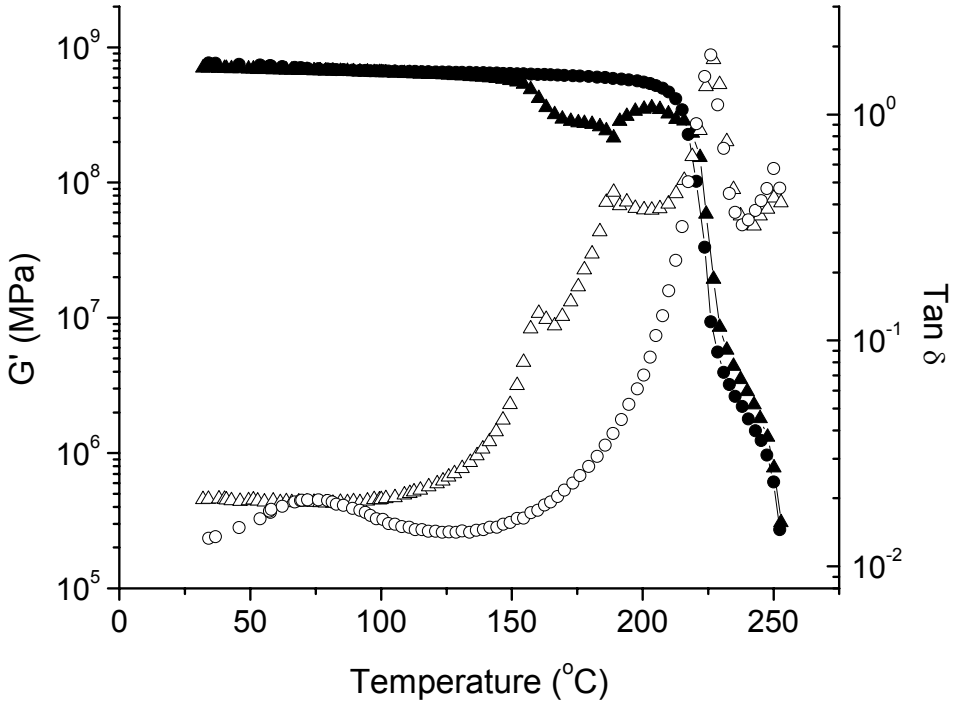

Figure 4.3. DMTA results of 1 wt% CNF-PAES saturated with water and CO_2 (▲) and neat CNF-PAES (●). The closed symbols represent the storage modulus and the open symbols represent the tan δ. The DMA was run in a nitrogen atmosphere at a heating rate of 10 ^{o}C/min. The DMA was run at a frequency of 1 s^{-1} and 1% strain.

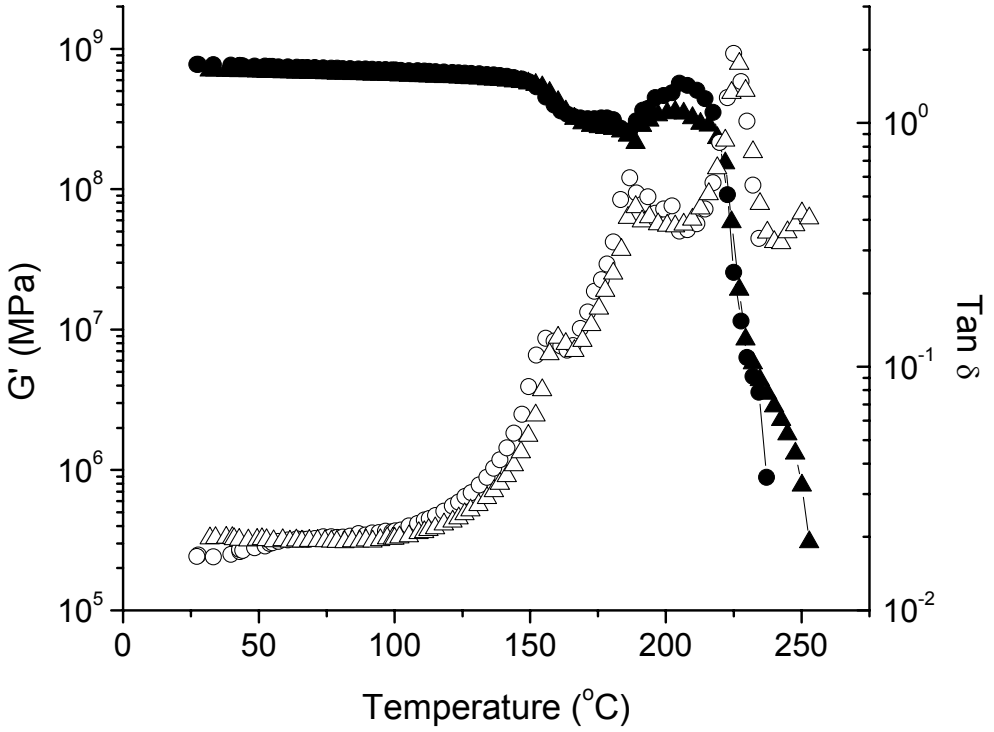

Figure 4.4. DMTA results of 1 wt% CNF-PAES saturated for release at 165 ^{o}C (●) and 220 ^{o}C (▲). The closed symbols represent the storage modulus and the open symbols represent the tan δ. The DMA was run in a nitrogen atmosphere at a heating rate of 10 ^{o}C/min. The DMA was run at a frequency of 1 s^{-1} and 1% strain.

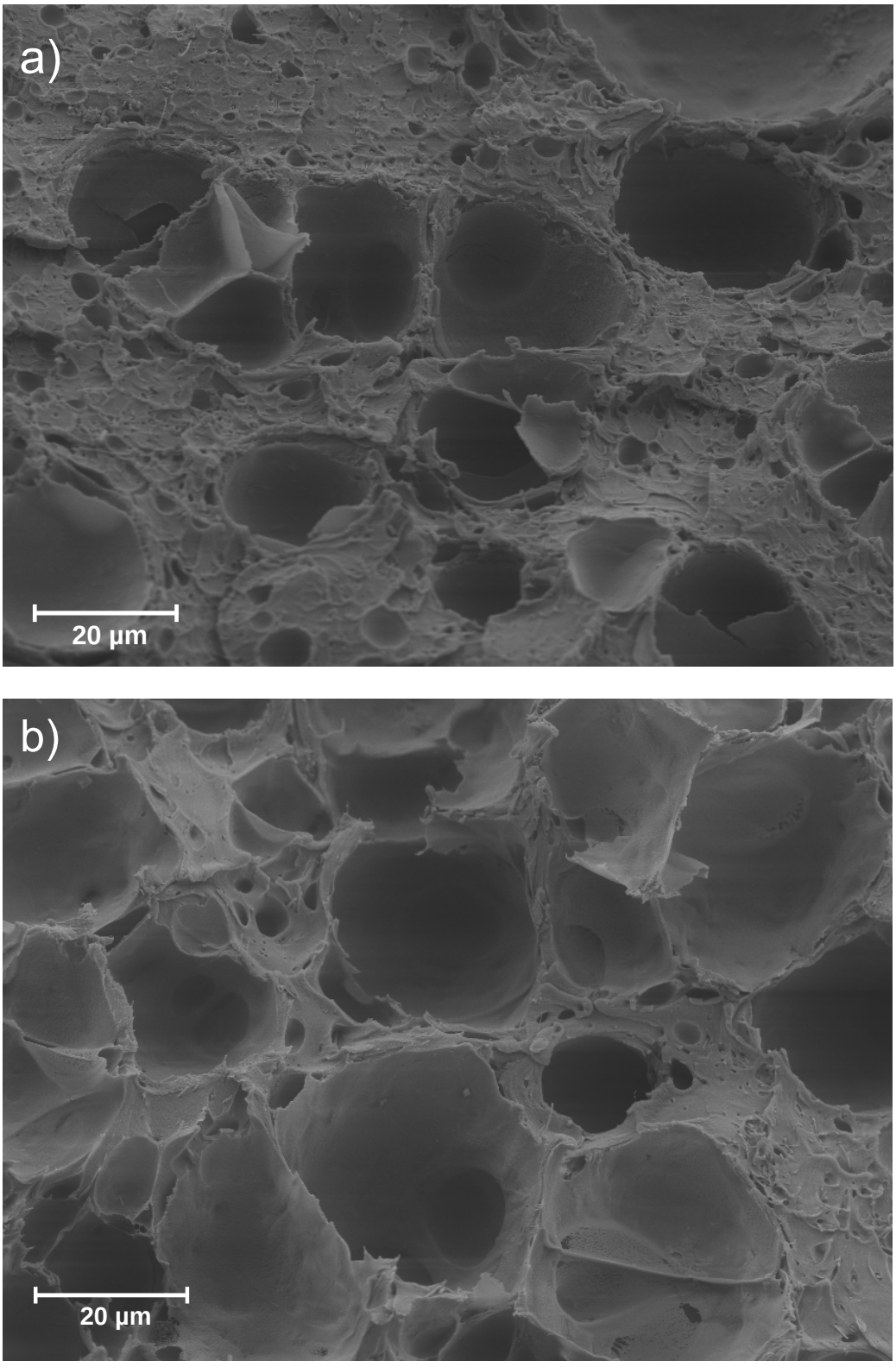
a)
20 µm
b)
20 µm

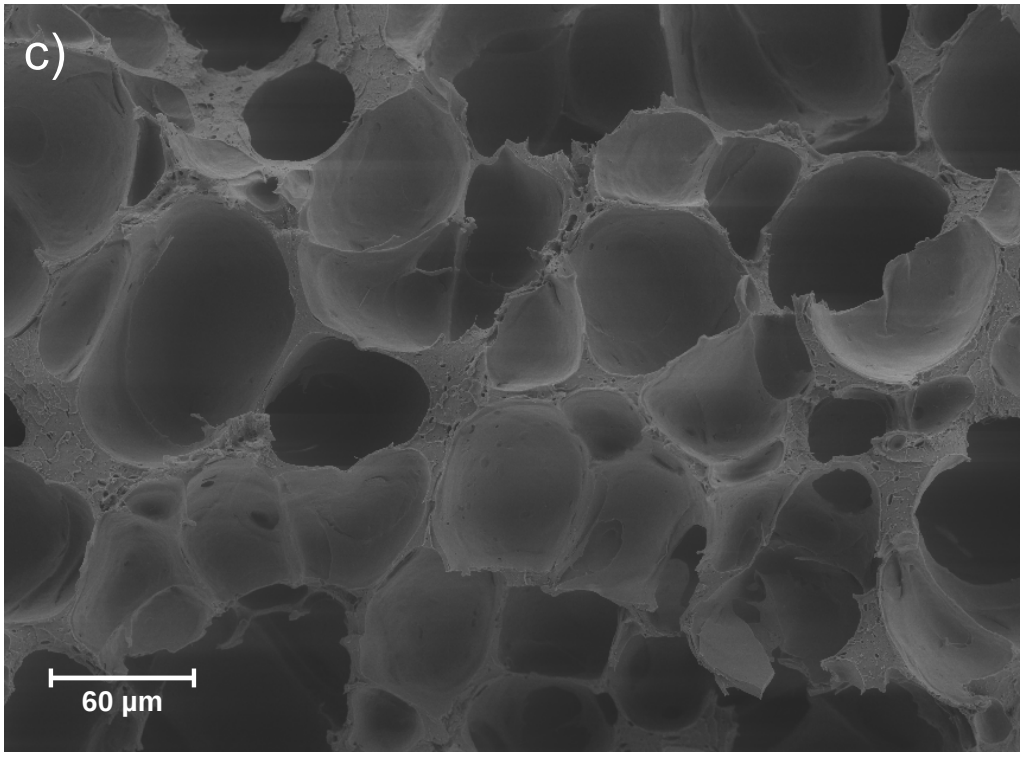
c)
60 µm

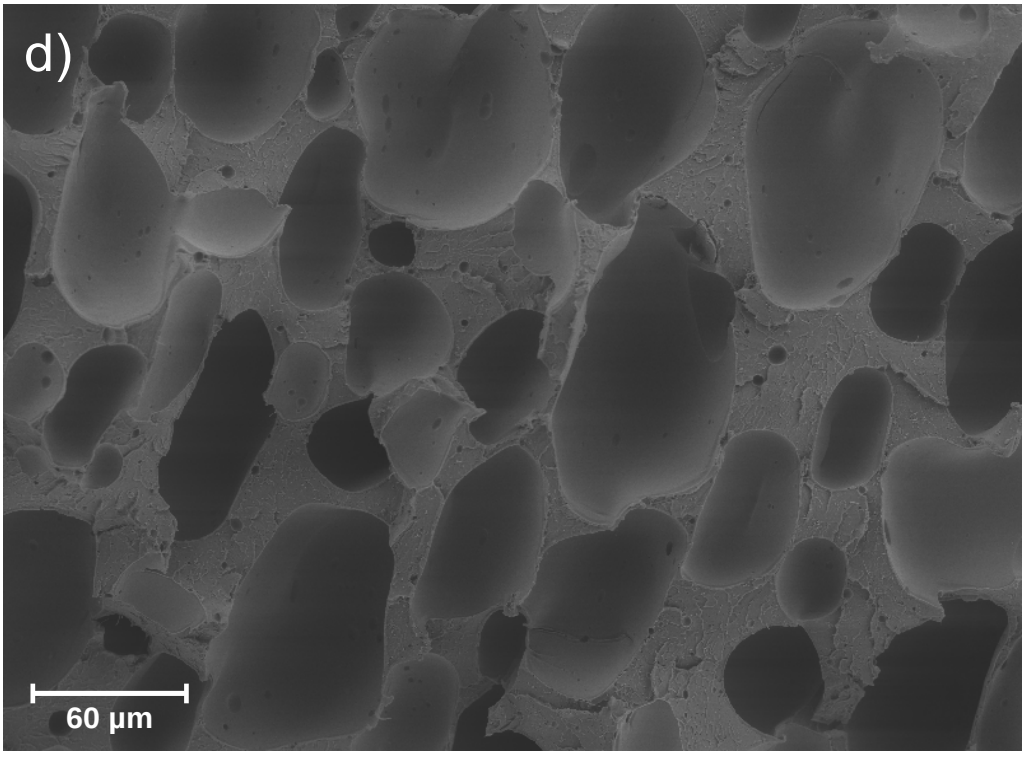
d)
60 µm

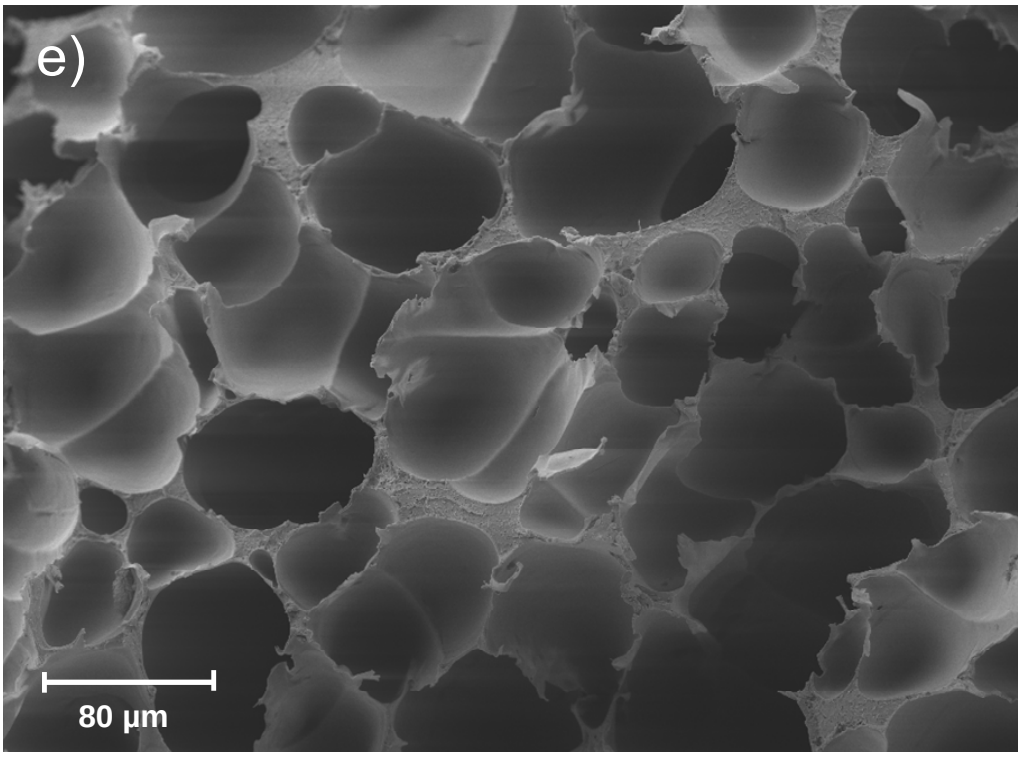

Figure 4.5. SEM micrograph of the CNF-PAES foam produced from a one-step batch process utilizing water and CO_2 as the blowing agents at a release temperature of a) 165 ^{o}C, b) 180 ^{o}C, c) 200 ^{o}C, d) 220 ^{o}C, e) 227 ^{o}C.

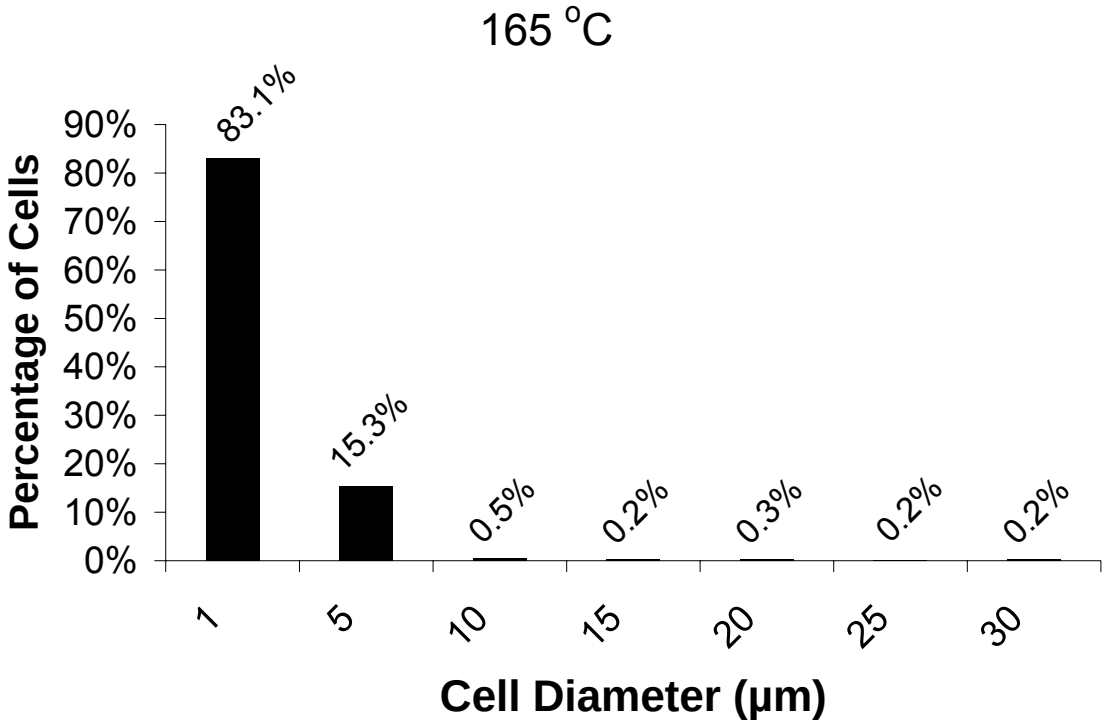
165 °C
Percentage of Cells
90%
80%
70%
60%
50%
40%
30%
20%
10%
0%
83.1%
15.3%
0.5%
0.2%
0.3%
0.2%
0.2%
1
5
10
15
20
25
30
Cell Diameter (µm)

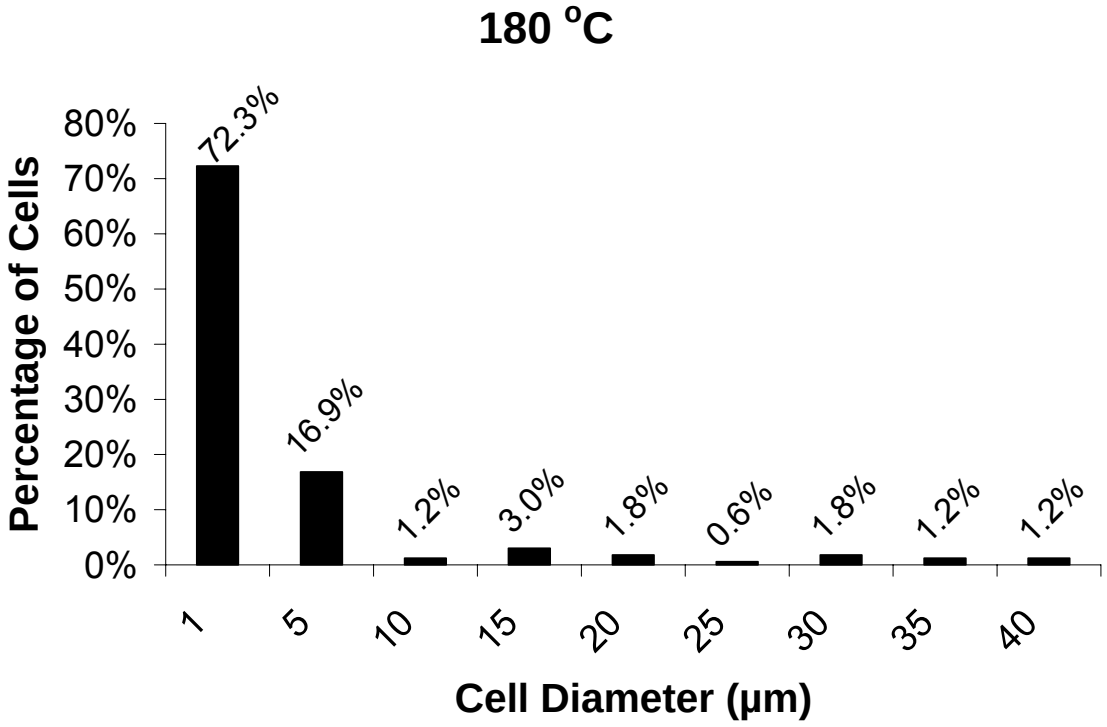
180 °C
Percentage of Cells
80%
70%
60%
50%
40%
30%
20%
10%
0%
72.3%
16.9%
1.2%
3.0%
1.8%
0.6%
1.8%
1.2%
1.2%
1
5
10
15
20
25
30
35
40
Cell Diameter (µm)

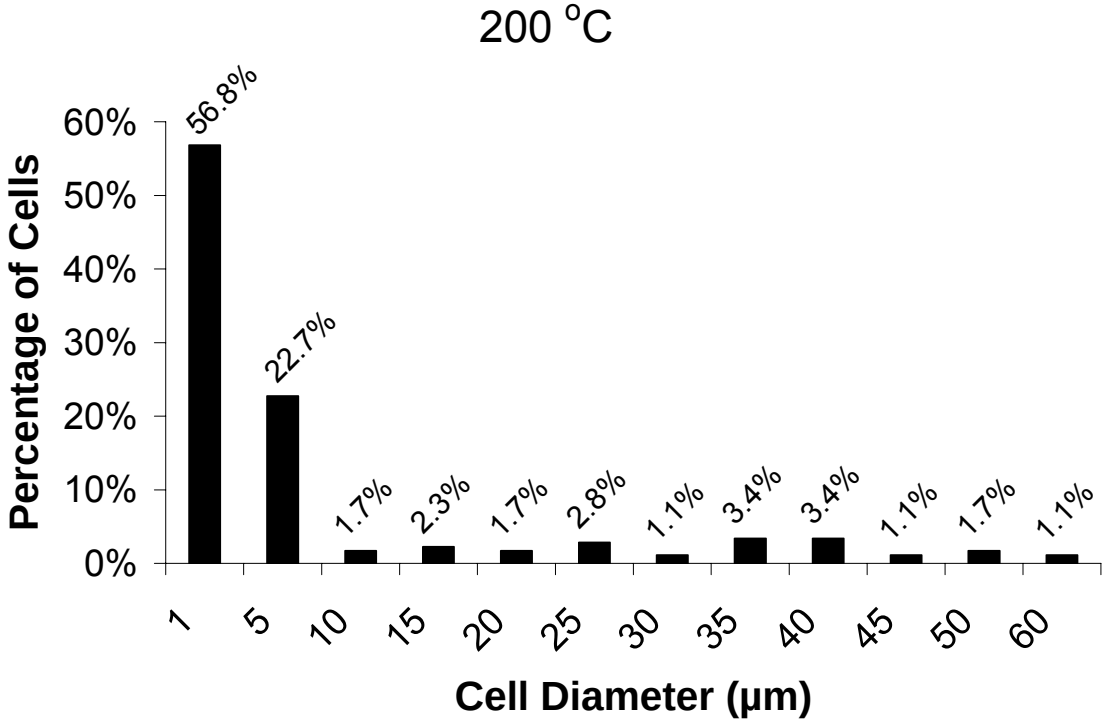
200 °C
Percentage of Cells
60%
50%
40%
30%
20%
10%
0%
56.8%
22.7%
1.7%
2.3%
1.7%
2.8%
1.1%
3.4%
3.4%
1.1%
1.7%
1.1%
1
5
10
15
20
25
30
35
40
45
50
60
Cell Diameter (µm)

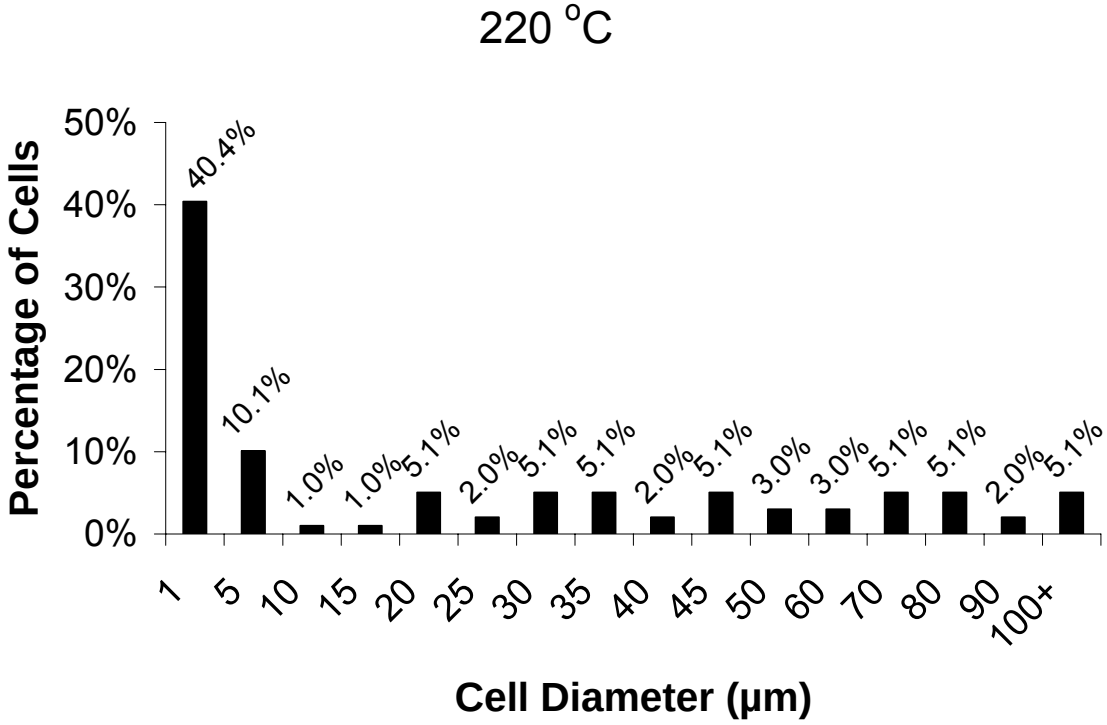
220 °C
Percentage of Cells
50%
40%
30%
20%
10%
0%
40.4%
10.1%
1.0%
1.0%
5.1%
2.0%
5.1%
5.1%
2.0%
5.1%
3.0%
3.0%
5.1%
5.1%
2.0%
5.1%
1
5
10
15
20
25
30
35
40
45
50
60
70
80
90
100+
Cell Diameter (µm)

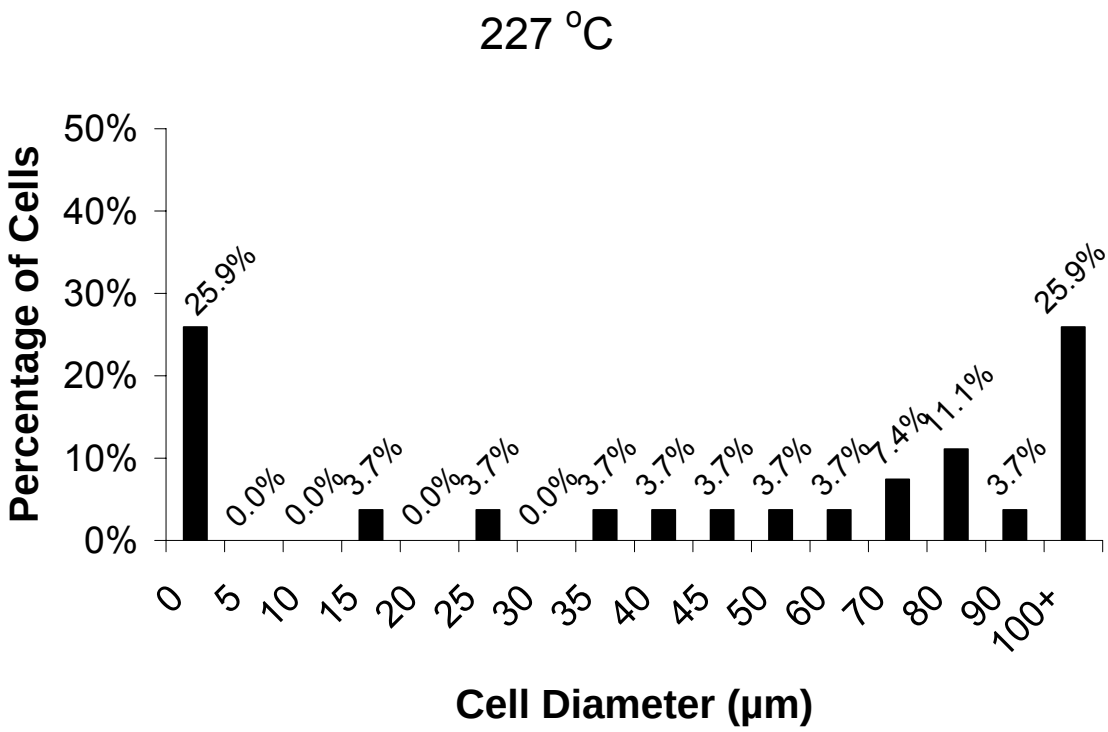

Figure 4.6. Cell size distribution of the CNF-PAES foam saturated with water and CO_2 at 165 °C, 180 °C, 200 °C, 220 °C, 227 °C.

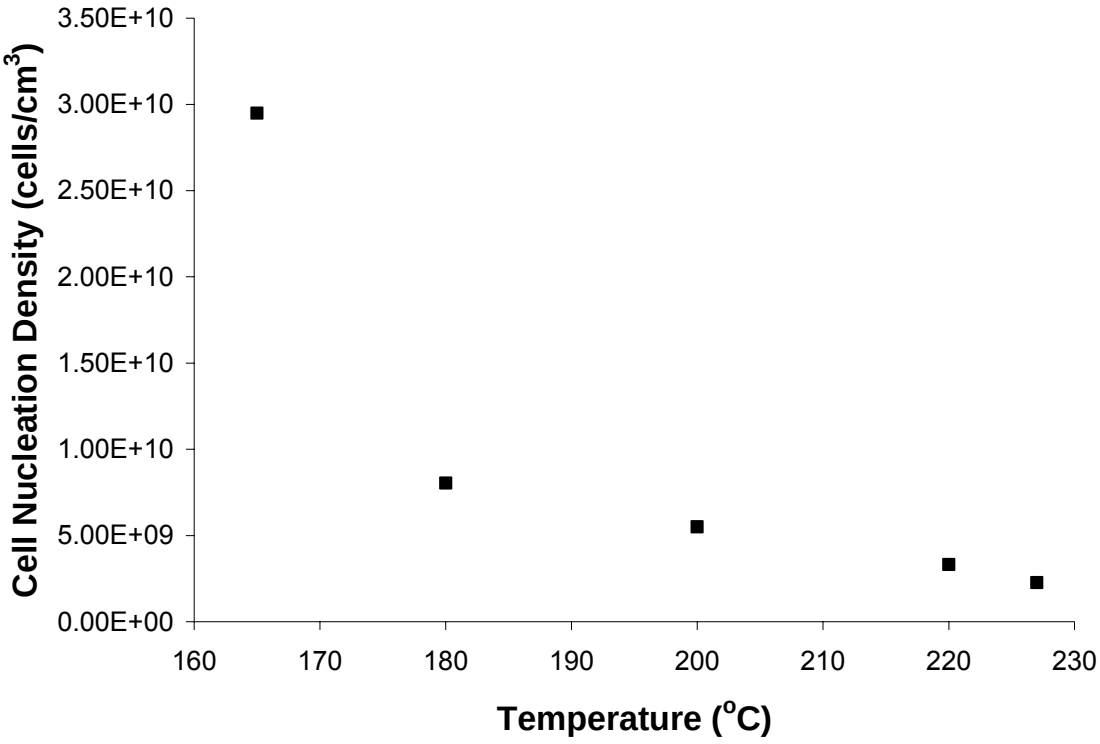

Figure 4.7. Effect of the release temperature on the cell nucleation density for CNF-PAES foamed with water and CO_2.

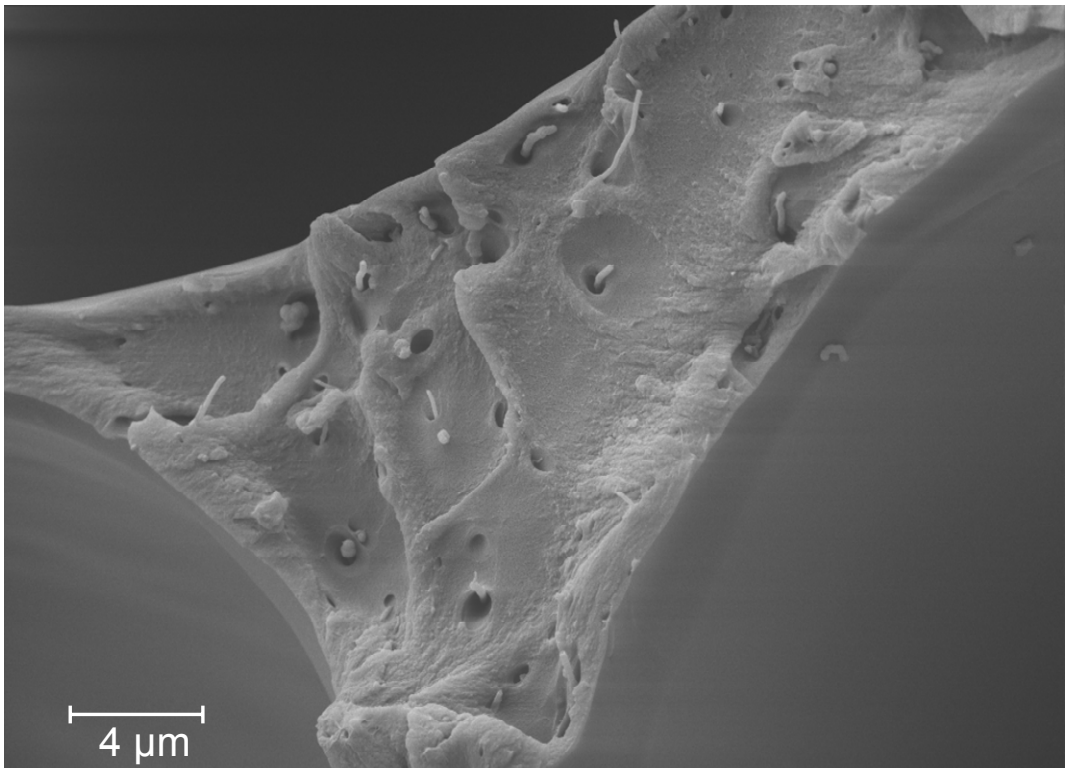

Figure 4.8. SEM micrograph of CNF-PAES foamed with water and CO_2 at a release temperature of 220 ^{o}C. The presence of heterogeneous nucleation can be seen in the micrograph.

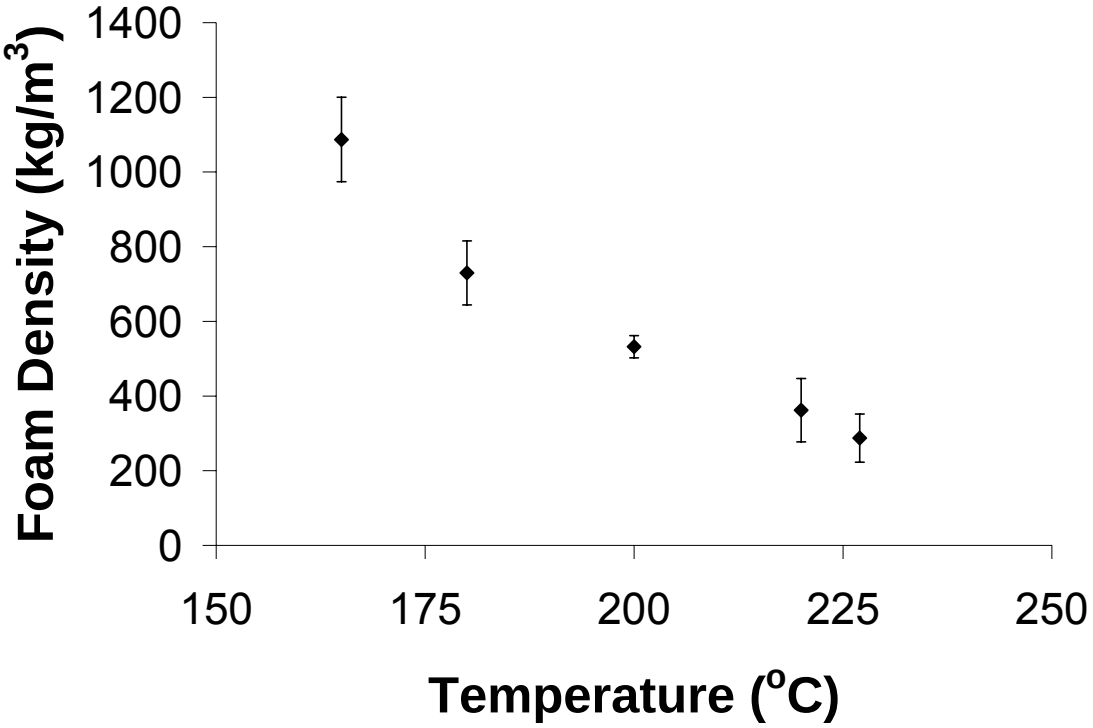

Figure 4.9. Effect of foaming temperature on the bulk density of the CNF-PAES foams.

5 Modeling of Cell Growth in Polymer Foaming with Dissolved Gas Blowing Agent by Incorporation of a Variable Viscosity Function

Desmond J. VanHouten[a], and Donald G. Baird[b]
[a]Macromolecular Science and Engineering, Virginia Polytechnic Institute and State University, Blacksburg VA 24061
[b]Department of Chemical Engineering, Virginia Polytechnic Institute and State University, Blacksburg VA 24061

Abstract

In this research, a method of modeling the cell growth of polymer foam produced from a dissolved gas blowing agent, which is also a plasticizer for the polymer, is presented. In previous cell growth models it is assumed that during the cell growth the viscosity of the polymer remains constant, but because the dissolved gas is a plasticizer the viscosity of the polymer changes during the cell growth. As the nucleated cells grow the dissolved gas diffuses out of the polymer and the viscosity increases due to the increase in the glass transition temperature. In the model presented an empirical function for viscosity is incorporated into the equations used to describe the cell growth. In the cell growth equations, the initial pressure inside the cell, the diffusivity for the gas/polymer system, Henry's law constant, and the cell nucleation density are required. Extensive experiments are necessary to obtain the physical parameters if they are not already presented in literature. Because of the lack of physical parameters for poly(arylene ether sulfone) with water and CO_2 used as the physical blowing agents, the model was not used quantitatively. Qualitative results exhibited that with the variable viscosity function, the cell growth does not occur as rapidly and the viscosity inhibits cell growth. This is believed to more closely follow the cell growth phenomena than when a constant viscosity term is used.

5.1 Introduction

Many models have been developed to describe the cell growth process in polymeric foam being produced from PBAs. Initially, a model was developed which described the cell growth process as a single bubble growing in an infinite amount of polymer.[1] Although, this provided a good starting point, the model has limitations because it only includes one cell. A model was later developed that described the cell growth as many cells growing close to each other.[2] In this model, each cell is surrounded by a finite shell of polymer that contributes to the growth. While this is an improvement over the initial model, it is still limited by certain assumptions.

The modeling of cell growth has assumed that the viscosity of the polymer is constant throughout the process. However, this assumption is not valid when foaming a polymer with a physical blowing agent that plasticizes the polymer. Many polymers have been reported to be plasticized by carbon dioxide[3], which is widely used as a physical blowing agent in many polymeric foaming processes[4-7]. The plasticization has been demonstrated to significantly reduced the viscosity of the polymers by lowering the glass transition temperature (T_g), and the viscosity reduction is dependent upon the concentration of the plasticizer[8, 9]. During the cell growth process, the PBA that diffused into the polymer during saturation contributes to cell growth and then diffuses out of the polymer. The cell growth and diffusion of the blowing agent out of the polymer leads to an increase in T_g which ultimately increases the viscosity, and therefore, the viscosity cannot be considered constant during the cell growth.

The goal of our research is to improve upon previous cell growth models by incorporating the increase in viscosity as a PBA, which plasticizes the polymer, diffuses

out of the polymer during cell growth. This paper addresses selecting a function to describe the change viscosity, as a result of the T_g increase, and incorporating this function into the finite shell model. Our research focuses on the foaming of poly(arylene ether sulfone) (PAES) with water and carbon dioxide (CO_2). This system is not ideal for modeling because there is a lack of data on the physical parameters on this polymer/gas system which inhibits accurate modeling. In this research, the equations and technique to solve them is presented, but the model cannot be evaluated quantitatively because of the lack of data on the initial pressure inside the cell before growth, the cell nucleation density, diffusivity, and Henry's law constant.

5.2 Cell Growth Modeling

Cell growth in polymer foams produced from dissolved gas blowing agents can be described as numerous cells growing in close proximity to each other in the saturated polymer melt. Each individual cell is assumed to be surrounded by a finite shell of polymer, which has a known concentration of blowing agents.[2, 10] The blowing agents in this shell of polymer provide the gas which is necessary for the cells to grow. Once the blowing agents have been used to nucleate cells and have diffused out of the polymer melt, the cell growth is inhibited.

A schematic of the cell growth is shown in Figure 5.1. In this figure, P_g is the gas (blowing agent) pressure inside of the cell, P_f is the pressure of the gas in the polymer melt, c is the concentration of gas in the polymer, R is the radius of the cell, and S is the radius of the polymer shell. As can been seen in the figure, there is a concentration gradient of gas in the polymer melt. This concentration gradient drives the diffusion of the gas from the polymer shell to the growing cell.

Several assumptions are made to facilitate the modeling of the cell growth, as follows:

1. The growing cell is spherical and grows symmetrically.
2. The combination of the polymer/gas melt is incompressible.
3. During the growth process, inertial effects are negligible.
4. The pressure at the boundary of the shell is equal to the pressure of the gas in the polymer melt at a given moment.
5. The gas in the bubble behaves as an ideal gas.
6. The diffusivity of the gas in the polymer is constant throughout the cell growth process.
7. The gas pressure in the cell is described by Henry's Law, which relates pressure to the concentration of the gas.
8. The cell growth occurs isothermally.
9. The polymer melt is described as a Newtonian fluid.

In order to model the cell growth, the process must be understood fundamentally to determine the governing equations. The cell growth is driven by the pressure inside the nucleated cell being greater than the pressure outside of the shell boundary. The higher pressure results in a force causing the cell to grow. However, the surface tension of the polymer melt, as well as, the viscous nature of the polymer melt leads to forces which resist the cell growth. This process is described by the conservation of momentum, which is given in Eq. (5.1), which is derived from the Cauchy momentum equation.

$$P_g - \frac{2\sigma}{R} = P_f - 2\int_{R_0}^{S} \frac{\tau_{rr} - \tau_{\theta\theta}}{r} dr \tag{5.1}$$

The components of the stress tensor, τ_{rr} and $\tau_{\theta\theta}$, are required to solve Eq. (5.1). A constitutive equation is required to obtain these stress components. In previous attempts, people have used the upper-convected Maxwell [10-12] and Oldroyd B[13, 14] models which predict constant viscosity. To simplify the calculations, previous models[2] have used a Newtonian fluid constitutive equation to determine the components of the stress tensor. The Newtonian fluid constitutive equation was chosen for the simulation because of the simplification in the calculations, so the variable viscosity dependence can be emphasized. The components of the stress tensor, τ_{rr} and $\tau_{\theta\theta}$, for a Newtonian fluid are described by Eq. (5.2):

$$\tau_{\theta\theta} - \tau_{rr} = 2\eta\left(d_{\theta\theta} - d_{rr}\right) = 6\mu\frac{R^2\dot{R}}{r^3} \tag{5.2}$$

By inserting the r and θ components of the stress tensor (Eq. (5.2)) into Eq. (5.1) and integrating, Eq. (5.1) becomes Eq. (5.3):

$$P_f - P_g - \frac{2\sigma}{R} = 4\mu R^2\dot{R}\left[\frac{1}{S^3} - \frac{1}{R_0^3}\right] \tag{5.3}$$

During cell growth, the pressure inside the cell decreases as the volume increases. This causes a concentration gradient in the polymer melt, which leads to diffusion of gas from the polymer melt into the growing cell. The conservation of mass is used to describe the transfer of the gas from the polymer melt to the cell. The conservation of mass is shown in Eq. (5.4).

$$\frac{dP_g}{dt} = \frac{3R_g DT}{R}\left(\frac{\partial c}{\partial r}\right)\Bigg|_{r=R} - \frac{3P_g}{R}\frac{dR}{dt} \tag{5.4}$$

The concentration profile of the gas in the polymer melt is needed to solve the conservation of mass (Eq.(5.4)) and is described by the diffusion equation. The diffusion equation is shown in Eq. (5.5). In this equation the fluid velocity, v_r, is described by Eq. (5.6).

$$\frac{\partial c}{\partial t} + v_r \frac{\partial c}{\partial r} = \frac{D}{r^2}\frac{\partial}{\partial r}\left(r^2 \frac{\partial c}{\partial r}\right) \tag{5.5}$$

$$v_r = \frac{R^2 \dot{R}}{r^2} \tag{5.6}$$

One initial and two boundary conditions are needed to solve the diffusion equation which are given in Eqs.(5.7), (5.8), (5.9), respectively:

$$c(r,0) = c_o \tag{5.7}$$

$$c(R,t) = c_{cell} \tag{5.8}$$

$$\frac{\partial c}{\partial r}(S,t) = 0 \tag{5.9}$$

5.3 Determination of Viscosity, η

In the model, a function needs to be incorporated to calculate the viscosity for a given concentration of dissolved blowing agent. This function can be obtained by first relating the viscosity to the plasticized T_g and then relating the plasticized T_g to the concentration of dissolved blowing agent. A relationship between the viscosity and concentration of dissolved blowing agent can then be obtained by combining these two relationships.

The Williams-Landel-Ferry (WLF) equation is used here to determine the viscosity of a polymer at different processing temperatures. The WLF equation is given in Eq. (5.10), and is valid up to $T_g + 100\ ^oC$.[15] In Eq. (5.10), the viscosity the polymer, η_T, at a temperature T is related to the visocity of the polymer, η_{Tg} at the T_g of the polymer. C_1 and C_2 are constants which are generally considered to be universal and have the values of 17.44 and 51.6 ^oK, respectively.

$$\log \frac{\eta_T}{\eta_{T_g}} = \frac{C_1\left(T - T_g\right)}{C_2 + \left(T - T_g\right)} \tag{5.10}$$

Bortner[16] suggested that the viscosity of a plasticized polymer can be estimated by deriving an equation based on the WLF equation. The equation can be derived by taking the ratio of the viscosity of the pure polymer to the viscosity of the plasticized polymer, as is shown in Eq. (5.11):

$$\frac{\eta_T^{polymer}}{\eta_T^{plasticized}} = \frac{10^{\left(\frac{-C_1\left(T - T_g^{polymer}\right)}{C_2 + \left(T - T_g^{polymer}\right)}\right)}}{10^{\left(\frac{-C_1\left(T - T_g^{plasticized}\right)}{C_2 + \left(T - T_g^{plasticized}\right)}\right)}} \tag{5.11}$$

It was determined for this equation to be accurate, the universal values for C_1 and C_2 should not be used, but rather they should be determined empirically. The constants can calculated by measuring the viscosity at various concentrations of the blowing agents, creating a master curve, and doing least squares to calculate C_1 and C_2[16]. Both a pressurized capillary rheometer and a slit-die rheometer have been used to effectively

determine the viscosity of plasticized polymers[8, 9]. With these constants, a function to estimate the T_g at intermediate points within the experimental range can be obtained.

An empirical relationship between dissolved gas concentration and plasticized T_g was obtained experimentally. As shown in Chapter 4, the plasticized T_g can be quantitatively determined by using dynamic mechanical thermal analysis (DMTA). To determine the concentration of dissolved blowing agent, thermogravimetric analysis (TGA) was used. By conducting DMTA and TGA on the polymer at different plasticization levels, data can be obtained relating the T_g to the dissolved gas concentration. This data can be fit experimentally to obtain an empirical formula relating the T_g to the concentration of blowing agent.

In the model the concentration at the bubble interface can be obtained through Henry's Law which is given in Eq. (5.12).

$$c_{cell} = k_H P_g \tag{5.12}$$

In Eq. (5.12), c_{cell} is the concentration of gas at the cell/polymer interface and k_H is Henry's Law constant. From the model, the pressure at any time t' can be obtained from Eq. (5.4). By combining Eq. (5.4) with Eq. (5.12), the concentration of the gas at the cell/polymer interface is estimated. This was then be used in conjunction with the empirical relationship relating the gas concentration to the plasticized T_g. The plasticized T_g was then be used to obtain the viscosity of the polymer at the cell/polymer interface.

5.4 Solving the System of Equations

To model the cell growth, the governing equations (Eqs (5.3) - (5.5)), need to be solved simultaneously. Because of the complex nature of the system of equations, an

analytical solution is not available and numerical simulation is required. MATLAB was used to solve the system of equations. To solve the two ordinary differential equations, the Runge-Kutta method (MATLAB function 'ode45') was used. To solve the diffusion equation, the partial differential equation was solved using the method of lines which reduced the PDE to a system of ordinary differential equations. The r-direction was broken into discrete points, called nodes. An ordinary differential equation was written to describe the concentration as a function of time. These ordinary differential equations were then solved using a stiff ordinary differential solver (MATLAB function 'ode15s').

A schematic for solving the set system of equations is shown in Figure 5.2. The system of governing equations is solved over a small time step, Δt. For this small time step the cell radius, gas concentration profile, and pressure can be determined. Once these values are calculated from the governing equations, the time step is incremented and the equations are solved again. This simulation is carried out until the final time, $t_{f,}$ is reached.

5.5 Determination of the Physical Parameters

Several physical parameters are necessary to model the cell growth. It is necessary to know the diffusivity, Henry's Law constant, and surface tension which are often obtained from literature. The surface tension is estimated from conducting a pendent drop test under various saturation pressure and temperatures [10]. It is also necessary to determine the cell nucleation density and P_g. The cell nucleation density is then used to calculate S, by dividing the volume of the polymer sample by the cell nucleation density which can then be used to calculate the radius of the polymer shell.

The initial cell radius, R_o, can be estimated from the Laplace equation[10, 17]. The viscosity of the polymer at the T_g, $\eta_g^{polymer}$, is assumed to be infinitely large.

5.6 Effect of Variable Viscosity on Cell Growth Modeling

Quantitatively modeling the cell growth of PAES saturated with water and CO_2 requires extensive experiments because of the limited data available for the cell nucleation density, diffusivity, k_H, and σ. Although the results obtained from the model cannot be compared to experimental values at this time, the model can still give qualitative insight on the affect viscosity has on cell growth.

To model the cell growth, an estimation of the physical parameters is shown in Table 5.1. These physical parameters were estimated from values which were reported in literature[10]. These values are only used as an estimation to assess how the variable viscosity function affects the cell growth model.

A comparison of the modeled cell growth with constant viscosity and with variable viscosity is shown in Figure 5.3. From this figure, it can be seen that when a constant viscosity is used, the cell growth is not as restricted and the cells are predicted to be ~45 μm. This is much larger than when the variable viscosity function is incorporated into the model. With the variable viscosity, the viscosity increases as the concentration of gas at the cell/polymer interface decreases. The increase in viscosity restricts the cell growth, which leads to a smaller cell diameter.

The pressure inside the growing cell is also affected by the incorporation of the variable viscosity function into the cell growth model. The pressure inside the cell during the cell growth is shown in Figure 5.4. The pressure is shown for modeling the cell growth with both a constant and a variable viscosity. It can be seen that with a constant

viscosity, the pressure inside the cell decreases rapidly and then slowly increases. The increase in pressure is attributed to the diffusion of the gas from the polymer melt occurring more quickly than the volume of the cell is increasing. When the variable viscosity function is incorporated into the model, the pressure initially decreases rapidly. However, as the viscosity increases and the cell growth is more restricted, the pressure begins to increase more rapidly. The pressure eventually increases to an equilibrium value. It is expected that this is a more accurate representation of the actual cell growth process.

5.7 Conclusions

This paper addresses the modeling of the cell growth in a polymer that is foamed with a dissolved gas blowing agent, which plasticizes the polymer. In previous modeling efforts, the viscosity of the polymer was assumed to be constant. This assumption is invalid because it is known that plasticization leads to a reduction in the viscosity. In this paper, empirical techniques, in conjunction with the WLF equation, were presented as a way to develop a function to describe the viscosity during the cell growth.

The incorporation of the variable viscosity function into the model was shown to control the cell growth, despite the lack qualitative results. The model could only be used qualitatively because of the lack of data on the diffusivity, k_H, and σ. From the qualitative results, it was shown that when the viscosity was modeled as increasing during the cell growth the cell growth did not occur uncontrollably. Initially, the cell growth was large, but as the blowing agents were used in the cell growth and diffused out of the polymer the viscosity of the polymer was increased which led to a decrease in the cell growth rate.

Eventually, when there was no longer any blowing agent present in the polymer the viscosity increased infinitely large and the cell growth ceased.

5.8 Nomenclature

P_g = pressure inside of cell
P_f = pressure at the boundary of the polymer shell
σ = surface tension
R = radius of the cell
τ_{rr} = r-component of the stress tensor
$\tau_{\theta\theta}$ = θ-component of the stress tensor
R_o = initial cell radius
S = outer radius of the polymer shell
d_{rr} = r-component of the rate of deformation tensor
$d_{\theta\theta}$ = θ-component of the rate of deformation tensor
η = viscosity of the polymer melt
c = concentration of the gas
c_{cell} = concentration of gas at the cell/polymer interface
D = diffusivity
R_g = ideal gas law constant
T = temperature
v_r = fluid velocity at the cell wall
η_T = viscosity of the polymer melt at a temperature T in WLF equation
η_{Tg} = viscosity of the polymer melt at the glass transition temperature in WLF equation
C_1 and C_2 = WLF constants
$\eta_T^{polymer}$ = viscosity of the polymer melt at a temperature T in modified WLF equation
$\eta_T^{plasticized}$ = viscosity of the plasticized polymer at temperature T in modified WLF equation
$T_g^{polymer}$ = glass transition temperature of the neat polymer
$T_g^{plasticized}$ = glass transition temperature of the plasticized polymer
k_H = Henry's Law Constant

5.9 References

1. Street, J.R., A.L. Fricke, and L.P. Reiss, *Dynamics of Phase Growth in Viscous, Non-Newtonian Liquids. Initial Stages of Growth.* Ind. Eng. Chem. Fundam., 1971. **10**: p. 54.

2. Amon, M. and C.D. Denson, *Study of Dynamics of Foam Growth: Analysis of Growth of Closely Spaced Spherical Bubbles.* Polym. Eng. Sci., 1984. **24**(13): p. 1026-1034.

3. Tomasko, D.L., et al., *A Review of CO_2 Applications in the Processing of Polymers.* Ind. Eng. Chem. Res., 2003. **42**: p. 6431-6456.

4. Krause, B., et al., *Microcellular Foaming of Amorphous High-T_g Polymers Using Carbon Dioxide.* Macromolecules, 2001. **34**: p. 874-884.

5. Kumar, V., *A Process for Making Microcellular Thermoplastic Parts.* Polym. Eng. Sci., 1990. **30**(20): p. 1323-1329.

6. Sato, Y., et al., *Solubilities and Diffusion Coefficients of Carbon Dioxide in Poly(vinyl acetate) and Polystyrene.* J. Supercrit. Fluid., 2001. **19**: p. 187-198.

7. Arora, K.A., A.J. Lesser, and T.J. McCarthy, *Preparation and Characterization of Microcellular Polystyrene Foams Processed in Supercritical Carbon Dioxide.* Macromolecules, 1998. **31**(4614-4620).

8. Bortner, M.J. and D.G. Baird, *Absorption of CO2 and subsequent viscosity reduction of an acrylonitrile copolymer.* Polym. J., 2004. **45**: p. 3399-3412.

9. Wilding, M.D., D.G. Baird, and A.P.R. Eberle, *Melt processability and foam suppression of high molecular weight polyethylenes plasticized with supercritical carbon dioxide.* Int. Polym. Proc., 2008. **23**(2): p. 228-237.

10. Leung, S.N., et al., *Computer Simulation of Bubble-Growth Phenomena in Foaming.* Ind. Eng. Chem. Res., 2006. **45**: p. 7823-7831.

11. Advani, S.G. and A. Arefmanesh, *Chapter 10: Bubble Growth and Collapse in Viscoelastic Liquids*, in *Advances in Transport Processes IX*, A.S. Mujumdar and

R.A. Mashelkar, Editors. 1993, Elsevier Science Publishers B.V.: New York. p. 445-499.

12. Otsuki, Y. and T. Kanai, *Numerical Simulation of Bubble Growth in Viscoelastic Fluid with Diffusion of Dissolved Foaming Agent.* Polym. Eng. Sci., 2005. **45**(9): p. 1277-1287.

13. Chen, X., J.J. Feng, and C.A. Bertelo, *Plasticization Effects on Bubble Growth During Polymer Foaming.* Polym. Eng. Sci., 2006. **46**: p. 97-107.

14. Everitt, S.L., O.G. Harlen, and H.J. Wilson, *Bubble Growth in a Two-Dimensional Viscoelastic Foam.* J. Non-Newton. Fluid., 2006. **137**: p. 46-59.

15. Ferry, J.D., *Viscoelastic Properties of Polymers*. 1980, New York, NY: John Wiley and Sons.

16. Bortner, M.J., *Ph.D. Thesis: Melt Processing of Metastable Acrylic Copolymer Carbon Precursors*, in *Department of Chemical Engineering*. 2003, Virginia Tech: Blacksburg, VA. p. 329.

17. Kweeder, J.A., et al., *The Nucleation of Microcellular Polystyrene Foam.* SPE ANTEC Tech. Papers., 1991. **37**: p. 1398-1400.

Table 5.1. Estimated Physical Parameters Used in the Cell Growth Modeling.

D	1×10^{-9} m^2/s
k_H	8.4×10^{-5} mol/(N*m)
R_o	0.179 μm
σ	1×10^{-3} N/m
S	60 μm
T_g	493 K
$P_{g,o}$	6.8×10^{6} N/m^2

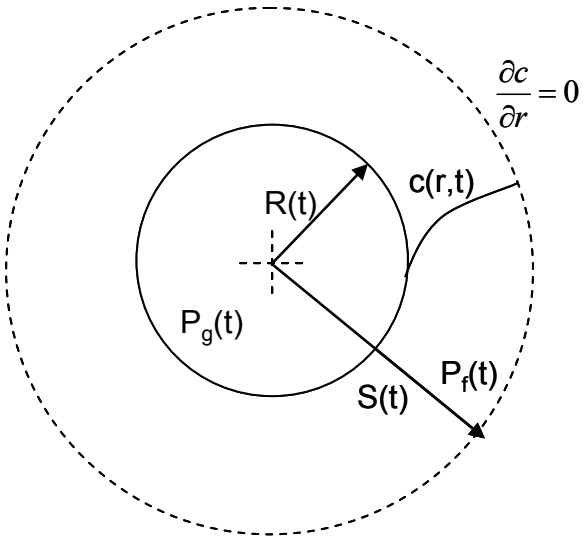

Figure 5.1. Schematic for the modeling of the cell growth. An individual cell is assumed to be surrounded by a finite shell of gas-saturated polymer melt.

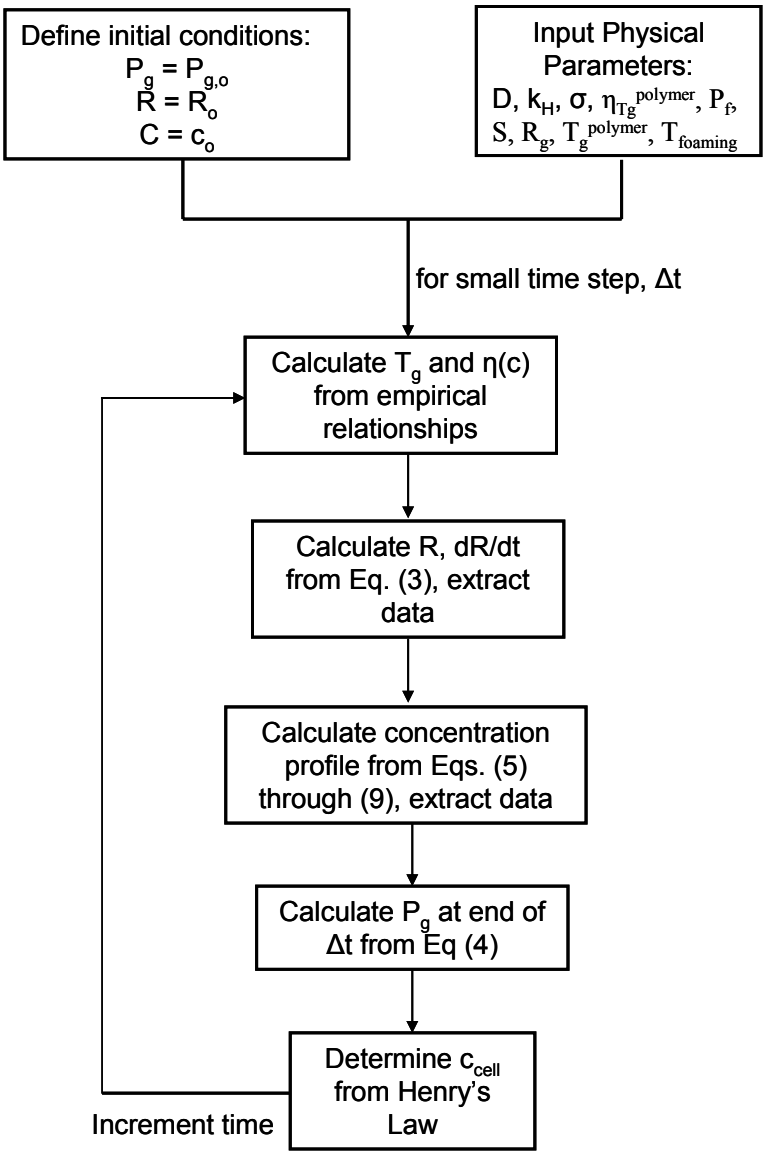

Figure 5.2. Schematic for the numerical simulation of the cell growth.

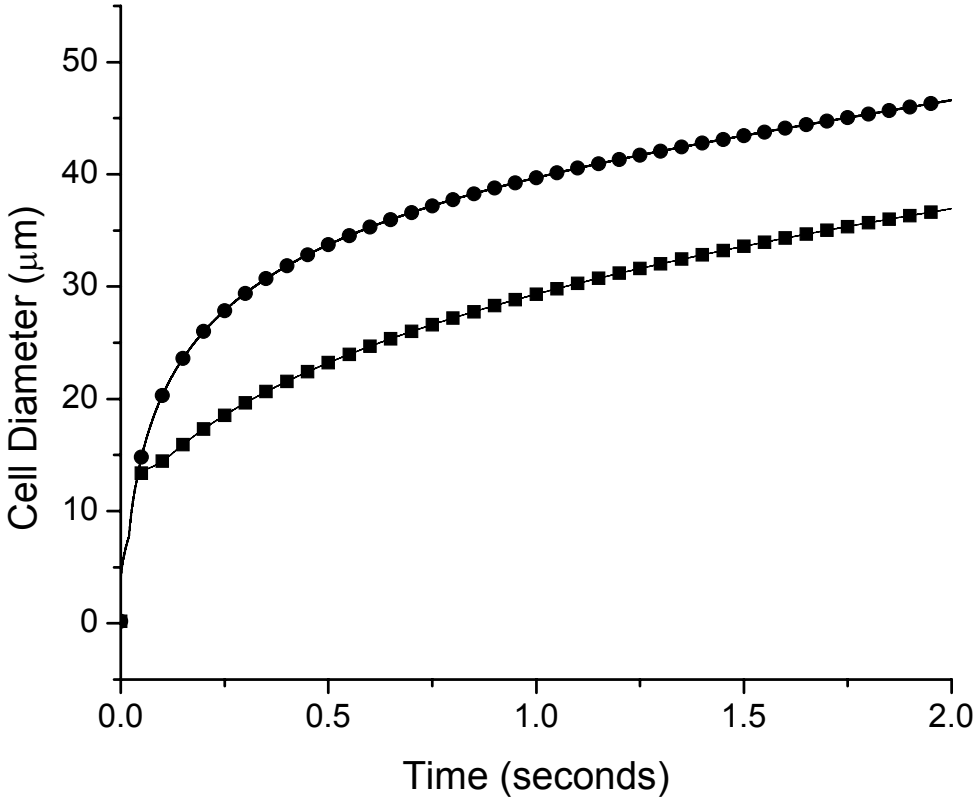

Figure 5.3. Comparison of the cell diameter in the cell growth model when a constant viscosity term (●) versus a variable viscosity function (■) is used.

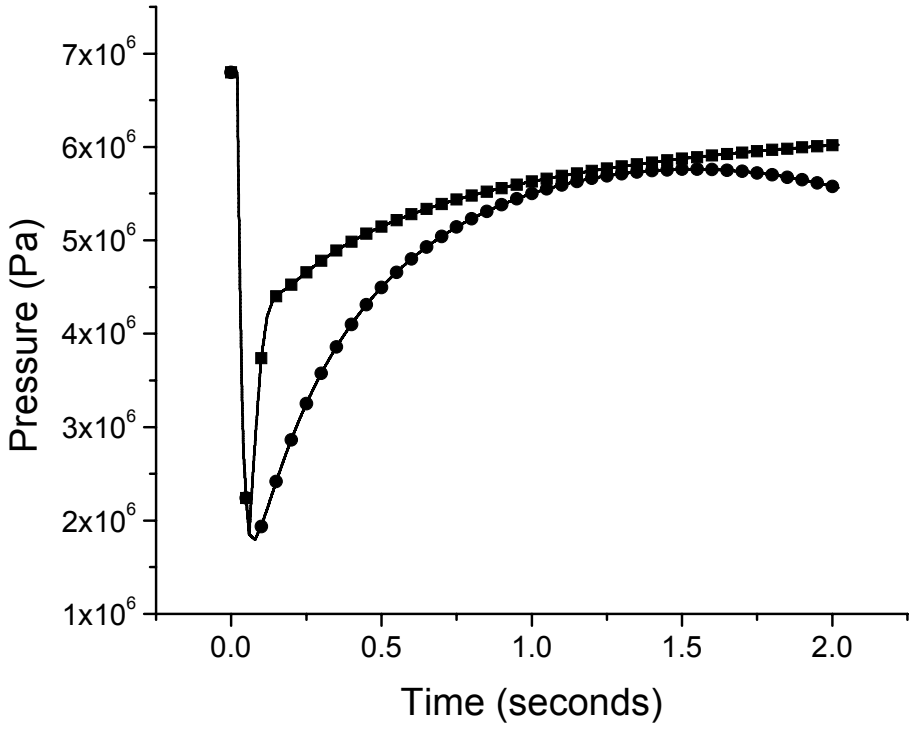

Figure 5.4. Comparison of the pressure inside the cell in the cell growth model when a constant viscosity term (●) versus a variable viscosity function (■) is used.

6 Recommendations

1) The production of the PAES and CNF-PAES foams was all conducted in a one-step batch process; however, it would be more desirable for industrial use to produce the foams from a continuous process. While there have been processes developed for continuous extrusion of foams, which use $scCO_2$ as the blowing agent, no work has incorporated both water and $scCO_2$ as blowing agents into a continuous foaming process. The die design is also of concern in continuous foam production on a single screw extruder. Many of the processes for single screw continuous foam production involve the use of filament dies, which do not produce a part that is useful.

2) While the cell growth model with the variable viscosity was able to qualitatively estimate the cell growth of a polymer with dissolved gas blowing agents that are plasticizers, quantitative modeling is desirable. The incorporation of a viscoelastic constitutive equation to describe the components of the extra stress tensor would provide for more accurate results. Both the upper convected Maxwell[1-3] and the Oldroyd B[4, 5] models have been used in the cell growth model with constant viscosity. The incorporation of either of these models would involve streamlining the program for obtaining the numerical analysis so that a solution could be obtained in a timely manner. By incorporating a viscoelastic constitutive equation, the solution becomes more computational intensive.

3) Another improvement that could be made to the cell growth model is to incorporate the Sanchez-Lacombe equation of state[6] to better describe the gas inside of the cell, than is possible with the ideal gas law. Because carbon dioxide is supercritical, the ideal gas law does not accurately describe the gas inside of the cell. The Sanchez-Lacombe would be a better option. More work would also have to be done with incorporating both the water vapor and the $scCO_2$, into whatever equation is used to describe the gas inside of the cell.

4) The current cell growth model was developed based on a single dissolved gas in the polymer. Research would have to be conducted on how to incorporate both water and $scCO_2$ into the cell growth model. It may be feasible to combine the physical parameters of the water and $scCO_2$.

6.1 Determination of the Physical Parameters in the Cell Growth Model for PAES with Water and CO_2

1) Henry's law constant, k_H, needs to be determined for the PAES foamed with water and $scCO_2$ in order to quantitatively model the cell growth. The value of k_H could be determined by subjecting the PAES to various saturation pressures, and then measuring the solubility of the gas in the polymer. A linear plot should be obtained when the concentration of gas vs. pressure is plotted, with the slope being the value for k_H.

2) The initial pressure inside of the cell, P_g, can be estimated by thermodynamic equilibrium based on the Sanchez-Lacombe equation of state[6]. As with using the Sanchez-Lacombe equation of state to describe the pressure of the gas in the cell, experiments would need to be conducted on using a combination of water and $scCO_2$.

3) The diffusivity of the blowing agents in the PAES can be determined experimentally. Various techniques are reviewed in section 2.1.3 of this dissertation.

4) The cell nucleation density, and ultimately the value of the shell diameter, can either be determined experimentally or calculated based on cell nucleation models[7-9]. Several models have been reported in literature to describe the cell nucleation density. Experimentally, the value of the cell nucleation density can be calculated by foaming a polymer, observing the cell morphology with scanning electron microscopy, and calculating the cell nucleation density.

6.2 References

1. Leung, S.N., et al., *Computer Simulation of Bubble-Growth Phenomena in Foaming.* Ind. Eng. Chem. Res., 2006. **45**: p. 7823-7831.

2. Advani, S.G. and A. Arefmanesh, *Chapter 10: Bubble Growth and Collapse in Viscoelastic Liquids*, in *Advances in Transport Processes IX*, A.S. Mujumdar and R.A. Mashelkar, Editors. 1993, Elsevier Science Publishers B.V.: New York. p. 445-499.

3. Otsuki, Y. and T. Kanai, *Numerical Simulation of Bubble Growth in Viscoelastic Fluid with Diffusion of Dissolved Foaming Agent.* Polym. Eng. Sci., 2005. **45**(9): p. 1277-1287.

4. Chen, X., J.J. Feng, and C.A. Bertelo, *Plasticization Effects on Bubble Growth During Polymer Foaming.* Polym. Eng. Sci., 2006. **46**: p. 97-107.

5. Everitt, S.L., O.G. Harlen, and H.J. Wilson, *Bubble Growth in a Two-Dimensional Viscoelastic Foam.* J. Non-Newton. Fluid., 2006. **137**: p. 46-59.

6. Sanchez, I.C. and R.H. Lacombe, *Statistical Thermodynamics of Polymer Solutions.* Macromolecules., 1978. **11**(6): p. 1145-1156.

7. Kweeder, J.A., et al., *The Nucleation of Microcellular Polystyrene Foam.* SPE ANTEC Tech. Papers., 1991. **37**: p. 1398-1400.

8. Ramesh, N.S., D.H. Rasmussen, and G.A. Campbell, *The Heterogeneous Nulceation of Microcellular Foams Assisted by the Survival of Microvoids in Polymers Containing Low Glass Transition Particles. Part I: Mathematical Modeling and Numerical Simulation.* Polym. Eng. Sci., 1994. **34**(22): p. 1685-1697.

9. Colton, J.S. and N.P. Suh, *The Nucleation of Microcellular Thermoplastic Foam With Additives: Part 1: Theorectical Considerations.* Polym. Eng. Sci., 1987. **27**(7): p. 485-492.

Appendix A: MATLAB Program for Cell Growth Modeling

```
function cellgrowthloopwetawplot
clear all
close all
global Diff Rend dRend Pinf Kh co Rbubbleo sigma eta Rshell  m C r
dCoutdr Rg T cbubble i tdivisions rdivisions Pend tgap Cout Cinitial pp
%*********************************************************************
%Enter in material properties
Diff = 1e-9; %(m^2/s)
Pgo = 6.8e6; %Gas pressure in bubble (N/m^2)
Kh = 8.4e-5; %(mol/(N*m))
Rbubbleo =.179e-6; %initial bubble size(m)
sigma = 1e-3; %interfacial tension coefficient (N/m)
etapoly =3e8; %Viscosity of the polymer(N/m*s)
etao = 3e6; %Initial Viscosity
Pinf = 8e6; %Pressure at outer boundary of polymer shell (N/m^2)
Rshell = 60e-6; %Radius of shell (m)
Rg = 8.314472; %universal gas constant (m^3*Pa/mol*K)
T = 493; %Temperature in K
Tgpoly = 493; %Glass Transition Temperature of Polymer in K
%*********************************************************************

%Define time range, increments, and the time and position mesh
tfinal = 2; %final time in seconds
numloops = 100; %number of time steps
tgap = tfinal/numloops;
tdivisions = 100; %number of time divisions within each time gap
rdivisions = 100;  %number of points in r-mesh

%System properties calculated from material parameters
co = Pgo*Kh; %Initial gas concentration in polymer melt (mol/m^3)
Cinitial = (Pgo*Kh)*ones(1,rdivisions);
Rend = Rbubbleo;

%Determination of the initial viscosity based on the gas concentration
Tgplast = -0.0893*co+493;
eta = etapoly/((10^((-5*(T-Tgpoly))/(120+T-Tgpoly)))/(10^((-5*(T-
Tgplast))/(120+T-Tgplast))));

%Fit a function to the initial concentration profile
pp = spline(linspace(Rbubbleo, Rshell, rdivisions),Cinitial);

%Define Solution Matrices
tRmat = zeros(tdivisions*numloops, 2);%solution matrix for Radius vs.
Time
tPmat = zeros(tdivisions*(numloops+1),2);  %solution matrix for
Pressure vs. Time
Cgaspolymat = zeros(tdivisions*numloops+1, rdivisions+1); %solutions
matrix for the concentration profile
Csurf = zeros(numloops+1, rdivisions+1);

%matrix for initial pressure is held constant
```

```
P(1:tdivisions,:) = ones(tdivisions,1)*Pgo;
tP = linspace(0, tgap, tdivisions);
tPmat(1:tdivisions,:) = [tP', P];

%Loop to incrementally step through the calculations over small time
steps
for i=1:1:numloops;

    %defines time increment
    tincrement = linspace((i-1)*tgap, i*tgap, tdivisions);

    %Carry over initial pressure for time step from previous time step
    Pend = P(tdivisions);

    %calculate concentration in bubble from Henry's Law
    cbubble = Pend*Kh;

    %Determine Rend and dRend from the Consveration of Motion
    [tR,Rbubble] = ode45(@eqnmotloop,tincrement,Rend); %check to see if
I want this as Rbubbleo or Rend

    Rend = Rbubble(tdivisions);
    dRend = (Rbubble(tdivisions)-Rbubble(tdivisions-
1))/(tgap/tdivisions);

    %Determine the concentration profile from Rend to Rshell
    diffeqn

    %compute dCdr evaluated at r=Rt
    [Cout,dCoutdr] = pdeval(m,r,[C(end,:)],Rend);

    %Fit a function to the concentration at the end of the time step
    pp = spline(linspace(Rbubbleo, Rshell, rdivisions),C(end,:));

    %Functions to determine eta from the concentration of gas at the
cell wall
    Tgplast = -0.0893*Cout+493;
    eta = etainf/((10^((-5*(T-Tgpoly))/(120+T-Tgpoly)))/(10^((-5*(T-
Tgplast))/(120+T-Tgplast))));

    %compute the pressure for the next time step from Conservation of
Mass
    [tP,P] = ode45(@conmasseqnloop,
linspace(i*tgap,(i+1)*tgap,tdivisions), Pend);

    %Puts the solutions of R vs t and P vs t for the time step in
solution matrix
    tRmat(((i-1)*tdivisions+1):i*tdivisions,:) = [tR, Rbubble*1e6];
    tPmat((i*tdivisions+1):(i+1)*tdivisions,:) = [tP, P];

    %Puts solution for concentration vs r and t into solution matrix
    Cgaspolymat(1,2:(rdivisions+1)) = r; %assigns the top row, starting
at column 2 to for the radius
```

```
    Cgaspolymat(((i-1)*tdivisions+2):i*tdivisions+1, 1) = [tR];
%assigns the 1 column starting at row 2 for time
    Cgaspolymat(((i-1)*tdivisions+2):i*tdivisions+1, 2:(rdivisions+1))
= C; %assigns rest of matrix starting at column 2 row 2 for
concentration

    %Assigns the concentration profile to the matrix for plotting
    Csurf(1,2:(rdivisions+1))= r;
    Csurf(i+1,1) = tR(1);
    Csurf(i+1,2:(rdivisions+1)) = C(end,:);

    figure(3);
    surf(Csurf(1,2:end), Csurf(2:end,1), Csurf(2:end,2:end)); hold on;
    xlabel('Distance r')
    ylabel('Time t')
end

%Plot of R vs time
figure(1)
plot(tRmat(:,1),tRmat(:,2))
xlabel('time t');
ylabel('solution R');

%Plot of P vs time
figure(2)
plot(tPmat(:,1),tPmat(:,2))
xlabel('time t');
ylabel('solution P');

%Surface plot of C vs position and time
figure(4)
surf(Csurf(1,2:end), Csurf(2:end,1), Csurf(2:end,2:end))
xlabel('Distance r')
ylabel('Time t')

%Outputs excel file of R and time
xlswrite('bubblegrowthvariableviscosity.xls', tRmat,
'variableviscosity')
xlswrite('cellpressurevariableviscosity.xls', tPmat,
'variableviscosity')
% --------------------------------------------------------------
function diffeqn
global  Rend Rbubbleo Rshell sol m C r i tdivisions rdivisions tgap

m = 2;
r = linspace(Rend, Rshell, rdivisions);
t = linspace((i-1)*tgap, i*tgap, tdivisions);

sol = pdepe(m,@diffpde,@diffpdeic,@diffpdebc,r,t);
% Extract the first solution component as u.
C = sol(:,:,1);
% Surface plot of C(r,t)
%figure(3)
%surf(r,t,C)
%title('Numerical solution computed with 100 mesh points.')
```

```
%xlabel('Distance r')
%ylabel('Time t')
% ------------------------------------------------------------
function [c,f,s] = diffpde(r,t,C,DCDr)
global Diff Rend dRend

c = 1/Diff;
f = DCDr;
s = (1/Diff)*(-(Rend^2*dRend)/r^2)*DCDr;
% ------------------------------------------------------------
function C0 = diffpdeic(r)
global co Cinitial pp
    C0 = ppval(pp,r);%initial amount of dissolve CO2 in polymer
% ------------------------------------------------------------
function [pl,ql,pr,qr] = diffpdebc(rl,cl,rr,cr,t)
global cbubble co
pl = cl-cbubble;
ql = 0;
pr = 0;
qr = 1;



%subroutine for the conservation of mass
function dPdt = conmasseqnloop(tP,P)
global Diff Rend dRend dCoutdr Rg T

dPdt = (3*Rg*Diff*T/Rend)*dCoutdr - (3*P/Rend)*dRend;



%subroutine for the equation of motion
function dRdt = eqnmotwetaloop(tR,Rbubble)
global Pinf Rbubbleo sigma eta Rshell Pend

dRdt = ((Pinf-Pend) - ((2*sigma)/Rbubble))*((1/(1/Rshell^3))-
(1/(1/Rbubbleo^3)))*(1/(4*eta*Rbubble^2));
```

Appendix B: DMTA Data

Temp °C	G' Pa	G" Pa	tan_delta	Temp °C	G' Pa	G" Pa	tan_delta
28.39	1.11E+08	1.26E+07	0.11377	135.4	1.16E+08	6.99E+06	0.06014
27.3	1.19E+08	1.12E+07	0.09383	138.04	1.17E+08	6.93E+06	0.05923
26.25	1.21E+08	1.07E+07	0.08799	141.43	1.15E+08	7.08E+06	0.06165
30.78	1.23E+08	1.05E+07	0.0848	144.72	1.13E+08	7.28E+06	0.06446
41.2	1.19E+08	9.76E+06	0.08226	147.82	1.14E+08	7.25E+06	0.06386
47.89	1.18E+08	1.04E+07	0.08814	150.69	1.14E+08	7.47E+06	0.06552
48.04	1.18E+08	9.81E+06	0.08283	154.02	1.14E+08	7.32E+06	0.06413
49.12	1.17E+08	9.46E+06	0.0806	157.29	1.15E+08	7.28E+06	0.06316
54.79	1.16E+08	9.36E+06	0.08051	160.16	1.16E+08	7.71E+06	0.06638
58.82	1.15E+08	9.17E+06	0.07996	163.01	1.17E+08	7.62E+06	0.06516
60.19	1.14E+08	9.64E+06	0.0848	166.4	1.18E+08	7.72E+06	0.06519
62.49	1.12E+08	9.38E+06	0.0835	169.57	1.19E+08	8.02E+06	0.06712
66.93	1.13E+08	9.04E+06	0.08025	172.61	1.20E+08	7.90E+06	0.06584
70.88	1.13E+08	9.21E+06	0.08162	175.77	1.21E+08	8.16E+06	0.0676
72.66	1.15E+08	8.80E+06	0.07644	178.69	1.21E+08	8.47E+06	0.06994
75.14	1.15E+08	8.57E+06	0.07472	181.79	1.22E+08	8.92E+06	0.07288
79.38	1.13E+08	8.31E+06	0.0735	185.2	1.23E+08	9.64E+06	0.07865
82.89	1.13E+08	8.18E+06	0.07257	188.18	1.21E+08	1.08E+07	0.0891
85.27	1.15E+08	7.93E+06	0.06915	191.22	1.25E+08	1.15E+07	0.0923
87.93	1.14E+08	8.44E+06	0.07399	193.94	1.26E+08	1.16E+07	0.09181
91.47	1.14E+08	7.99E+06	0.07004	197.14	1.25E+08	1.17E+07	0.09309
95.09	1.14E+08	7.66E+06	0.06724	200.59	1.25E+08	1.26E+07	0.10093
97.63	1.14E+08	7.69E+06	0.06723	203.64	1.24E+08	1.36E+07	0.10969
98.86	1.14E+08	7.35E+06	0.06427	206.44	1.22E+08	1.37E+07	0.11204
100.78	1.14E+08	7.30E+06	0.06381	208.8	1.19E+08	1.52E+07	0.12773
104.65	1.15E+08	7.21E+06	0.0629	211.82	1.13E+08	1.63E+07	0.14447
108.04	1.15E+08	7.11E+06	0.0616	214.38	1.06E+08	1.82E+07	0.17158
110.41	1.15E+08	7.08E+06	0.06136	216.66	9.48E+07	2.14E+07	0.22563
113.16	1.17E+08	7.02E+06	0.0602	219.13	7.85E+07	2.43E+07	0.30959
116.59	1.16E+08	6.97E+06	0.05989	221.44	5.34E+07	2.45E+07	0.45854
120.23	1.15E+08	7.10E+06	0.06185	223.96	2.10E+07	1.34E+07	0.63831
123.02	1.16E+08	7.01E+06	0.06032	227.24	1.23E+07	4.43E+06	0.36189
125.46	1.16E+08	6.99E+06	0.06021	229.54	9.87E+06	1.18E+06	0.11923
128.9	1.16E+08	7.07E+06	0.06123	232.46	7.93E+06	4.92E+05	0.06197
132.64	1.16E+08	7.43E+06	0.06406	234.5	6.46E+06	2.35E+05	0.03639
				237.27	4.64E+06	48189.8	0.01038

Temp °C	G' Pa	G" Pa	tan_delta	Temp °C	G' Pa	G" Pa	tan_delta
31.41	7.71E+08	1.35E+07	0.01748	131.19	6.63E+08	2.17E+07	0.03273
29.47	7.73E+08	1.34E+07	0.01727	134.03	6.57E+08	2.31E+07	0.03517
27.78	7.75E+08	1.30E+07	0.01685	136.5	6.51E+08	2.49E+07	0.03829
27.23	7.74E+08	1.29E+07	0.01666	138.84	6.44E+08	2.67E+07	0.04153
33.31	7.70E+08	1.28E+07	0.01657	141.37	6.36E+08	2.95E+07	0.04636
39.66	7.65E+08	1.30E+07	0.01697	144.07	6.24E+08	3.33E+07	0.05327
43.07	7.63E+08	1.33E+07	0.01746	147.02	6.10E+08	3.90E+07	0.06387
42.88	7.61E+08	1.35E+07	0.01776	149.43	5.84E+08	4.84E+07	0.08289
44.13	7.59E+08	1.33E+07	0.01758	152.27	5.37E+08	5.99E+07	0.1116
48.52	7.55E+08	1.36E+07	0.01807	155.71	4.55E+08	5.95E+07	0.13068
52.38	7.52E+08	1.38E+07	0.01838	158.82	3.99E+08	5.08E+07	0.12727
54.06	7.50E+08	1.41E+07	0.0188	161.28	3.62E+08	4.40E+07	0.12138
54.99	7.48E+08	1.42E+07	0.01892	163.55	3.42E+08	3.99E+07	0.11675
57.3	7.46E+08	1.43E+07	0.01917	165.84	3.31E+08	4.03E+07	0.12194
60.71	7.43E+08	1.45E+07	0.01947	168.55	3.22E+08	4.62E+07	0.1433
64.05	7.40E+08	1.46E+07	0.01966	171.26	3.18E+08	5.34E+07	0.16781
66.11	7.38E+08	1.45E+07	0.01959	173.63	3.19E+08	6.48E+07	0.20342
67.93	7.37E+08	1.44E+07	0.01958	176.2	3.22E+08	7.31E+07	0.22729
70.6	7.34E+08	1.45E+07	0.01972	178.29	3.21E+08	8.46E+07	0.26329
73.72	7.32E+08	1.47E+07	0.02004	180.6	3.12E+08	1.01E+08	0.32511
76.77	7.29E+08	1.46E+07	0.02002	183.38	2.73E+08	1.32E+08	0.4842
78.95	7.27E+08	1.45E+07	0.0199	186.7	2.60E+08	1.54E+08	0.59445
80.98	7.25E+08	1.45E+07	0.01996	189.11	3.08E+08	1.59E+08	0.51555
83.67	7.23E+08	1.46E+07	0.02014	191.46	3.66E+08	1.70E+08	0.46409
86.78	7.20E+08	1.49E+07	0.02063	193.4	3.75E+08	1.86E+08	0.49768
89.34	7.18E+08	1.46E+07	0.02039	196.11	4.50E+08	1.92E+08	0.42592
91.81	7.16E+08	1.49E+07	0.02075	199.16	4.64E+08	2.06E+08	0.44312
94.2	7.13E+08	1.49E+07	0.02083	202.26	4.87E+08	2.23E+08	0.45684
96.72	7.11E+08	1.50E+07	0.02112	205.01	5.68E+08	2.04E+08	0.35934
98.96	7.09E+08	1.49E+07	0.021	208.01	5.49E+08	2.00E+08	0.36438
100.26	7.07E+08	1.50E+07	0.02118	211.42	5.07E+08	1.96E+08	0.38547
102.34	7.05E+08	1.50E+07	0.02133	214.42	4.42E+08	1.96E+08	0.44253
105.32	7.01E+08	1.56E+07	0.02222	217.32	3.52E+08	2.00E+08	0.56806
108.55	6.98E+08	1.58E+07	0.02268	219.83	2.16E+08	1.80E+08	0.83183
110.96	6.95E+08	1.63E+07	0.0235	222.71	9.15E+07	1.16E+08	1.26831
112.86	6.92E+08	1.64E+07	0.02376	224.98	2.56E+07	4.94E+07	1.92538
115.18	6.89E+08	1.69E+07	0.02454	227.64	1.15E+07	1.69E+07	1.47916
118.24	6.85E+08	1.75E+07	0.02549	229.83	6.34E+06	6.44E+06	1.01562
121.33	6.81E+08	1.82E+07	0.0268	232.13	4.64E+06	2.57E+06	0.55489
123.69	6.77E+08	1.88E+07	0.02784	234.26	3.58E+06	1.20E+06	0.33594
125.91	6.73E+08	1.97E+07	0.02931	237.1	8.86E+05	1.77E+06	1.9999
128.33	6.68E+08	2.03E+07	0.0304				

Temp °C	G' Pa	G" Pa	tan_delta	Temp °C	G' Pa	G" Pa	tan_delta
36.17	7.65E+08	1.05E+07	0.01379	144.24	6.44E+08	9.59E+06	0.01489
35.5	7.64E+08	1.05E+07	0.01373	146.69	6.42E+08	9.88E+06	0.01538
34.75	7.65E+08	1.03E+07	0.01343	149.28	6.40E+08	1.00E+07	0.01563
34.17	7.65E+08	1.02E+07	0.01331	152.04	6.38E+08	1.04E+07	0.0163
36.78	7.60E+08	1.03E+07	0.01355	154.45	6.36E+08	1.04E+07	0.01636
45.73	7.50E+08	1.11E+07	0.01483	157.27	6.34E+08	1.10E+07	0.01727
53.7	7.39E+08	1.20E+07	0.01624	159.81	6.32E+08	1.12E+07	0.01773
57.77	7.32E+08	1.27E+07	0.01734	162.39	6.29E+08	1.18E+07	0.01868
57.31	7.29E+08	1.28E+07	0.01758	164.74	6.27E+08	1.21E+07	0.01929
57.98	7.25E+08	1.30E+07	0.01789	167.45	6.24E+08	1.27E+07	0.02039
62.33	7.18E+08	1.32E+07	0.01843	170.02	6.21E+08	1.35E+07	0.02173
67.01	7.12E+08	1.37E+07	0.01929	173.26	6.17E+08	1.44E+07	0.02338
69.18	7.07E+08	1.38E+07	0.01953	176	6.13E+08	1.55E+07	0.02521
69.81	7.04E+08	1.38E+07	0.01959	179.35	6.08E+08	1.68E+07	0.02766
71.95	7.00E+08	1.38E+07	0.01966	182.51	6.03E+08	1.85E+07	0.03065
76.05	6.95E+08	1.37E+07	0.01972	185.59	5.97E+08	2.05E+07	0.03432
79.53	6.90E+08	1.35E+07	0.01953	188.58	5.90E+08	2.29E+07	0.03878
81.32	6.87E+08	1.33E+07	0.01929	191.81	5.83E+08	2.60E+07	0.04459
82.9	6.85E+08	1.29E+07	0.01885	194.66	5.74E+08	2.99E+07	0.05205
85.58	6.82E+08	1.27E+07	0.01862	197.87	5.65E+08	3.44E+07	0.06099
89.07	6.78E+08	1.23E+07	0.01807	200.32	5.53E+08	3.89E+07	0.07024
91.97	6.76E+08	1.20E+07	0.0177	202.86	5.41E+08	4.55E+07	0.08418
94.01	6.74E+08	1.17E+07	0.01734	205.04	5.22E+08	5.48E+07	0.10487
95.86	6.73E+08	1.13E+07	0.01679	207.51	4.98E+08	6.39E+07	0.12848
98.3	6.71E+08	1.09E+07	0.01624	209.86	4.67E+08	7.75E+07	0.16593
100.66	6.70E+08	1.08E+07	0.01611	212.55	4.16E+08	9.41E+07	0.22626
102.86	6.68E+08	1.04E+07	0.0155	214.99	3.44E+08	1.10E+08	0.31891
105.33	6.67E+08	1.03E+07	0.01538	217.38	2.27E+08	1.14E+08	0.50379
107.93	6.65E+08	9.99E+06	0.01502	220.46	1.02E+08	9.31E+07	0.91123
110.7	6.64E+08	9.89E+06	0.01489	223.65	3.32E+07	4.89E+07	1.4745
113.13	6.62E+08	9.62E+06	0.01453	226.02	9.35E+06	1.71E+07	1.83237
115.63	6.61E+08	9.60E+06	0.01453	228.56	5.58E+06	6.15E+06	1.10154
118.09	6.60E+08	9.42E+06	0.01428	230.86	3.94E+06	2.79E+06	0.70747
120.84	6.58E+08	9.40E+06	0.01428	233.11	3.21E+06	1.43E+06	0.44661
123.4	6.57E+08	9.30E+06	0.01416	235.31	2.63E+06	9.69E+05	0.36895
126.02	6.55E+08	9.32E+06	0.01422	237.97	2.21E+06	7.18E+05	0.32443
128.73	6.54E+08	9.26E+06	0.01416	240.36	1.79E+06	6.09E+05	0.34112
131.03	6.52E+08	9.36E+06	0.01434	243	1.46E+06	5.50E+05	0.37639
133.81	6.51E+08	9.21E+06	0.01416	245.16	1.24E+06	5.15E+05	0.41586
136.46	6.49E+08	9.39E+06	0.01447	247.39	9.68E+05	4.56E+05	0.47052
139.08	6.48E+08	9.41E+06	0.01453	250.04	6.09E+05	3.50E+05	0.57533
141.53	6.46E+08	9.62E+06	0.01489	252.28	2.72E+05	1.29E+05	0.47235

Temp °C	G' Pa	G" Pa	tan_delta	Temp °C	G' Pa	G" Pa	tan_delta
32.01	7.04E+08	1.39E+07	0.01978	138.84	6.01E+08	1.99E+07	0.03309
34.02	7.03E+08	1.39E+07	0.01984	141.38	5.95E+08	2.12E+07	0.03566
38.06	7.01E+08	1.39E+07	0.0199	143.96	5.89E+08	2.32E+07	0.03945
40.23	7.00E+08	1.39E+07	0.01984	146.58	5.80E+08	2.59E+07	0.04454
40.83	6.99E+08	1.37E+07	0.01966	149.33	5.70E+08	2.97E+07	0.05205
42.76	6.97E+08	1.36E+07	0.01953	151.95	5.56E+08	3.51E+07	0.06312
46.12	6.95E+08	1.35E+07	0.01941	154.5	5.33E+08	4.28E+07	0.08019
49.42	6.93E+08	1.35E+07	0.01953	157.16	4.87E+08	5.49E+07	0.11266
51.22	6.91E+08	1.36E+07	0.01966	160.27	4.19E+08	5.52E+07	0.1318
52.91	6.89E+08	1.34E+07	0.01947	163.14	3.59E+08	4.44E+07	0.12386
55.44	6.87E+08	1.32E+07	0.01928	166.32	3.18E+08	3.69E+07	0.11606
58.79	6.85E+08	1.33E+07	0.01947	169.28	2.95E+08	3.76E+07	0.12758
61.54	6.83E+08	1.31E+07	0.01918	172.51	2.83E+08	4.19E+07	0.14804
63.77	6.81E+08	1.32E+07	0.01935	175.28	2.77E+08	4.80E+07	0.17302
65.84	6.79E+08	1.30E+07	0.01917	177.65	2.74E+08	5.61E+07	0.20511
68.57	6.77E+08	1.31E+07	0.01929	180.66	2.69E+08	6.51E+07	0.24148
71.73	6.75E+08	1.30E+07	0.01929	183.56	2.59E+08	7.85E+07	0.30245
74.35	6.73E+08	1.29E+07	0.01923	186.02	2.41E+08	9.83E+07	0.40822
76.65	6.71E+08	1.29E+07	0.01917	188.91	2.14E+08	9.70E+07	0.45235
78.76	6.69E+08	1.28E+07	0.01911	191.18	2.84E+08	1.12E+08	0.39532
81.57	6.67E+08	1.27E+07	0.01905	193.92	3.10E+08	1.27E+08	0.4105
84.44	6.64E+08	1.28E+07	0.01923	197.17	3.37E+08	1.29E+08	0.38386
87.21	6.62E+08	1.27E+07	0.01917	200.54	3.49E+08	1.32E+08	0.37897
89.47	6.60E+08	1.28E+07	0.01935	203.45	3.56E+08	1.34E+08	0.37694
91.95	6.58E+08	1.26E+07	0.01917	206.56	3.47E+08	1.33E+08	0.38323
94.71	6.56E+08	1.28E+07	0.01947	209.76	3.22E+08	1.29E+08	0.40105
97.35	6.54E+08	1.29E+07	0.01978	212.75	2.93E+08	1.31E+08	0.44641
99.36	6.52E+08	1.29E+07	0.01972	215.85	2.85E+08	1.46E+08	0.511
100.01	6.51E+08	1.28E+07	0.01973	218.91	2.32E+08	1.52E+08	0.65267
101.88	6.48E+08	1.29E+07	0.01996	221.84	1.53E+08	1.29E+08	0.8488
105.39	6.46E+08	1.30E+07	0.02014	224.25	5.86E+07	7.80E+07	1.33049
108.95	6.43E+08	1.33E+07	0.02075	227.1	1.93E+07	3.38E+07	1.74845
110.98	6.40E+08	1.34E+07	0.021	229.35	8.54E+06	1.16E+07	1.35463
112.61	6.38E+08	1.36E+07	0.02137	232.02	5.77E+06	4.38E+06	0.7589
115.06	6.35E+08	1.38E+07	0.02173	234.62	4.37E+06	2.04E+06	0.4658
118.18	6.32E+08	1.42E+07	0.02253	237.36	3.50E+06	1.24E+06	0.35569
121.46	6.29E+08	1.46E+07	0.0232	239.96	2.85E+06	9.23E+05	0.32435
123.7	6.25E+08	1.49E+07	0.02387	242.53	2.28E+06	7.34E+05	0.32133
125.82	6.22E+08	1.55E+07	0.02486	244.83	1.80E+06	6.42E+05	0.35618
127.98	6.19E+08	1.59E+07	0.02576	247.64	1.31E+06	5.00E+05	0.38085
130.97	6.15E+08	1.67E+07	0.02711	250.12	7.77E+05	3.31E+05	0.4265
134.1	6.10E+08	1.76E+07	0.02888	252.84	3.06E+05	1.25E+05	0.40715
136.64	6.06E+08	1.87E+07	0.03089				